How Stromal Interaction Molecule 1 (STIM1) and Store Operated Calcium Entry (SOCE) affect mitochondrial energy metabolism and neuronal function

Inaugural-Dissertation

zur Erlangung des Doktorgrades der
Mathematisch-Naturwissenschaftlichen Fakultät
der Heinrich-Heine-Universität Düsseldorf

vorgelegt von

Nadine Henke
aus Wuppertal

Düsseldorf, Oktober 2012

Aus der Klinik für Neurologie des
Universitätsklinikums Düsseldorf
und dem Institut für Physikalische Biologie
der Heinrich-Heine-Universität Düsseldorf

Gedruckt mit der Genehmigung der
Mathematisch-Naturwissenschaftlichen Fakultät der
Heinrich-Heine-Universität Düsseldorf

Referent: Prof. Dr. Axel Methner

Koreferent: Prof. Dr. Dieter Willbold

Tag der mündlichen Prüfung: 11.12.2012

In the furnaces of the stars the elements evolved from hydrogen. When oxygen and neon captured successive α particles, the element calcium was born. [1]

David E. Clapham

Summary

Ca^{2+} ions are critically involved in a broad range of cellular functions and are indispensably linked to cellular signaling events. Once a plasma-membrane bound receptor is activated to elicit a Ca^{2+} signal, Ca^{2+} is quickly released from the endoplasmic reticulum (ER) to trigger a cytosolic Ca^{2+} increase. The thereby lowered ER-Ca^{2+} content has to be refilled to permit the next Ca^{2+} signal and to preserve the physiologic activity of the ER. This refilling process, termed store-operated Ca^{2+} entry (SOCE), is facilitated through the ER resident Ca^{2+} binding protein STIM1 (stromal interaction molecule 1) and the Ca^{2+} channel ORAI1. So far, SOCE was mainly investigated in non-excitable cells of the immune system although expression of STIM1 was also reported for excitable cells like neurons.

In the course of this thesis, we investigated the expression pattern of STIM1 and the closely related STIM2 in murine and human tissues and different cell types of the brain. Since we clearly detected STIM1 and 2 in neurons, we set out to investigate the role of SOCE on neuronal network activity and on pathological hyperexcitability as observed during epilepsy. We observed a clear participation of SOCE to neuronal excitability in these experiments and next decided to investigate the role of SOCE in cellular resistance against oxidative stress which plays a role in neurological diseases like epilepsy, Parkinson's or Alzheimer's disease as well as ischemia-reperfusion injuries observed after stroke.

First we studied resistance against oxidative stress in STIM1 wild type (WT) and knock out (KO) fibroblasts as a model for reduced SOCE capacity. STIM1 KO cells exhibited increased sensitivity towards endogenous oxidative stress which was diminished by expression of STIM1-YFP. We explained the enhanced sensitivity of STIM1 KO fibroblasts to oxidative stress by impaired adaption of mitochondrial metabolism and morphology to energy needs resulting in a pronounced basal oxidative stress level due to the absence of STIM1.

In the third study presented here, we switched to a more neuronal model, the murine hippocampal HT22 cell line. Unexpectedly, we observed a different effect of reduced SOCE activity in these cells compared to the results obtained in fibroblasts. HT22 cells do not rely on STIM1 for the regulation of oxidative stress resistance. Instead we observed a protective effect of reduced ORAI1 expression and disclosed ORAI1 to be the Ca^{2+} channel facilitating detrimental Ca^{2+} influx in the final phase of the cell death induced by oxidative stress.

We conclude that STIM1 and physiologic SOCE function are essential for neuronal excitability and impact on mitochondrial morphology and cellular energy production in fibroblasts but not in hippocampal HT22 cells. Instead we discovered ORAI1 to be the main Ca^{2+} entry channel in the course of the oxidative-stress induced cell death program in HT22 cells.

Zusammenfassung

Ca^{2+} Ionen sind an einer Vielzahl zellulärer Prozesse beteiligt und sind unverzichtbar für die zelluläre Signalübertragung. Nach Aktivierung vieler plasmamembrangebundener Rezeptoren wird Ca^{2+} aus dem Endoplasmatischen Retikulum (ER) freigesetzt, was die zytosoläre Ca^{2+}-Konzentration erhöht. Es ist wichtig, den dadurch verringerte Ca^{2+}-Gehalt des ERs wieder aufzufüllen, um die nächsten Ca^{2+}-Signale zu ermöglichen und die physiologische Funktion des ERs zu bewahren. Dieser Auffüllungsprozess wird als speichergesteuerter Ca^{2+}-Einstrom (store-operated Ca^{2+} entry, SOCE) bezeichnet und durch ein im ER lokalisiertes, Ca^{2+}-bindendes Protein namens STIM1 (stromal interaction molecule 1) und einen Ca^{2+}-Kanal namens ORAI1 ermöglicht. SOCE ist bisher in nicht-erregbaren Zellen des Immunsystems am besten untersucht, obwohl STIM1 Expression auch in erregbaren Zellen des Nervensystems beobachtet wurde.

In dieser Arbeit untersuchten wir das Expressionsmuster von STIM1 und dem nahe verwandten STIM2 in verschiedenen Geweben der Maus und des Menschen, sowie in verschiedenen Zelltypen des Hirns. Da STIM1 und 2 in Neuronen nachweisbar waren, untersuchten wir die Rolle von SOCE in neuronaler Netzwerkaktivität und in pathologischer Über-Erregbarkeit, wie sie in Epilepsie zu beobachten ist. Wir konnten eine klare Beteiligung von SOCE an neuronaler Erregbarkeit beobachten und entschlossen uns, im weiteren Verlauf dieser Arbeit, die Wirkung von SOCE auf das Zellüberleben während oxidativem Stress zu untersuchen, da dieser häufig beteiligt ist an neurologischen Erkrankungen wie z.B. Epilepsie, Alzheimer oder Parkinson und Schlaganfällen.

Als Model für reduzierte SOCE Aktivität untersuchten wir zunächst die Resistenz von STIM1 wildtyp (WT) und knockout (KO) Fibroblasten gegenüber oxidativem Stress. KO-Zellen zeigten eine erhöhte Sensitivität gegenüber endogenem oxidativen Stress, was durch die Expression von STIM1-YFP gemindert werden konnte. Diese erhöhte Sensitivität ließ sich dadurch erklären, dass die Anpassung von mitochondrialem Metabolismus und Morphologie an den Energiebedarf der Zelle in STIM1 KO Fibroblasten gestört ist, was zu einem erhöhten Maß an basalem oxidativen Stress durch Abwesenheit von STIM1 führt.

In der dritten, hier präsentierten Arbeit wechselten wir zu der murinen hippokampalen HT22 Zelllinie. Hier beobachteten wir durch reduzierte SOCE Aktivität einen von den Ergebnissen aus Fibroblasten abweichenden Effekt. HT22 sind für die Regulation der Resistenz gegenüber oxidativem Stress nicht auf STIM1 angewiesen. Stattdessen war ein protektiver Effekt durch verringerte ORAI1 Expression zu beobachten. Wir konnten ORAI1 als den entscheidenden Ca^{2+}-Kanal identifizieren, der für den verhängnisvollen Ca^{2+}-Einstrom im Zelltodprogramm, induziert durch oxidativen Stress, verantwortlich ist.

Zusammenfassend schließen wir, dass STIM1 und physiologische SOCE Aktivität für neuronale Erregbarkeit essentiell sind und die mitochondriale Morphologie sowie die zelluläre Energieproduktion in Fibroblasten aber nicht in HT22 beeinflussen. Stattdessen ist ORAI1 in HT22 der wichtigste Ca^{2+}-Kanal im Verlauf des durch oxidativen Stress induzierten Zelltodprogrammes.

Table of contents

Introduction **7**

Ca^{2+} signaling *7*
Neuronal Ca^{2+} signaling *7*
Store-operated Ca^{2+} entry *8*
Ca^{2+} and cell death *9*

Oxidative stress *10*
GSH system *11*
Oxidative glutamate toxicity *12*

Aims of the thesis **12**

Publications **13**

Store-operated calcium entry modulates neuronal network activity in a model of chronic epilepsy *13*

Stromal interaction molecule 1 (STIM1) is involved in the regulation of mitochondrial shape and bioenergetics and plays a role in oxidative stress *24*

The plasma membrane channel ORAI1 mediates detrimental calcium influx caused by endogenous oxidative stress *36*

Summary of the results **46**

Store-operated calcium entry modulates neuronal network activity in a model of chronic epilepsy *46*

Stromal interaction molecule 1 (STIM1) is involved in the regulation of mitochondrial shape and bioenergetics and plays a role in oxidative stress *46*

The plasma membrane channel ORAI1 mediates detrimental calcium influx caused by endogenous oxidative stress *47*

Discussion **48**

References **53**

Appendix **57**
Abbreviations *57*
List of publications *59*
Acknowledgement/Danksagung *61*
Declaration/Erklärung *63*

Introduction

Ca^{2+} signaling

Ca^{2+} ions are extremely important mediators of signaling in all kind of cells. Retaining the cytoplasmic Ca^{2+} concentration in the nanomolar range while high Ca^{2+} amounts are stored in the endoplasmic reticulum (ER) or located in the extracellular space enables the cell to quickly respond with elevations of the cytosolic-Ca^{2+} concentration in a spatiotemporal tightly controlled way to different stimuli like receptor activation or changes in plasma membrane potential. To render this possible, a considerable amount of energy in form of adenosine triphosphate (ATP) needs to be produced to tightly regulate the distribution of Ca^{2+} ions within the cell. Once a Ca^{2+} signal is triggered, the cytosol is flooded with Ca^{2+} within seconds, facilitating further downstream effects as diverse as muscle contraction, secretion, proliferation, apoptosis or even embryonic development of fertilized egg cells (1) (2).

Neuronal Ca^{2+} signaling

Besides Na^{+} and K^{+}, Ca^{2+} ions are indispensable for the physiological activity of excitable cells like neurons. Ca^{2+} signaling is critically involved in synaptic transmitter release and modifies the responsiveness of the neuron to prolonged stimulation through activation of Ca^{2+}-activated K^{+} channels, a process called adaptation. Also the hippocampal effects of long-term potentiation and depression underlying the processes of learning and memory are critically dependent on Ca^{2+} signaling events (3).
In order to generate cytosolic Ca^{2+} signals, a neuron can allow Ca^{2+} influx from the extracellular space through different types of plasma-membrane Ca^{2+} channels, classified by their mode of activation into voltage-dependent Ca^{2+} channels (VDCC) and ligand-gated Ca^{2+} channels (LGCC). VDCC are further subdivided into L-, N-, P-, Q, R- and T-type Ca^{2+} channels, depending on channel conductance, activation voltage, speed of inactivation and sensitivity to different drugs and toxins (4) (5) and their activation during an action potential for example induces pre-synaptic neurotransmitter release (3). LGCCs instead are largely independent from membrane potential but are gated by binding of their specific ligand. Prominent examples for LGCC are NMDA (N-Methyl-D-aspartate) and some types of AMPA (2-amino-3-(3-hydroxy-5-methyl-isoxazol-4-yl)propanoic acid) receptors which are located at the postsynaptic membrane and open in response to binding of the neurotransmitter glutamate (6) (7). Alternatively, through activation of G_q-protein coupled receptors like metabotropic glutamate receptors 1 and 5 (mGluR1 and mGluR5), Ca^{2+} can also be released from internal stores either through the generation of inositol 1,4,5-triphosphate (IP3), which binds and opens IP3 receptors 1-3 (IP3R1-3) in the ER membrane (8) (9) or through opening of ryanodine receptors, what can occur dependently or independently from a small IP3-induced cytosolic Ca^{2+} increase (10).

Considering these complex mechanisms for Ca^{2+} signaling in neurons it is not surprising that a dysfunction of one of these signaling modulators critically disturbs neuronal physiology leading to different neurological diseases like Parkinson's or Alzheimer's disease, stroke, amyotrophic lateral sclerosis, epilepsy or even schizophrenia (11).

Store-operated Ca^{2+} entry

Cytosolic Ca^{2+} signals can be evoked by G_q-coupled surface receptors, e.g. mGluR1 and mGluR5, or tyrosin-kinase-coupled receptors like B- and T-cell receptors, through the generation of IP3 and diacylglycerol (DAG) from phosphatidylinositol 4,5-bisphosphate (PIP2) by phospholipase C (PLC). IP3 quickly diffuses from its spot of generation at the plasma membrane to the ER membrane to bind and open IP3R1-3 thereby inducing Ca^{2+} release from the ER lumen and a sudden increase in cytosolic Ca^{2+} concentration. The depletion of the ER-Ca^{2+} content in turn activates plasma membrane channels called Ca^{2+}-release activated Ca^{2+} (CRAC) channels leading to store-operated Ca^{2+} entry (SOCE) (12) (13).

The mechanism of activation of these CRAC channels has been a subject of long lasting debates and discussions (14). One model explained the activation of CRAC channels in the plasma membrane in response to ER-Ca^{2+}-store depletion by direct coupling through the IP3R receptors (15). In contrast to this model, Randriamampita and Tsien described the existence of a diffusible messenger, called Ca^{2+} influx factor (CIF), which was released from the ER in response to store depletion and able to induce Ca^{2+} influx when applied to macrophages, astrocytoma cells and fibroblasts (16). This CIF was shown to activate Ca^{2+}-independent phospholipase A_2 ($iPLA_2$) which then in turn activated CRAC channels through generation of lysophospholipids (17).

The discussion about the different CRAC-activation models was suddenly interrupted in 2005, when stromal interaction molecule 1 (STIM1) was identified in an RNA interference (RNAi) screen as the main sensor of ER-Ca^{2+} content which activated Ca^{2+} influx via the plasma membrane in response to store depletion (18) (19). STIM1 is a single-transmembrane protein located in the ER membrane with a luminal EF hand sensing the Ca^{2+} content of the ER. Upon store depletion STIM1 clusters into punctae near the plasma membrane (20) and activates ORAI1 channels by direct binding to their N- and C-termini via its CRAC-activation domain (21). Mutation of the luminal EF-hand motif generates a constitutively active STIM1 that is located in punctae within close proximity to the plasma membrane, independently from ER-Ca^{2+} concentration (22) (23). In overexpression experiments ORAI1 alone remarkably inhibited SOCE whereas expression of STIM1 slightly increased Ca^{2+} entry induced by store depletion. Only co-expression of ORAI1 and STIM1 highly increased SOCE pointing out the importance of the correct stoichiometry between STIM1 and ORAI1 (24). Manjarres et al. identified the optimal ORAI1:STIM1 ratio showing the largest increase in SOCE being 1:1, a ratio of 4:1 still increased SOCE but less strongly than the 1:1 did and further increasing the ratio up to 10:1 inhibited SOCE. In addition to STIM1 and

ORAI1 also the sarcoplasmic/endoplasmic reticulum Ca^{2+} ATPase (SERCA) co-assembles into punctae induced by store depletion to permit quick shuttling of entering Ca^{2+} into the ER (25) (26).

Interestingly a regulatory function of STIM1 also on VDCC was described. Whereas STIM1 activates ORAI1 channels in response to store depletion it simultaneously binds the C-terminus of the L-type VDCC $Ca_V1.2$, which results in acute inhibition of depolarization-induced channel opening and subsequent internalization of the $Ca_V1.2$ (27) (28). $Ca_V1.2$ is widely expressed in excitable cells, amongst others in cells of the cortex, hippocampus and cerebellum (29). Thus, this interconnection between different Ca^{2+}-signaling pathways has to be kept in mind especially for the interpretation of Ca^{2+} signaling in neurons, where SOCE and VDCC-signaling co-exist.

Ca^{2+} and cell death

The link between Ca^{2+} and cell death is complex. One needs to distinguish the spontaneous and uncontrolled death of a cell induced by traumatic injury called necrosis from the programed cell death known as apoptosis which is dependent on the availability of ATP and proceeds in a very controlled way not only in response to irreversible stress or damage but also during normal development (30) (31). The main characteristics of apoptosis include cytosolic and nuclear condensation together with DNA fragmentation and membrane blebbing resulting in the formation of apoptotic bodies which can be eliminated by macrophages (32) (33). Two different ways to induce apoptosis are known, the extrinsic pathway, which is mediated by surface receptors and activated for example by cytotoxic lymphocytes, and the so called intrinsic pathway which is regulated by mitochondria and activated from within the cell in response to damage to cellular organelles (34).

During commitment of the extrinsic apoptosis pathway, CD95/FAS-receptor signaling provokes sustained Ca^{2+} release from the ER which is necessary for the induction of apoptosis (35). Typical for the intrinsic apoptosis pathway is an excess of mitochondrial Ca^{2+}, which induces swelling and subsequent rupture of the outer mitochondrial membrane followed by release of cytochrome c, a well-known mediator of apoptosis (34) (36). Also in the cytosol, Ca^{2+} can trigger or inhibit apoptosis by Ca^{2+}-dependent enzymes like the calpains, a family of cysteine proteases that include pro- and anti-apoptotic members (37) (38). Next to its role during induction of apoptosis, Ca^{2+} can also be recruited as a messenger during commitment of programmed cell death. The plasma membrane Ca^{2+} ATPase (PMCA) (39) (40) or the Na^+/Ca^{2+} transporter type 1 (NCX) (34) can both serve as substrates for caspases and cleavage results in inactivation and subsequent increase of cytosolic Ca^{2+} further accelerating the execution of cell death. Furthermore different studies suggest regulatory functions on cellular Ca^{2+} homeostasis for B-cell lymphoma 2 (BCL-2), an extensively studied inhibitor of apoptosis, and other pro- and antiapoptotic members of the BCL-2 family, e.g. BAX (Bcl-2–associated X protein), BAK (Bcl-2 homologous antagonist killer) and BCL-XL (BCL2-like 1) (41) (42) (43) (44).

As STIM1 and ORAI1 are important players in Ca^{2+} signaling, a link of these molecules to apoptosis appears possible and was demonstrated in different scenarios. First Chiu et al. observed an activation of STIM1 and concomitant SOCE in cervical epithelial cells in response to planting on soft substrate resulting in calpain activation and subsequent apoptosis. Inhibition of SOCE by siRNA mediated knock down of STIM1 increased survival of these cells on soft substrate (45). Also in different cancer cell lines, reduction of SOCE by downregulation of either ORAI1 or STIM1 transcripts resulted in increased resistance to apoptosis (46) (47). Contrarily, malignant melanoma cells were dependent on an intact SOCE machinery to sustain activation of protein kinase B, which phosphorylates AKT, a pro-survival factor. Disturbance of SOCE by knock down of STIM1 reduced the phosphorylation state of AKT underlining the importance of Ca^{2+} signaling for survival of these tumor cells (48). Also in glioblastoma cells SOCE was demonstrated to be important for cell survival and proliferation and reduction of SOCE induced apoptosis (49). Hawkins et al. identified a glutathionylation site at cysteine 56 of STIM1 which was glutathionylated in response to oxidative stress leading to constitutive activation of STIM1 independently from ER-Ca^{2+} store filling, what finally caused cell death (50). In contrast to this publication, Berna-Erro et al. observed no change in viability of cultured hippocampal neurons derived from STIM1 KO mice in comparison to WT controls after exposure to hypoxia (51).

Oxidative stress

In respiring cells, a continuous production of reactive oxygen species (ROS) at complex I (52) (53) and III (54) (55) of the mitochondrial electron transport chain together with minor sources of ROS like peroxisomes or nicotinamide-adenine dinucleotide phosphate (NADPH) oxidases (56) need to be balanced by detoxifying antioxidative mechanisms. An imbalance between the production and detoxification of ROS inevitably leads to the occurrence of a phenomenon called oxidative stress which is well known to be responsible for the process of aging and furthermore involved in development and progression of various diseases e.g. Parkinson's or Alzheimer's disease, myocardial infarction, stroke, rheumatoid arthritis, diabetes, amyotrophic lateral sclerosis or even schizophrenia (56) (57) (58).

The primary reactive oxygen species directly produced at the mitochondria is the superoxide anion ($O2^{\bullet-}$) from which other kinds of ROS like H_2O_2 or hydroxyl radicals ($^{\bullet}OH$) can be generated (59). These highly reactive compounds have the tendency to quickly oxidize other molecules like nucleic acids, proteins or lipids and can thereby cause serious damage in the worst case leading to cell death.

In order to detoxify these continuously produced ROS, a variety of antioxidative-defense mechanisms have evolved, including non-enzymatic antioxidants e.g. ascorbic acid, α-tocopherol or glutathione (GSH) or antioxidative enzymes like superoxide dismutase (SOD), which dismutates superoxide anions to H_2O_2 that subsequently is converted to O_2 and H_2O by catalase, or glutathione peroxidase, that detoxifies H_2O_2, with participation of GSH, to H_2O (60).

If these basal antioxidative-defense mechanisms are not sufficient to neutralize the endogenously produced ROS or additional oxidative stress is triggered by exposure to reactive chemicals, a signaling cascade is activated which induces expression of additional antioxidative-defense genes transcriptionally controlled by a cis-acting element termed ARE (antioxidant-response element) (61). The transcription factor which regulates ARE-dependent transcription is nuclear factor (erythroid-derived 2)-like 2 (NRF2). In resting conditions NRF2 is located in the cytosol and bound by kelch like-ECH-associated protein 1 (KEAP1) and Cullin 3, which mark NRF2 for degradation by the proteasomal system resulting in a very short half-life of NRF2 (62). If the level of oxidative stress increases, KEAP1 dissociates from NRF2, allowing translocation of NRF2 to the nucleus, where it binds AREs and initiates transcription of antioxidative-defense genes (63).

GSH system

GSH, a tripeptide composed of glutamate, cysteine and glycine, is one of the major antioxidants and the most abundant thiol of low molecular weight not only in animal but also in plant cells (64). It is synthesized in an ATP-dependent two-step reaction, with the first step being the rate-limiting reaction. First, glutamate is ligated to cysteine by the enzyme γ-glutamylcysteine ligase (GCL) and the emerging dipeptide γ-glutamylcysteine is then fused to glycine by the enzyme glutathione synthase resulting in the tripeptide GSH (64). Once generated in the cytosol, GSH can either be secreted to the extracellular space, transported into different cellular organelles like mitochondria or the nucleus, or fulfill its role as an antioxidant directly in the cytoplasm (65).

GSH can either directly detoxify ROS or act as a cofactor of ROS-scavenging enzymes, the glutathione peroxidases. In both reactions, the enzymatic or non-enzymatic detoxification of ROS, two GSH molecules are oxidized, building a covalent disulfide bond, resulting in a GSH disulfide molecule (GSSG). GSSG is continuously regenerated to GSH by the NADPH-dependent enzyme GSH reductase keeping the GSH/GSSG ratio as high as possible (64). Small changes in the redox status of the cell can significantly alter the GSH/GSSG ratio which influences cell fate into either a proliferating (reducing environment with higher GSH/GSSG ratio) or more differentiating (oxidizing environment with lower GSH/GSSG ratio) condition (66).

Next to its function as an antioxidant GSH is also involved in the regulation of protein activity. Dependent on the oxidation state of a cell, protein sulfhydryl groups can be activated by oxidation and serve as a target for GSH which forms a mixed disulfide. The resulting glutathionylation influences the activity of proteins like chaperones or cell cycle regulators (67). Recently, also STIM1 was shown to be glutathionylated in response to the redox state of the cell, what lead to Ca^{2+} entry independently of the ER- Ca^{2+} filling state (50).

Oxidative glutamate toxicity

The rate-limiting step during the synthesis of GSH is the ligation of glutamate to cysteine to form γ-glutamylcysteine. The substrate cysteine is the reduced form of cystine which is imported into the cell by system X_c^-, a cystine/glutamate antiporter. By application of millimolar amounts of glutamate to the culture medium this antiporter is blocked, cystine import is stopped and the cell runs short in cysteine which in turn leads to oxidative stress induced by GSH depletion (68).

The mouse hippocampal cell line HT22 serves as an excellent model for this oxidative glutamate toxicity as it lacks ionotropic glutamate receptors and remains therefore unaffected from excitotoxicity, a form of programmed cell death also induced by glutamate. Application of glutamate to the culture medium of HT22 induces a very well defined sequence of events which, after about 16 hours, results in cell death caused by oxidative stress. In the first hours, the level of GSH is continuously reduced, while the load of ROS slowly increases. When the GSH level drops below a certain threshold, 12-lipoxygenase (12-LOX) is activated which strongly enhances ROS production (69). In the final phase, soluble guanylyl cyclase (sGC) is activated which leads to the production of cyclic guanosinmonophosphate (cGMP) and opening of so far unknown Ca^{2+} channels. The resulting strong cytosolic Ca^{2+} rise eventually finalizes the cell death program (70).

Aims of the thesis

In the course of this study the role of store-operated Ca^{2+} entry for neuronal function was characterized. As nerve cells are particularly prone to oxidative stress-induced injury, and Ca^{2+} ions fulfill important functions herein, an effect of STIM1 and ORAI1 expression on oxidative stress resistance was hypothesized and investigated.

Publications

Store-operated calcium entry modulates neuronal network activity in a model of chronic epilepsy

Julius A. Steinbeck[1,2*], Nadine Henke[3*], Jessica Opatz[3], Joanna Gruszczyńska-Biegała[4], Lars Schneider[3], Stephan Theiss[3], Nadine Hamacher[3], Barbara Steinfarz[1], Stefan Golz[5], Oliver Brüstle[1], Jacek Kuźnicki[4] & Axel Methner[3]#

[1]Institute of Reconstructive Neurobiology, [2]Department of Neurology, University of Bonn, Sigmund-Freud-Str. 25, 53127 Bonn, Germany, [3]Department of Neurology, Heinrich Heine University Düsseldorf, Moorenstr. 5, 40225 Düsseldorf, Germany; [4]Laboratory of Neurodegeneration, International Institute of Molecular and Cell Biology, 4 Ks. Trojdena Street, 02-109 Warsaw, Poland, [5]Institute for Target Research, Bayer HealthCare AG, 42096 Wuppertal, Germany,
* equally contributed

The presented manuscript was published in the Journal of “Experimental Neurology” (71).

Contribution of Nadine Henke, shared first author:

Experimental design: 20%
Execution and analysis of experiments: 30%
Manuscript writing: 25%

Experimental Neurology 232 (2011) 185–194

Contents lists available at SciVerse ScienceDirect

Experimental Neurology

journal homepage: www.elsevier.com/locate/yexnr

Store-operated calcium entry modulates neuronal network activity in a model of chronic epilepsy

Julius A. Steinbeck [a,b,1], Nadine Henke [c,1], Jessica Opatz [c], Joanna Gruszczynska-Biegala [d], Lars Schneider [c], Stephan Theiss [c], Nadine Hamacher [c], Barbara Steinfarz [a], Stefan Golz [e], Oliver Brüstle [a], Jacek Kuznicki [d], Axel Methner [c,*]

[a] Institute of Reconstructive Neurobiology, University of Bonn, Sigmund-Freud-Str. 25, 53127 Bonn, Germany
[b] Department of Neurology, University of Bonn, Sigmund-Freud-Str. 25, 53127 Bonn, Germany
[c] Department of Neurology, Heinrich Heine University Düsseldorf, Moorenstr. 5, 40225 Düsseldorf, Germany
[d] Laboratory of Neurodegeneration, International Institute of Molecular and Cell Biology, 4 Ks. Trojdena Street, 02-109 Warsaw, Poland and Nencki Institute of Experimental Biology PAN, 3 Pastuer, 02-093 Warsaw, Poland
[e] Target Discovery Technologies, Bayer Pharma AG, 42096 Wuppertal, Germany

ARTICLE INFO

Article history:
Received 29 July 2011
Accepted 23 August 2011
Available online 30 August 2011

Keywords:
STIM1
STIM2
Epilepsy
Store-operated calcium entry
Network activity

ABSTRACT

Store-operated Ca^{2+} entry (SOCE) over the plasma membrane is activated by depletion of intracellular Ca^{2+} stores and has only recently been shown to play a role in CNS processes like synaptic plasticity. However, the direct effect of SOCE on the excitability of neuronal networks *in vitro* and *in vivo* has never been determined. We confirmed the presence of SOCE and the expression of the calcium sensors STIM1 and STIM2, which convey information about the calcium load of the stores to channel proteins at the plasma membrane, in neurons and astrocytes. Inhibition of SOCE by pharmacological agents 2-APB and ML-9 reduced the steady-state neuronal Ca^{2+} concentration, reduced network activity, and increased synchrony of primary neuronal cultures grown on multi-electrode arrays, which prompted us to elucidate the relative expression of STIM proteins in conditions of pathologic excitability. Both proteins were increased in brains of chronic epileptic rodents and strongly expressed in hippocampal specimens from medial temporal lobe epilepsy patients. Pharmacologic inhibition of SOCE in chronic epileptic hippocampal slices suppressed interictal spikes and rhythmized epileptic burst activity. Our results indicate that SOCE modulates the activity of neuronal networks *in vitro* and *in vivo* and delineates SOCE as a potential drug target.

Introduction

Ca^{2+} transients control a vast array of cellular functions from short-term responses such as contraction and secretion to long-term regulation of cell growth and proliferation. Cytosolic Ca^{2+} increases in response to activation of cell-surface receptors and subsequent generation of the second messenger inositol 1,4,5-trisphosphate (IP3), which interacts with its receptors (IP3R1-3) on the membrane of the endoplasmic reticulum (ER). Opening of these IP3R Ca^{2+} channels releases luminally-stored Ca^{2+} from the ER. Depletion of ER Ca^{2+} stores results in activation of store-operated channels (SOCs) at the plasma membrane, mediating capacitative or store-operated Ca^{2+} entry (SOCE) from the extracellular space followed by removal of cytosolic Ca^{2+} and replenishment of luminal Ca^{2+} through sarcoplasmic/endoplasmic reticulum Ca^{2+}-ATPases (SERCA). Based on electrophysiological and molecular properties, two main types of SOCs were proposed: the highly Ca^{2+}-selective I_{CRAC} currents mediated by the ORAI family of proteins carrying the highly Ca^{2+}-selective I_{CRAC} currents (Feske et al., 2006; Vig et al., 2006), and non-selective Ca^{2+} permeable TRPC (C-type transient receptor potential) channels (Huang et al., 2006). The Ca^{2+} sensor that conveys information about the Ca^{2+} load of the ER lumen to SOCs is stromal interaction molecule 1 (STIM1). STIM1 senses luminal Ca^{2+} concentration via an amino-terminal EF hand Ca^{2+}-binding domain and in response to store depletion rearranges into punctate structures close to

Abbreviations: SOCE, Store-operated calcium entry; STIM, Stromal interaction molecule; 2-APB, 2-aminoethoxydiphenyl borate; IP3, Inositol 1,4,5-trisphosphate; IP3R, IP3 receptor; ER, Endoplasmic reticulum; SOC, Store-operated channels; ICRAC, Calcium-release activated calcium current; TRPC, C-type transient receptor potential; NMDA, *N*-Methyl-D-aspartate; PDL, Poly-D-lysine; MEA, Multi-electrode array; DMEM, Dulbecco's Modified Eagle Medium; FBS, Fetal bovine serum; FAM, Fluorescein amidite; TAMRA, 5-carboxytetramethylrhodamine; HPRT, Hypoxanthine phosphoribosyltransferase; GAPDH, Glyceraldehyde-3-phosphate dehydrogenase; RIPA, Radioimmunoprecipitation assay buffer; PBS-T, Phosphate buffered saline-tween; HBSS, Hanks' Balanced Salt solution; EGTA, Ethylene glycol-bis(2-aminoethylether)-*N,N,N′,N′*-tetraacetic acid; PFA, Paraformaldehyde; aCSF, Artificial cerebrospinal fluid; FCS, Fetal calf serum; PBS, Phosphate buffered saline; GFAP, Glial fibrillary acidic protein; ANOVA, Analysis of variance; DG, Dentate gyrus; KA, Kainic acid; MEF, Mouse embryonic fibroblast; TG, Thapsigargin; CTRL, Control; SE, Status epilepticus; WT, Wild type; KO, Knock out.

* Corresponding author at: Dept. of Neurology, Heinrich Heine Universität Düsseldorf, Moorenstr. 5, 40225 Düsseldorf, Germany. Fax: +49 40 42803 5101.
E-mail address: axel.methner@gmail.com (A. Methner).
[1] Equally contributed.

0014-4886/$ – see front matter © 2011 Elsevier Inc. All rights reserved.
doi:10.1016/j.expneurol.2011.08.022

the plasma membrane while still remaining in the ER. STIM1 then activates members of the ORAI family of Ca^{2+}-influx channels through direct interaction (Liou et al., 2005; Park et al., 2009; Roos et al., 2005), resulting in Ca^{2+} entry by I_{CRAC} into the cell. As a third element SERCA was shown to co-assemble into STIM1-ORAI1 punctae facilitating the quick shuttling of entering Ca^{2+} into the ER (Manjarrés et al., 2010). In contrast to STIM1, the function of STIM2 is still less clear. STIM2 has been proposed to act as an important sensor of basal ER Ca^{2+} levels and was claimed to be the main regulator of resting ER Ca^{2+} levels in non-excitable HeLa cells (Brandman et al., 2007) and in neurons (Gruszczynska-Biegala et al., 2011).

The role of SOCE and specifically the ER Ca^{2+} sensor STIM1 is best defined in non-excitable cells like immune cells, where it mediates rapid responses such as mast cell degranulation as well as long-term responses that involve new gene transcription (Feske, 2007). However, some effort has been made to elucidate the role of STIM proteins and SOCE also in excitable cells, especially neurons. STIM1 is expressed in cultured neurons and in brain sections with the most prominent expression in cell bodies and dendrites of pyramidal neurons and in Purkinje and granule neurons of the cerebellum (Klejman et al., 2009). STIM1 expression increases during *in vitro* differentiation to relatively high and stable levels in mature neuronal cultures and was found to be present in fractions enriched for postsynaptic densities, suggesting that it may function at or near synapses (Keil et al., 2010). STIM1 and Orai1 were also confirmed in sensory neurons at both the transcript and protein levels (Gemes et al., 2011). Others hardly detected any STIM1 mRNA in pure primary hippocampal neurons of mice isolated by laser capture microscopy and obtained only very weak STIM1 signal from brain lysates in immunoblot analyses (Berna-Erro et al., 2009) and suggested that STIM2 is the main regulator of SOCE in the brain. However, in a parallel work, we compared absolute copy numbers of STIM1 and STIM2 mRNA in hippocampal neurons and showed that STIM2 transcripts are only about twofold more abundant than STIM1 in laser-dissected hippocampal neurons (Gruszczynska-Biegala et al., 2011).

In summary, it appears clear that STIM proteins are present in the brain whereas their role in neuronal function is still uncertain. Blocking of SOCE with Lanthanum attenuated spontaneous Ca^{2+} transients in synaptic boutons, which are important for short-term synaptic plasticity and may also contribute to long-term plasticity (Emptage et al., 2001). Inhibition of SOCE with 2-aminoethoxydiphenyl borate (2-APB) and SKF-96365 in hippocampal slice preparations accelerated the decay of NMDA-induced Ca^{2+} transients without affecting their peak amplitude, and attenuated tetanus-induced dendritic Ca^{2+} accumulation and long-term potentiation at Schaffer collateral-CA1 synapses (Baba et al., 2003) suggesting a link between SOCE and neuroplasticity. Finally, a SOCE influx pathway was also demonstrated in bag cell neurons of *Aplysia* (Kachoei et al., 2006) and in flight neurons of *Drosophila melanogaster* (Agrawal et al., 2010). Blockade of SOCE increased neuronal excitability in dorsal root ganglion neurons (Gemes et al., 2011). Recently, STIM1 was shown to directly suppress depolarization-induced opening of the voltage-gated Ca^{2+} channel $Ca_V1.2$ by binding to the C terminus of this channel, which led to acute inhibition of gating and long-term internalization of the channel from the membrane (Park et al., 2010; Wang et al., 2010).

In this contribution, we tried to pharmacologically elucidate the function of SOCE in the nervous system by the use of dissociated cortical cultures grown on multi-electrode arrays (Otto et al., 2003), which allows a highly sensitive and reproducible assessment of network activity. These data hinted to a role of SOCE in network activity, which is an important determinant of epilepsy. We therefore studied the expression of STIM1 and STIM2 in tissues from chronic epileptic rats and humans and the function of SOCE in a model of chronic epileptiform activity in organotypic hippocampal slice cultures. These experiments showed that STIM proteins are upregulated in conditions of chronic excitability and suggested that SOCE modulates the activity of neuronal networks, which delineates SOCE as a potential drug target in the treatment of chronic epilepsy.

Materials and methods

Cell culture

For the analysis of network activity, cryopreserved primary dissociated cortical cultures of the embryonic rat (embryonic day 18, E18, QBM Cell Science) were employed (Otto et al., 2003). After thawing, the cells were plated at a final density of 10^5 cells on PDL-/laminin-precoated MEAs or coverslips. Neuronal cultures were incubated in a humidified atmosphere (5% CO_2/95% air) at 37 °C. For analysis of STIM1 expression, freshly prepared pure primary embryonic cortical neurons (embryonic day 18, E18) and postnatal astrocytes (postnatal day 0/1, P0/1) were plated on PDL-/laminin-coated or PDL only-coated coverslips. For preparation of astrocytes, P0-1 Wistar rat pups were anesthetized and decapitated, the brain was removed and the neocortex dissected for each brain hemisphere sparing the hippocampi. Meninges were removed and tissue fragments were crudely fragmented. Cell separation was achieved by trituration and by filtration through sterile nylon gauze with a pore size of 60 μm. Astrocytes were cultivated in presence of DMEM supplemented with 10% FBS in a humidified atmosphere (10% CO_2/95% air) at 37 °C with medium renewal every 2–4 days. For removal of non-astroglial contaminations, confluent astrocyte cultures were incubated on a shaker over night, followed by medium renewal. Pure astrocyte cultures were cultivated in the presence of serum-free, chemically defined medium for the generation of astrocyte-conditioned medium. For the preparation of cortical neurons, E18 Wistar rat pups were decapitated, the brain removed, and neocortex tissue prepared as described for the preparation of astrocytes. Cell separation was achieved by trypsinizing the tissue, followed by trituration and by filtration through sterile nylon gauze with a pore size of 30 μm. Cortical neurons were cultivated in the presence of astrocyte-conditioned medium in a humidified atmosphere (10% CO_2/95% air) at 37 °C.

Extracellular microelectrode recordings and signal analysis

Extracellular microelectrode recordings and signal analysis were performed as described (Otto et al., 2003). Network activity was recorded on MEAs (Multi Channel Systems) with 64 titanium nitride electrodes (30 μm diameter and 200 μm spacing) at 37 °C using sterile conditions. Signals from all 64 electrodes were simultaneously sampled at 25 kHz, visualized and stored using the standard software MC-Rack (Multi Channel Systems). Spike and burst detection was performed offline using a specialized software (SPANNER 2.0, Result, Germany).

Whole body panel

For relative quantitation of STIM1 and STIM2 mRNA levels in human tissues, a TaqMan™ real-time PCR assay was employed on a 7900 HT Sequence Detection system (Applied Biosystems) according to the manufacturer's protocols. For first strand cDNA synthesis, 85 μg of total RNA was incubated for 1.5 h at 37 °C with 2 U/μl Omniscript reverse transcriptase (Qiagen) in the supplied buffer plus 9.5 μM random hexamer primer, 0.5 mM per dNTP, and 3000 U RnaseOut (Invitrogen) in a final volume of 680 μl. The resulting cDNA was diluted 1:10 with water and directly used in PCR (5 μl per reaction). PCR primers and probes were: STIM1 forward: 5′-CTGACGGAGCCACAGCAT; reverse: 5′-CACTCATGTGGAGGGAGGAC, FAM™/TAMRA™-labeled probe 5′-TCTCAGAGGGATTTGACCCATTCCG, and STIM2 forward: 5′-ACTGGCTCTGCCGCAACT; reverse: 5′-GCATGGTGGACTCAGTGACA, probe 5′-ATAGCCCGGCGCTCATGACAGAT. The real-time PCR thermal protocol was set to 2 min at 50 °C, followed by 10 min at 95 °C, followed by 40 cycles of 15 s at 95 °C and 1 min at 60 °C. To normalize the amount of cDNA per assay, the expression of reference genes hypoxanthine phosphoribosyltransferase, gapdh, and

β-actin was measured in parallel assays. Relative expression was calculated using normalized expression values.

Immunoblotting

For immunoblot analysis, cells were harvested and directly lysed in RIPA buffer containing Complete Mini Protease Inhibitor Cocktail (ROCHE). Protein concentrations were determined using the bicinchoninic acid assay protein quantitation kit from Interchim and for each sample 50 μg of total protein were loaded into the wells of a NuPAGE Novex 4–12% Bis-Tris Mini Gel (Invitrogen). Proteins were blotted onto a nitrocellulose membrane using the iBlot Gel Transfer device (Invitrogen) and successful blotting was verified by staining with Ponceau S. The membrane was blocked with 3% milk in phosphate buffered saline with 0.5% Tween-20 (PBS-T) for 1 h at room temperature with gentle shaking. Primary antibodies were diluted in 3% milk in PBS-T for incubation on the membrane at 4 °C with light shaking over night. Antibodies were used as follows: mouse anti-GOK/STIM1 (#G7210) from BD Bioscience was diluted 1:250, rabbit anti-GAPDH (#2118) from Cell Signaling 1:2500 and rabbit anti-STIM2 (#4123) from ProSci 1:1000. After washing with PBS-T three times the membrane was placed into secondary antibody solution and incubated at room temperature for 1 h in the dark. IRDye 800CW Goat Anti-Mouse IgG and IRDye 680 Goat Anti-Rabbit IgG were diluted 1:20000 in 3% milk in PBS-T. Afterwards the membrane was washed in PBS-T three times and scanned on a Licor Odyssey Infrared Imaging System.

Real-time PCR analysis

Total RNA of primary astrocytes and neurons was isolated with the RNeasy Mini Kit (Qiagen) and transcribed into cDNA using the High-Capacity cDNA Reverse Transcription Kit from Applied Biosystems. Quantitative PCR was performed on an ABI 7500 real time cycler using TaqMan universal PCR Mastermix (ABI) and different primer-probe sets in a final reaction volume of 20 μl. As endogenous control served the hypoxanthin-phosphoribosyltransferase (HPRT) gene amplified with individually designed primers and a FAM/TAMRA probe all synthesized by MWG-Biotech. All the other transcripts were amplified by primer-probe sets of the Universal probe library from Roche. Probes were FAM/dark-quencher labeled and obtained from Roche and primers were also synthesized by MWG-Biotech.

SOCE and agents

Pure primary cortical astrocytes or neurons, grown on cover-slips coated with poly-D-lysine or poly-D-lysine with laminin, were incubated for 30 min with 1 μM Fura-2 acetoxymethyl ester (Molecular Probes) in HBSS (Gibco) at 37 °C in an atmosphere of 5% CO_2. Cover slips were washed twice with HBSS and placed into a flow chamber. Calcium imaging was done on an Olympus IX81 fluorescence microscope with the cell^R imaging software. Every 5 s two pictures were taken (excitation wavelength 340 and 380 nm) and the ratio of both was calculated for each single cell. During measurement the HBSS buffer was changed to EGTA buffer (HBSS containing 1 μM Thapsigargin (Molecular Probes), 0.5 mM EGTA, 2 g/l Glucose and 20 mM HEPES (Gibco) without Ca^{2+}) after 6 min and back to HBSS buffer containing Ca^{2+} again after another 6 min. If not indicated differently, chemicals were obtained from Sigma.

In vivo experimental epilepsy

C57Bl6 mice were subjected to a pilocarpine-induced status epilepticus (SE), terminated with diazepam after 40 min. After the development of chronic seizures (4 weeks after SE) animals were transcardially perfused using 4% PFA, the brain removed, cryopreserved in 30% sucrose and cut into 30 μm cryosections.

In vitro experimental epilepsy

Horizontal hippocampal slices (400 μm) containing the hippocampus, entorhinal cortex, and adjacent areas of the temporal cortex were prepared from 9-day-old Wistar rats (Charles River) and cultured in interphase conditions in a humidified 5% CO_2 atmosphere at 35 °C. Cultures were started in horse serum-containing medium, which was gradually replaced until day 5 in culture by a serum-free, defined solution based on DMEM–F12 and including the N2 and B27 supplements (Cytogen) (Benninger et al., 2003; Opitz et al., 2007). On day 6 in culture 3 μM kainic acid (Sigma-Aldrich) was added for 48 h. More than 90% of slices cultured under these conditions revealed a remarkable preservation of the hippocampal architecture including the preservation of the major neuronal subpopulations. The application of kainic acid induced a mild gliosis as well as mossy fiber sprouting as a neuropathological hallmark of epilepsy (data not shown).

Electrophysiology

For extracellular recordings one slice at a time was transferred to a recording chamber and continuously superfused with aCSF at 1–2 ml/min. This aCSF contained (in mM) 125 NaCl, 5 KCl, 1.25 NaH_2PO_4, 2 $CaCl_2$, 1 $MgCl_2$, 25 $NaHCO_3$, and 25 D-glucose (gassed with 95% O2/5% CO_2, pH 7.4, 300–305 mosmol/kg). Recordings were performed at ambient temperature. The dentate gyrus was visualized using an upright microscope equipped with infrared differential interference contrast and 5× objective (Zeiss). For recordings an aCSF-filled glass microelectrode was placed into the granule cell layer of the dentate gyrus at a depth of 40–100 μm. Signals were amplified 100× and filtered at 2 kHz (EXT 10-2F, NPI), digitized at 20 kHz and recorded using pClamp 10 software (Molecular Devices). Field excitatory postsynaptic potentials could be recorded in the dentate gyrus for at least 3 weeks after the application of kainic acid, confirming the functional integrity of the preparation. All electrophysiological recordings were analyzed using Clampfit 9 (Axon Instruments) and Microsoft Excel.

Medial temporal lobe epilepsy specimen

Three specimens from patients suffering from medial temporal lobe epilepsy were obtained from Albert Becker (Dept. of Neuropathology, University of Bonn) after routine selective hippocampectomy diagnosed as hippocampal sclerosis Wyler IV. The local ethics committee approved the use of the material; all patients provided written informed consent. Samples of human hippocampi were fixed for 30 min in 4% PFA and cut into 20 μm cryosections.

Immunohistochemistry

Sections were digested for antigen retrieval with pepsin (Dako, 100 mg/ml in 0.2 N HCl) and incubated with primary and secondary antibodies in blocking solution containing 8% FCS, 0.3% Triton X-100 in PBS for 16 and 4 h, respectively. We applied mouse IgG monoclonal antibodies to Stim1, (1:75 Abnova #H00006786-M01) and neuronal nuclei (1:50, Chemicon) as well as rabbit polyclonal antibodies to Stim2 (1:100 Cell Signaling #4917) and GFAP (DAKO; 1:800). All of the antigens were visualized using corresponding Cy3- and Cy5-conjugated goat secondary antibodies (Jackson). All immunohistochemical stainings were observed on a Zeiss Axioimager upright fluorescence microscope equipped with the apotome technology to reconstruct optical sections. For comparison of fluorescence intensities chronic epileptic and control hippocampi were always stained in parallel and imaged using identical exposure times and post acquisition image processing.

Statistical analysis

Data were summarized as mean ± S.E.M. and the statistical significance assessed using two-tailed *t*-tests or analysis of variance (ANOVA) with Tukey's Multiple Comparison Test as indicated.

Results

STIM1 and STIM2 are expressed in the murine and human nervous system

We first set out to investigate the relative expression of STIM1 and STIM2 in the murine nervous system by comparing the protein abundance in mouse tissues using immunoblotting with specific antibodies and normalization to the expression of glycerin-aldehyde-3-phosphate dehydrogenase (GAPDH). The specificity of the antibodies was shown by the use of mouse embryonic fibroblasts derived from STIM1 respectively STIM2-deficient mice. This quantification revealed a prominent expression of both STIM1 and STIM2 at intermediate levels in the cerebrum and to a lesser extent in cerebellum and even lower in the spinal cord (Fig. 1A). Both proteins were most prominently expressed in liver and lung, STIM1 also showed a strong expression in the spleen, which harbors a large amount of immune cells where STIM1 expression and function is best described. These data suggest that STIM1 and STIM2 are to a significant amount expressed in the murine nervous system.

We then analyzed *STIM1* and *STIM2* expression in a variety of human tissues using quantitative RT-PCR. In contrast to mouse tissue, *STIM1* turned out to be most prominently expressed in the excitatory tissues of CNS and skeletal muscle and not in spleen (Fig. 1B). Within the human brain, we observed the highest expression level in the cortex and hippocampus, both regions where a large amount of neurons prevail (Fig. 1C). *STIM2* expression, in contrast, was highest in the ovary

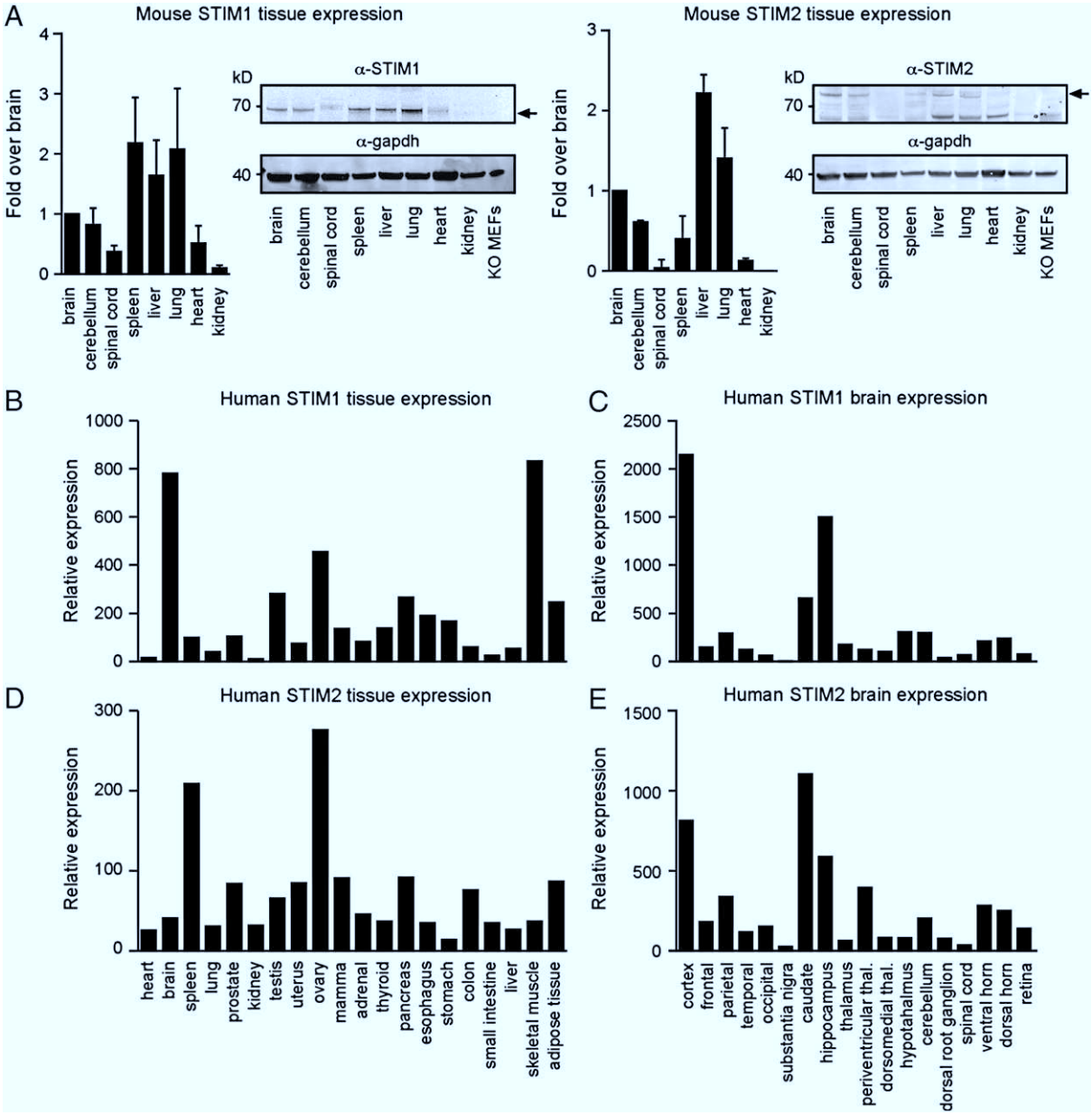

Fig. 1. STIM1 and STIM2 are expressed in the murine and human nervous system. A) Relative abundance of STIM1 and STIM2 protein in mouse tissues as quantified by immunoblotting using specific antisera demonstrated by lack of signal in KO MEFs. GAPDH served as loading control; size is indicated. Bar graphs represent the mean ± SEM from densitometric analysis of three independent blots. B-D) Relative amount of *STIM1* and *STIM2* mRNA in human tissues measured by quantitative real-time PCR normalized to the expression of housekeeping genes hypoxanthine phosphoribosyltransferase (*HPRT*), *GAPDH*, and β-actin.

and spleen with brain showing a rather low expression level (Fig. 1D). Within the human brain, the highest expression level was found in the cortex and hippocampus, similar to *STIM1* (Fig. 1E). These data suggest significant differences between mice and humans in regard to the relative expression levels of STIM1 and STIM2.

STIM1 is predominantly expressed in primary astrocytes and STIM2 in neurons

We then determined the relative expression of STIM proteins in the two main cell types present in the central nervous system by investigating their abundance in primary cultures containing only astrocytes or neurons. Cortical neurons were generated from embryonic day 18 rats and astrocytes from postnatal rats and were characterized by immunocytochemistry using β-tubulin III for neurons and GFAP (glial fibrillary acidic protein) for astrocytes (not shown). Both cultures contained STIM1 and STIM2 as shown by immunoblotting (Fig. 2A). To quantitate the relative expression, we used quantitative RT-PCR using *GFAP* and β-tubulin III as controls showing an approximately 1.7-fold increased expression of *STIM1* in astrocytes over neurons, whereas *STIM2* was increased 1.9-fold in neurons (Fig. 2C) in line with a recent report (Gruszczynska-Biegala et al., 2011).

Inhibition of SOCE decreases steady-state intracellular Ca^{2+} in primary neurons but not in astrocytes

We next studied the effect of ML-9, which was shown to inhibit SOCE and the I_{CRAC} current through inhibition of punctae formation (Smyth et al., 2008) on steady-state intracellular Ca^{2+} and SOCE using Fura-2AM Ca^{2+} imaging of single cortical rat neurons or astrocytes. ML-9 is effective in cells of the nervous system as it was previously shown to inhibit thapsigargin-mediated translocation of STIM1 and STIM2 to membrane fractions in neurons (Gruszczynska-Biegala et al., 2011). Our analysis demonstrated several profound differences between the two cell types. Resting Ca^{2+} levels were much higher in neurons than in astrocytes. In neurons, removal of extracellular Ca^{2+} with EGTA and addition of the SERCA inhibitor thapsigargin led to an immediate reduction in intracellular $[Ca^{2+}]$ followed by a small transient increase. Astrocytes, in contrast, reacted with a Ca^{2+} peak and a subsequent increase in cytosolic $[Ca^{2+}]$ in response to thapsigargin in EGTA (Fig. 3A black lines). The application of ML-9 resulted in a strong decrease in cytosolic $[Ca^{2+}]$ in the neurons, whereas astrocytes showed an increase in cytosolic $[Ca^{2+}]$. Such an increase in intracellular $[Ca^{2+}]$ was observed in previous reports (Norwood et al., 2000; Smyth et al., 2008) and attributed to release of Ca^{2+} from intracellular stores by ML-9. In neurons, ML-9 greatly attenuated the thapsigargin-releasable Ca^{2+} increase, which was not evident in astrocytes. Only in astrocytes, ML-9 led to a sharp decline in intracellular $[Ca^{2+}]$, when extracellular Ca^{2+} was removed with EGTA and SERCA pumps inhibited with thapsigargin (Fig. 3A). Also after re-addition of extracellular Ca^{2+}, astrocytes exhibited a much stronger store-operated Ca^{2+} entry as compared to neurons. ML-9 had a much stronger effect on this Ca^{2+} influx, where it blocked 76% of Ca^{2+} influx in astrocytes and 36% in neurons, indicating that some Ca^{2+} entry may occur through ML-9 insensitive channels particularly in neurons (Fig. 3B).

In summary, these results suggest that neurons and astrocytes differ dramatically in the regulation of the intracellular Ca^{2+} homeostasis and particularly SOCE. In neurons, SOCE (or rather ML-9-inhibitable Ca^{2+} influx) seems to be involved in the maintenance of steady-state Ca^{2+}, whereas astrocytes rather behave like non-excitable cells.

Inhibition of SOCE dampens network activity of primary dissociated cortical cultures grown on multi-electrode arrays

Multi-electrode arrays (MEAs) allow a highly sensitive and reproducible assessment of network activity by culturing dissociated cortical cells directly "on chip" (Fig. 4A). In these cultures, spontaneous electrical activity and signal propagation of evolving neuronal networks can be observed non-invasively in real time at 64 electrodes embedded into the chip. After 3 weeks *in vitro*, networks exhibit regular bursting

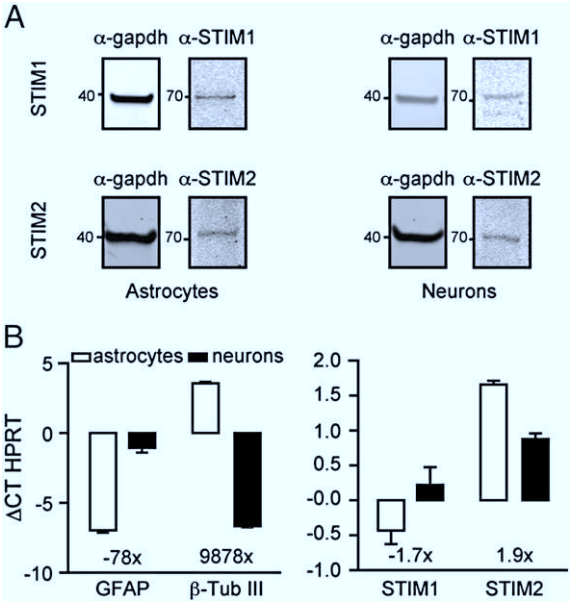

Fig. 2. STIM1 is predominantly expressed in primary astrocytes and STIM2 in neurons. A) STIM1 and STIM2 immunoblots showing expression in pure astrocytic and pure neuronal cultures. GAPDH served as loading control; size is indicated. B) Relative expression of *STIM1* and *STIM2* mRNA in these cultures shown by quantitative real-time PCR using the ΔCT method and *HPRT* as housekeeping control. Fold differences are shown below. Expression of *GFAP* and β-tubulin III served as controls to demonstrate the purity of the cultured cells.

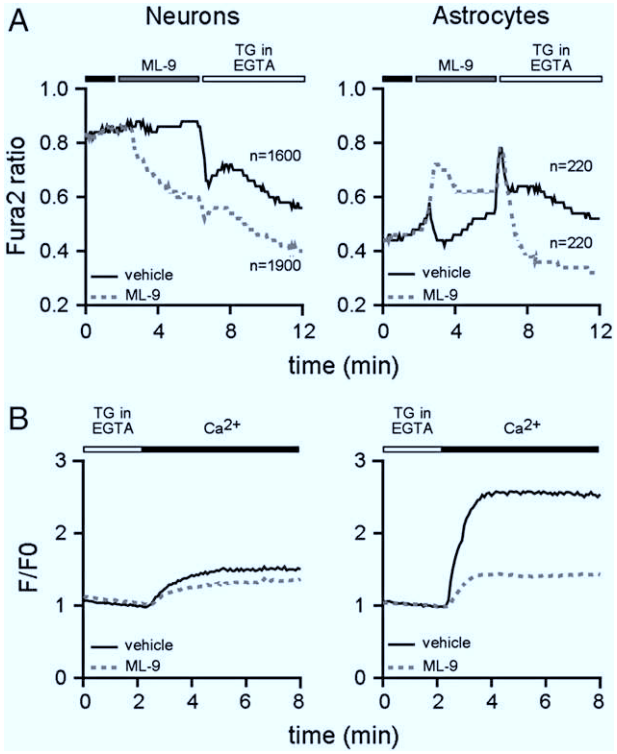

Fig. 3. Inhibition of SOCE decreases steady-state intracellular Ca^{2+} in primary neurons but not in astrocytes. Pure primary neurons or astrocytes were obtained from embryonic rats at E18 and cultured *in vitro* for 10 days. Cytosolic Ca^{2+} was measured as Fura-2 ratio in response to A) 50 μM ML-9 and 1 μM thapsigargin (TG) in the absence of extracellular Ca^{2+} (EGTA) and B) after re-addition of extracellular Ca^{2+}.

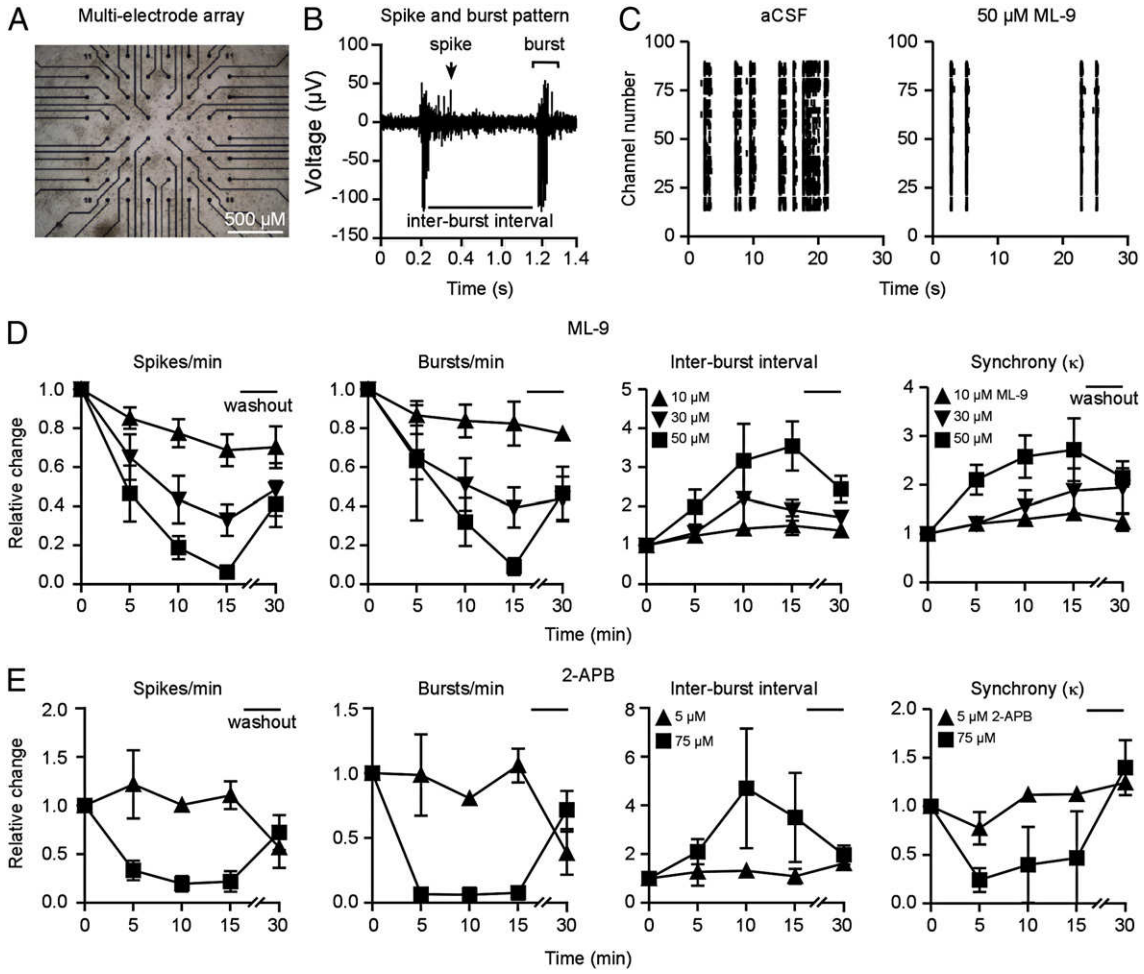

Fig. 4. Inhibition of SOCE dampens network activity of primary dissociated cortical cultures grown on multi-electrode arrays. A) Dissociated cortical cultures were grown on multi-electrode arrays and visualized by phase-contrast microscopy. Black discs correspond to electrodes. B) Typical trace recorded from one MEA-electrode showing the parameters used for statistical analysis. C) Spike raster plot of spontaneously active cryopreserved cortical neurons on one MEA in artificial CSF (aCSF) or 50 µM ML-9. Each bar represents one spike; electrode numbers are displayed on the vertical axis. The network exhibits correlated burst activity across several electrodes, which is dampened and synchronized by ML-9. D) Concentration- and time-dependent effect of ML-9 and E) 2-APB on the amount of spikes and bursts per minute as well as the network activity using Cohen's kappa as measure of synchrony of the activity on all 64 electrodes on the chip. Each data point corresponds to the mean ± SEM of at least three independent experiments. The horizontal bar indicates washout after 18 min.

activity consisting of single spikes or bursts, which can be measured quantitatively by the spike and burst rate per minute and the inter-burst interval (Fig. 4B). This technique allows highly sensitive and reproducible measurements of concentration-dependent effects on neuronal network activity (Gramowski et al., 2004; Johnstone et al., 2010).

Mature neuronal cultures derived from dissociated cortical cells exhibited highly synchronous network activity on MEAs (Fig. 4C left panel). ML-9 reversibly reduced spike and burst rate in a concentration-dependent manner, however retaining the burst structure of network activity at increased inter-burst intervals. Reduced network activity induced by ML-9 occurred in fewer but more regular, shorter bursts with fewer spikes per burst and fewer irregular spikes between bursts, thus leading to increased synchrony shown by an increased kappa value (Figs. 4C and D). We repeated these measurements with 2-APB, probably the most extensively utilized SOCE inhibitor, which was first described as a membrane-permeable inhibitor of the inositol 1,4,5-trisphosphate receptor. A low concentration of 5 µM 2-APB had no significant effect on neuronal network activity, but addition of 75 µM 2-APB reversibly reduced spike and burst rate similar to ML-9. However, 75 µM of 2-APB effectively suppressed nearly all neuronal bursting activity and rather induced a transition to sparse single spike firing—a network state with reduced synchrony suggesting insufficient excitatory synaptic transmission for bursting induced by 2-APB at this concentration (Fig. 4E). For both substances, all effects were quickly reversed after washout of the applied substances. We conclude that inhibition of SOCE with two independent and different well-characterized agents resulted in a profound reduction of neuronal network activity, albeit with different network burst behavior.

STIM1 and STIM2 levels are increased in the chronic epileptic hippocampus

The effect of SOCE inhibition by 2-APB and ML-9, which both reduced and partly synchronized network activity of primary cultures grown on multi-electrode arrays, suggested a role for SOCE in neuronal network activity. This prompted us to investigate the abundance of both proteins in pilocarpine-induced chronic epilepsy, an *in-vivo* model for increased neuronal network activity. Pilocarpine induces a single episode of status epilepticus, which then triggers a progressive structural and functional neuronal reorganization associated with the emergence of recurrent unprovoked seizures. This is accompanied by the conversion of hippocampal pyramidal neurons from regular firing, which is the predominant spiking mode in normal conditions (Azouz et al., 1996), to burst firing a few days after status epilepticus (Sanabria et al., 2001). Spontaneously bursting pyramidal cells can recruit the entire CA1 population of pyramidal cells into synchronized discharges (Sanabria et al., 2001). The role of SOCE and STIM1 in particular has not been studied in this model before.

We examined the expression of STIM1 and STIM2 in the hippocampal subfields of chronic epileptic mice and controls using immunohistochemistry. We observed a considerable upregulation of mainly perinuclear STIM1 in all three major hippocampal neuronal layers (dentate gyrus, CA1 and CA3, Fig. 5A). The upregulation of STIM1 was also evident in immunoblots at least for the dentate gyrus, whereas only very little STIM1 was present in the CA1 and CA3 regions rendering quantification impossible (Fig. 5A insert). The same upregulation was evident for perinuclear and nuclear STIM2, which was expressed in all hippocampal neuronal layers and upregulated in the chronic epileptic hippocampus as compared to control tissue (Fig. 5B).

STIM1 and STIM2 are highly expressed in a hippocampal specimen from a patient with medial temporal lobe epilepsy

To verify the expression of STIM1 and STIM2 in the human hippocampus under conditions of pathologic hyperexcitability, we then examined hippocampal specimen from patients undergoing hippocampectomy, diagnosed as Ammon's horn sclerosis °IV according to Wyler. Immunohistochemical analysis revealed a strong expression of STIM1 and STIM2 by neuronal cells in the human epileptic dentate gyrus and CA1 (Fig. 6). Importantly, STIM1 immunoreactivity extended far into neuronal processes compatible with a juxta-membranous localization of the protein, which is necessary for Ca^{2+} influx. Unfortunately, immunohistochemistry performed on an autopsy specimen of control patients did not show any specific staining, possibly due to rapid protein turnover (Klosen et al., 1993).

Inhibition of store-operated Ca^{2+} entry rhythmizes burst activity in epileptic hippocampal slice cultures

Based on this potential role of STIMs and SOCE in epileptic activity, we then set out to directly test the effect of pharmacologic SOCE inhibition on epileptiform activity. We used a model of chronic epileptiform activity, created by transient application of kainic acid (KA, 3 μM, 48 h) to organotypic hippocampal slice cultures. KA treatment induced epileptiform burst activity, which was recorded in the granule cell layer of the dentate gyrus in all experiments described here. It was, however, it was also detectable in the CA3 and CA1 region. This burst activity showed a considerable degree of inter-slice variation with regard to burst duration, frequency and amplitudes, however individual slice activity was stable for several hours during extracellular field potential recordings (data not shown). For pharmacological SOCE inhibition only slices with a baseline burst frequency of four to eight bursts (defined as >5 spikes per second with at least two consecutive spikes exhibiting high-frequency activity >50 Hz) per minute were chosen. Baseline activity was recorded for at least 20 min followed by the application of 100 μM ML-9 or 75 μM 2-APB for 10 min and subsequent wash out of the drug for at least 30 min (Fig. 7A).

Application of ML-9 ($n=5$) acutely increased the frequency of epileptiform bursts from 6.6 ± 2.5 bursts to 10.6 ± 2.5 bursts per minute 2 min after application of the drug. However, with a latency of 5–10 min during drug application and most prominent after the application of ML-9, burst frequencies decreased again to pre-treatment levels (6.3 ± 0.5 bursts per minute, 2 min after drug application, Fig. 7B). This effect was accompanied by qualitative changes of the bursts themselves. Before drug application single bursts consisted of 6.9 ± 1.9 individual spikes per burst, which did not change during drug application (6.7 ± 1.8) but increased markedly after drug application to 20.8 ± 3.9 (Fig. 7C). Before and during drug application, interictal spikes were a frequent phenomenon but were completely absent in the rhythmic phase following ML-9 wash-out, indicated by the sharp decline of the inter-burst interval variability (Fig. 7D, 20 intervals per condition and slice, note decrease in variability). In these experiments, 2-APB showed the same but less pronounced effects (Figs. 7B–D right panels). These results indicate that inhibition of SOCE suppresses interictal spikes and rhythmizes epileptic burst activity in chronic epileptic hippocampal slice cultures.

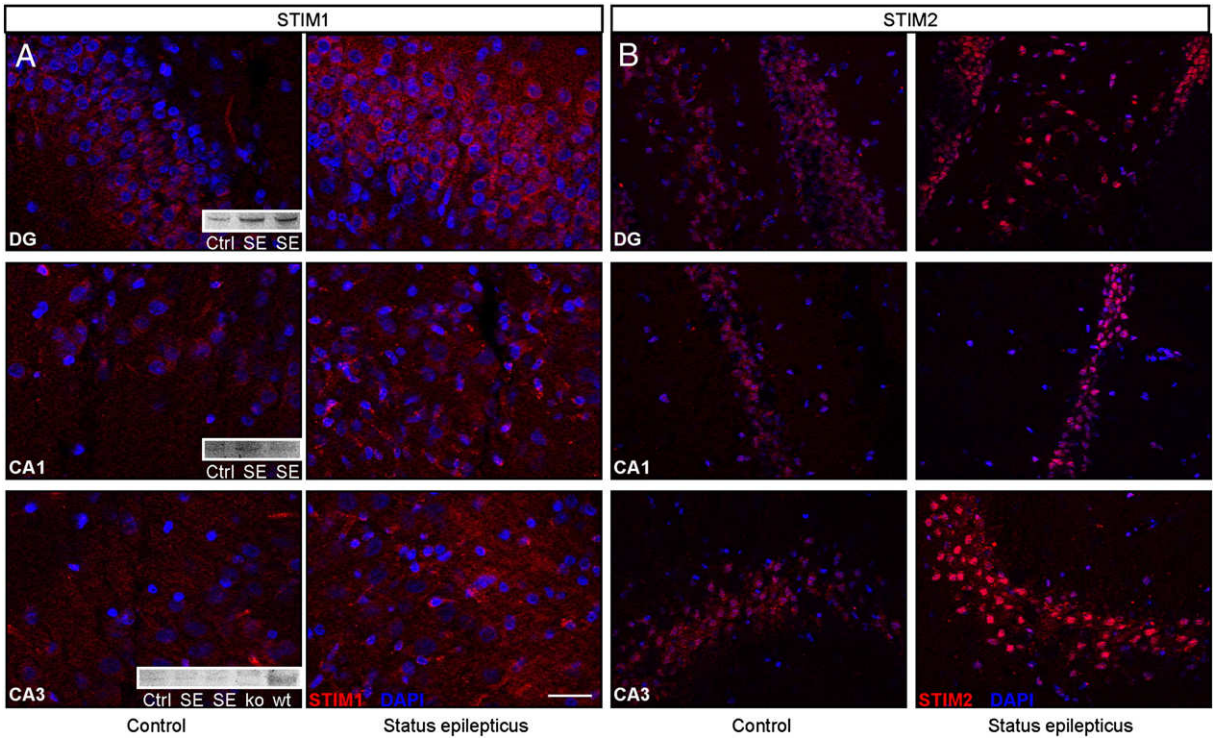

Fig. 5. STIM1 and STIM2 levels are increased in chronic epileptic mice. Immunohistochemical analysis of A) STIM1 and B) STIM2 expression in the hippocampus (dentate gyrus, DG and CA1/3) 4 weeks after sham-control or pilocarpine-induced status epilepticus in mice. Inserts in A) show STIM1 western blots of respective regions after hippocampal microdissections from individual animals after control (CTRL) or status epilepticus (SE) treatment as well as embryonic fibroblasts from wild type (WT) or STIM1 knock out (KO) animals. Scale bar, 30 μm.

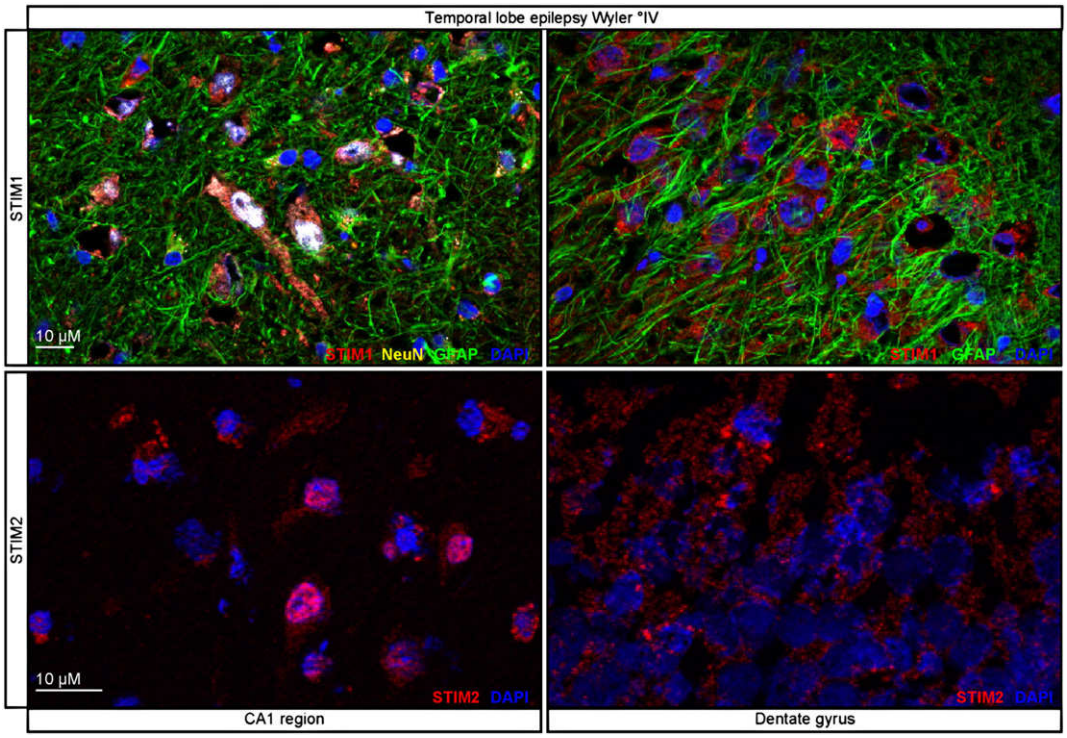

Fig. 6. STIM1 and STIM2 are highly expressed in a hippocampal specimen from a patient with medial temporal lobe epilepsy. Immunohistochemical analysis STIM1 (upper row) and STIM2 (lower row) expression in hippocampal specimen (DG and CA1) from medial temporal lobe epilepsy patients.

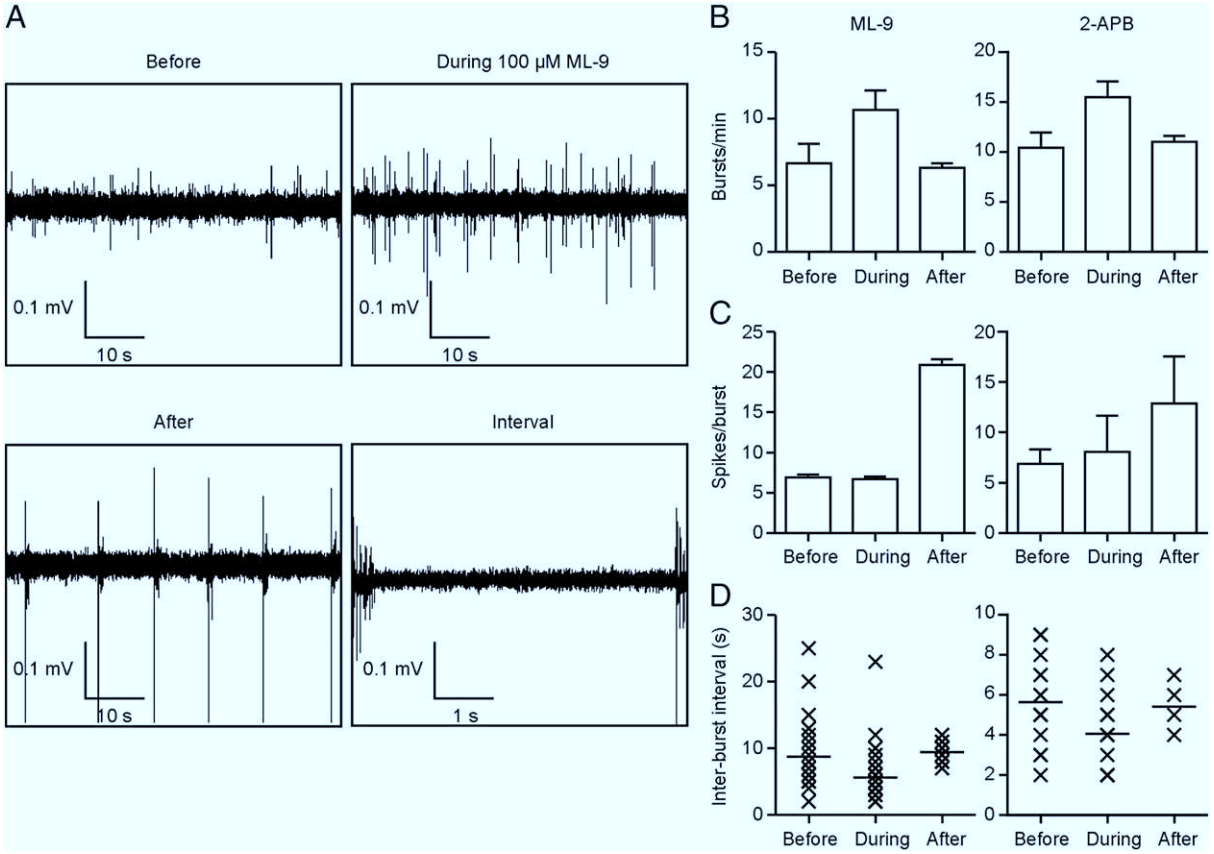

Fig. 7. Inhibition of store-operated Ca^{2+} entry rhythmizes burst activity in epileptic hippocampal slice cultures. A) Epileptiform spike and burst activities were recorded from all hippocampal subfields (shown is a typical recording from the dentate gyrus) during field potential recordings before, during, and after (5–10 min) application of 100 µM ML-9. Note the absence of interictal spike activity in the inter-burst interval after wash out of the drug. B-D) Quantification ($n = 5$) of B) burst per min, C) spikes per min, and D) the inter-burst interval before, during, and after application of 100 µM ML-9 and 75 µM 2-APB.

Discussion

Our results confirm the presence of SOCE and the expression of the calcium sensors STIM1 and STIM2 in neurons and astrocytes. Several studies have reported expression of STIM1 and STIM2 in the brain and in cultured neurons to different extends (Keil et al., 2010; Klejman et al., 2009; Park et al., 2010; Skibinska-Kijek et al., 2009; Wang et al., 2010). Our results are in line with a previous report that suggested that STIM1 expression is stronger in astrocytes and STIM2 in neurons (Gruszczynska-Biegala et al., 2011). STIM1 is however clearly detectable in neurons, which is in contrast to a previous report by Berna-Erro et al., who detected almost no STIM1 expression at the RNA and protein level in primary hippocampal neurons (Berna-Erro et al., 2009). We also, for the first time, evaluated the expression levels of STIM1 and STIM2 in human tissue, which showed a very prominent expression of STIM1 mRNA in the human brain. It is well possible that the high expression of STIM1 mRNA in human brain stems from a higher expression in astrocytes as the human brain contains approximately tenfold more astrocytes then the rodent brain. However, the pronounced expression in the remaining dentate gyrus and CA1 neurons in the mesial temporal lobe epilepsy specimen argues against a predominantly astrocytic expression of STIM1 in the human brain at least in this condition.

The analysis of the cytosolic Ca^{2+} content in neurons and astrocytes revealed a higher cytosolic Ca^{2+} concentration in neurons compared to astrocytes, which is in line with the increased STIM2 expression in neurons as STIM2 not only increases the Ca^{2+} concentration in the ER, but also in the cytosol via activation of the plasma membrane Ca^{2+} channel Orai1 (Brandman et al., 2007). ML-9-sensitive and thus most probably STIM2-mediated Ca^{2+} entry contributes to the neuronal baseline [Ca^{2+}], which suggest a role for SOCE in the maintenance of steady-state cytosolic Ca^{2+} levels in neurons. This is in line with previous results, which showed a decline in resting [Ca^{2+}] after inhibition of Ca^{2+} entry into sympathetic neurons by Lanthanum (Wanaverbecq et al., 2003). Also, dorsal root ganglion neurons displayed a fall in resting cytoplasmic [Ca^{2+}] after bath Ca^{2+} withdrawal and a subsequent elevation of cytoplasmic [Ca^{2+}] after Ca^{2+} reintroduction. This was amplified by store depletion with thapsigargin, significantly reduced by blockers of SOCE, and unaffected by antagonists of voltage-gated membrane Ca^{2+} channels (Gemes et al., 2011).

Not much is known about the role of SOCE in the brain. Our results suggest an involvement of SOCE in neuronal network activity. Pharmacological inhibition of SOCE resulted in a remarkable decrease in neuronal network activity measured with MEAs concomitantly with a decrease of the intracellular Ca^{2+} concentration measured by Fura-2 single cell imaging. It appears likely that this reduction in cytosolic Ca^{2+} concentration has a direct impact on membrane potential thereby impeding depolarization and generation of action potentials. Missing Ca^{2+} might also indirectly alter neuronal membrane potential by inactivation of Ca^{2+}-sensitive potassium channels and thereby increase the threshold for the generation of action potentials. Also synaptic transmitter release is a highly Ca^{2+}-dependent process. Therefore, the lowered cytosolic Ca^{2+} concentration might lead to a reduced neuronal network activity by inhibiting synaptic signal transduction.

The inhibitory and synchronizing effect of SOCE inhibition in the MEA experiments prompted us to examine the expression profiles of STIM1 and STIM2 in conditions of pathologic hyperexcitability. Interestingly, we found increased protein levels in the chronic epileptic hippocampus after pilocarpine-induced status epilepticus as compared to control tissue. We also found a strong expression of STIM1 and STIM2 in human hippocampal specimens after resection for Ammon's horn sclerosis. Despite the lack of adequate control tissue especially STIM1 showed a pronounced punctate and membraneous staining pattern associated with the SOCE activating state and localization of the protein, which is in line with recent reports showing elevated SOCE and I_{CRAC} after axonal injury by spinal nerve ligation (Gemes et al., 2011). We then used an *in vitro* model to directly assess the effects of SOCE inhibition in epileptic tissue. The addition of kainic acid to explanted juvenile rat hippocampal slice preparations initiates *in vitro* epileptogenesis. At the morphological level, this process is reflected by mossy fiber sprouting, a hallmark of hippocampal epilepsy (Sharma et al., 2007). At the functional level, spontaneous epileptic bursts develop within 1 week after kainic acid exposure and may be recorded for several weeks. The defined concentration, local extent and duration of the kainic acid treatment contributes to the relatively low inter-slice variability of epileptic discharges, as compared to *in vivo* kainic acid or other status epilepticus models (Bragin et al., 1999; Curia et al., 2008; Sharma et al., 2007).

Functional assessment of SOCE inhibiting drugs 2-APB and ML-9 depressed inter-burst activity and rhythmized epileptic burst activity in this model, which might be the correlate of synchrony seen in the MEA experiments. However, the increase in burst intensity and the absence of interictal spikes after drug application resemble a sustained enhancement of epileptic activity. These findings are compatible with a recent report showing that pharmacological blockade of SOCE elevated neuronal burst firing in dorsal root ganglion neurons (Gemes et al., 2011). Similar to the effect in epileptic slice models, SOCE inhibition by ML-9 application to mature dissociated neuronal cultures on MEAs reduced network activity, simultaneously sharpening burst structure and increasing synchrony by abolishing inter-burst activity. In contrast to its effect in slices, inhibiting SOCE by an effective dose of 2-APB almost completely suppressed network bursting in dissociated cultures, possibly suggesting an enhanced mechanism of reduced excitatory synaptic transmission, which plays a pivotal role in burst generation. Compared to organotypic slices, dissociated cultures may provide better accessibility to 2-APB, allowing for the observed stronger effect in these. Furthermore, 2-APB also has direct effects on Orai3 and to a lesser extent on Orai1, which it directly activates independently of internal Ca^{2+} stores and STIM1 (Dehaven et al., 2008). Therefore, 2-APB may suppress neuronal network activity along several pathways.

We can conclude from the presented data that STIM proteins and SOCE contribute in a noteworthy manner to cellular ion homeostasis and neuronal network activity under physiological and pathological conditions. Our results also delineate SOCE as a potential drug target.

Acknowledgments

This work was funded by the Deutsche Forschungsgemeinschaft ME1922/9-1 and SFB TR3, project D2. JG-B and JK were funded from statutory funds of the International Institute of Molecular and Cell Biology and the Nencki Institute of Experimental Biology (JK).

References

Agrawal, N., Venkiteswaran, G., Sadaf, S., Padmanabhan, N., Banerjee, S., Hasan, G., 2010. Inositol 1,4,5-trisphosphate receptor and dSTIM function in *Drosophila* insulin-producing neurons regulates systemic intracellular calcium homeostasis and flight. J. Neurosci. 30, 1301–1313.

Azouz, R., Jensen, M.S., Yaari, Y., 1996. Ionic basis of spike after-depolarization and burst generation in adult rat hippocampal CA1 pyramidal cells. J. Physiol. (Lond.) 492 (Pt 1), 211–223.

Baba, A., Yasui, T., Fujisawa, S., Yamada, R.X., Yamada, M.K., Nishiyama, N., Matsuki, N., Ikegaya, Y., 2003. Activity-evoked capacitative Ca2+ entry: implications in synaptic plasticity. J. Neurosci. 23, 7737–7741.

Benninger, F., Beck, H., Wernig, M., Tucker, K.L., Brüstle, O., Scheffler, B., 2003. Functional integration of embryonic stem cell-derived neurons in hippocampal slice cultures. J. Neurosci. 23, 7075–7083.

Berna-Erro, A., Braun, A., Kraft, R., Kleinschnitz, C., Schuhmann, M.K., Stegner, D., Wultsch, T., Eilers, J., Meuth, S.G., Stoll, G., Nieswandt, B., 2009. STIM2 regulates capacitive Ca2+ entry in neurons and plays a key role in hypoxic neuronal cell death. Sci. Signal. 2, ra67.

Bragin, A., Engel, J., Wilson, C.L., Vizentin, E., Mathern, G.W., 1999. Electrophysiologic analysis of a chronic seizure model after unilateral hippocampal KA injection. Epilepsia 40, 1210–1221.

Brandman, O., Liou, J., Park, W.S., Meyer, T., 2007. STIM2 is a feedback regulator that stabilizes basal cytosolic and endoplasmic reticulum Ca2+ levels. Cell 131, 1327–1339.

Curia, G., Longo, D., Biagini, G., Jones, R.S.G., Avoli, M., 2008. The pilocarpine model of temporal lobe epilepsy. J. Neurosci. Methods 172, 143–157.

Dehaven, W.I., Smyth, J.T., Boyles, R.R., Bird, G.S., Putney, J.W., 2008. Complex actions of 2-aminoethyldiphenyl borate on store-operated calcium entry. J. Biol. Chem. 283, 19265–19273.
Emptage, N.J., Reid, C.A., Fine, A., 2001. Calcium stores in hippocampal synaptic boutons mediate short-term plasticity, store-operated Ca2+ entry, and spontaneous transmitter release. Neuron 29, 197–208.
Feske, S., 2007. Calcium signalling in lymphocyte activation and disease. Nat. Rev. Immunol. 7, 690–702.
Feske, S., Gwack, Y., Prakriya, M., Srikanth, S., Puppel, S.-H., Tanasa, B., Hogan, P.G., Lewis, R.S., Daly, M., Rao, A., 2006. A mutation in Orai1 causes immune deficiency by abrogating CRAC channel function. Nature 441, 179–185.
Gemes, G., Bangaru, M.L.Y., Wu, H.-E., Tang, Q., Weihrauch, D., Koopmeiners, A.S., Cruikshank, J.M., Kwok, W.-M., Hogan, Q.H., 2011. Store-operated Ca2+ entry in sensory neurons: functional role and the effect of painful nerve injury. J. Neurosci. 31, 3536–3549.
Gramowski, A., Jügelt, K., Weiss, D.G., Gross, G.W., 2004. Substance identification by quantitative characterization of oscillatory activity in murine spinal cord networks on microelectrode arrays. Eur. J. Neurosci. 19, 2815–2825.
Gruszczynska-Biegala, J., Pomorski, P., Wisniewska, M.B., Kuznicki, J., 2011. Differential roles for STIM1 and STIM2 in store-operated calcium entry in rat neurons. PLoS One 6, e19285.
Huang, G.N., Zeng, W., Kim, J.Y., Yuan, J.P., Han, L., Muallem, S., Worley, P.F., 2006. STIM1 carboxyl-terminus activates native SOC, I(crac) and TRPC1 channels. Nat. Cell Biol. 8, 1003–1010.
Johnstone, A.F.M., Gross, G.W., Weiss, D.G., Schroeder, O.H.-U., Gramowski, A., Shafer, T.J., 2010. Microelectrode arrays: a physiologically based neurotoxicity testing platform for the 21st century. Neurotoxicology 31, 331–350.
Kachoei, B.A., Knox, R.J., Uthuza, D., Levy, S., Kaczmarek, L.K., Magoski, N.S., 2006. A store-operated Ca(2+) influx pathway in the bag cell neurons of Aplysia. J. Neurophysiol. 96, 2688–2698.
Keil, J.M., Shen, Z., Briggs, S.P., Patrick, G.N., 2010. Regulation of STIM1 and SOCE by the ubiquitin–proteasome system (UPS). PLoS One 5, e13465.
Klejman, M.E., Gruszczynska-Biegala, J., Skibinska-Kijek, A., Wisniewska, M.B., Misztal, K., Blazejczyk, M., Bojarski, L., Kuznicki, J., 2009. Expression of STIM1 in brain and puncta-like co-localization of STIM1 and ORAI1 upon depletion of Ca(2+) store in neurons. Neurochem. Int. 54, 49–55.
Klosen, P., Maessen, X., van den Bosch de Aguilar, P., 1993. PEG embedding for immunocytochemistry: application to the analysis of immunoreactivity loss during histological processing. J. Histochem. Cytochem. 41, 455–463.
Liou, J., Kim, M.L., Heo, W.D., Jones, J.T., Myers, J.W., Ferrell, J.E., Meyer, T., 2005. STIM is a Ca2+ sensor essential for Ca2+-store-depletion-triggered Ca2+ influx. Curr. Biol. 15, 1235–1241.
Manjarrés, I.M., Rodríguez-García, A., Alonso, M.T., García-Sancho, J., 2010. The sarco/endoplasmic reticulum Ca(2+) ATPase (SERCA) is the third element in capacitative calcium entry. Cell Calcium 47, 412–418.
Norwood, N., Moore, T.M., Dean, D.A., Bhattacharjee, R., Li, M., Stevens, T., 2000. Store-operated calcium entry and increased endothelial cell permeability. Am. J. Physiol. Lung Cell. Mol. Physiol. 279, L815–L824.
Opitz, T., Scheffler, B., Steinfarz, B., Schmandt, T., Brüstle, O., 2007. Electrophysiological evaluation of engrafted stem cell-derived neurons. Nat. Protoc. 2, 1603–1613.
Otto, F., Görtz, P., Fleischer, W., Siebler, M., 2003. Cryopreserved rat cortical cells develop functional neuronal networks on microelectrode arrays. J. Neurosci. Methods 128, 173–181.
Park, C.Y., Hoover, P.J., Mullins, F.M., Bachhawat, P., Covington, E.D., Raunser, S., Walz, T., Garcia, K.C., Dolmetsch, R.E., Lewis, R.S., 2009. STIM1 clusters and activates CRAC channels via direct binding of a cytosolic domain to Orai1. Cell 136, 876–890.
Park, C.Y., Shcheglovitov, A., Dolmetsch, R., 2010. The CRAC channel activator STIM1 binds and inhibits L-type voltage-gated calcium channels. Science 330, 101–105.
Roos, J., DiGregorio, P.J., Yeromin, A.V., Ohlsen, K., Lioudyno, M., Zhang, S., Safrina, O., Kozak, J.A., Wagner, S.L., Cahalan, M.D., Veliçelebi, G., Stauderman, K.A., 2005. STIM1, an essential and conserved component of store-operated Ca2+ channel function. J. Cell Biol. 169, 435–445.
Sanabria, E.R., Su, H., Yaari, Y., 2001. Initiation of network bursts by Ca2+-dependent intrinsic bursting in the rat pilocarpine model of temporal lobe epilepsy. J. Physiol. (Lond.) 532, 205–216.
Sharma, A.K., Reams, R.Y., Jordan, W.H., Miller, M.A., Thacker, H.L., Snyder, P.W., 2007. Mesial temporal lobe epilepsy: pathogenesis, induced rodent models and lesions. Toxicol. Pathol. 35, 984–999.
Skibinska-Kijek, A., Wisniewska, M.B., Gruszczynska-Biegala, J., Methner, A., Kuznicki, J., 2009. Immunolocalization of STIM1 in the mouse brain. Acta Neurobiol. Exp. 69, 413–428.
Smyth, J.T., Dehaven, W.I., Bird, G.S., Putney, J.W., 2008. Ca2+-store-dependent and -independent reversal of Stim1 localization and function. J. Cell Sci. 121, 762–772.
Vig, M., Peinelt, C., Beck, A., Koomoa, D.L., Rabah, D., Koblan-Huberson, M., Kraft, S., Turner, H., Fleig, A., Penner, R., Kinet, J.-P., 2006. CRACM1 is a plasma membrane protein essential for store-operated Ca2+ entry. Science 312, 1220–1223.
Wanaverbecq, N., Marsh, S.J., Al-Qatari, M., Brown, D.A., 2003. The plasma membrane calcium-ATPase as a major mechanism for intracellular calcium regulation in neurones from the rat superior cervical ganglion. J. Physiol. (Lond.) 550, 83–101.
Wang, Y., Deng, X., Mancarella, S., Hendron, E., Eguchi, S., Soboloff, J., Tang, X.D., Gill, D.L., 2010. The calcium store sensor, STIM1, reciprocally controls Orai and CaV1.2 channels. Science 330, 105–109.

Stromal interaction molecule 1 (STIM1) is involved in the regulation of mitochondrial shape and bioenergetics and plays a role in oxidative stress

Nadine Henke[1], Philipp Albrecht[1], Annika Pfeiffer[1], Diamandis Toutzaris[1], Klaus Zanger[2], and Axel Methner[1,3]#

[1]Heinrich Heine Universität Düsseldorf, Medical faculty, Department of Neurology, Moorenstr. 5, D-40225 Düsseldorf/Germany [2]Heinrich Heine Universität Düsseldorf, Medical faculty, Center for Anatomy and Brain Research, Moorenstr. 5, D-40225 Düsseldorf/Germany [3]Focus Program Translational Neuroscience (FTN), Rhine Main Neuroscience Network (rmn2), Johannes Gutenberg University Medical Center Mainz, Department of Neurology, Langenbeckstr. 1, D-55131 Mainz/Germany

The presented manuscript is accepted for publication in the “Journal of Biological Chemistry” (72).

Contribution of Nadine Henke, first author:

Experimental design: 50%
Execution and analysis of experiments: 90%
Manuscript writing: first draft, overall 50%

THE JOURNAL OF BIOLOGICAL CHEMISTRY VOL. 287, NO. 50, pp. 42042–42052, December 7, 2012

Stromal Interaction Molecule 1 (STIM1) Is Involved in the Regulation of Mitochondrial Shape and Bioenergetics and Plays a Role in Oxidative Stress*

Received for publication, September 8, 2012 Published, JBC Papers in Press, October 17, 2012, DOI 10.1074/jbc.M112.417212

Nadine Henke[‡], Philipp Albrecht[‡], Annika Pfeiffer[‡], Diamandis Toutzaris[‡], Klaus Zanger[§], and Axel Methner[‡¶1]

From the [‡]Department of Neurology and the [§]Center for Anatomy and Brain Research, Medical Faculty, Heinrich Heine Universität Düsseldorf, D-40225 Düsseldorf, Germany and the [¶]Focus Program Translational Neuroscience, Rhine Main Neuroscience Network, Johannes Gutenberg University Medical Center Mainz, Department of Neurology, D-55131 Mainz, Germany

Background: Store-operated Ca^{2+} entry is regulated by the sensor STIM1 and the channel ORAI1.
Results: Deficiency alters mitochondrial shape and increases mitochondrial activity resulting in increased susceptibility to oxidative stress and cell death by nuclear translocation of apoptosis-inducing factor.
Conclusion: Store-operated Ca^{2+} entry regulates mitochondrial function and vulnerability.
Significance: STIM1 plays a role in oxidative stress by regulating mitochondrial function.

Calcium ions are involved in a plethora of cellular functions including cell death and mitochondrial energy metabolism. Store-operated Ca^{2+} entry over the plasma membrane is activated by depletion of intracellular Ca^{2+} stores and is mediated by the sensor STIM1 and the channel ORAI1. We compared cell death susceptibility to oxidative stress in STIM1 knock-out and ORAI1 knockdown mouse embryonic fibroblasts and in knock-out cells with reconstituted wild type and dominant active STIM1. We show that STIM1 and ORAI1 deficiency renders cells more susceptible to oxidative stress, which can be rescued by STIM1 and ORAI1 overexpression. STIM1 knock-out mitochondria are tubular, have a higher Ca^{2+} concentration, and are metabolically more active, resulting in constitutive oxidative stress causing increased nuclear translocation of the antioxidant transcription factor NRF2 triggered by increased phosphorylation of the translation initiation factor eIF2α and the protein kinase-like endoplasmic reticulum kinase PERK. This leads to increased transcription of antioxidant genes and a high basal glutathione in STIM1 knock-out cells, which is, however, more rapidly expended upon additional stress, resulting in increased release and nuclear translocation of apoptosis-inducing factor with subsequent cell death. Our data suggest that store-operated Ca^{2+} entry and STIM1 are involved in the regulation of mitochondrial shape and bioenergetics and play a role in oxidative stress.

Calcium ions are involved in a plethora of cellular functions ranging from short term responses such as contraction and secretion to long term regulation of cell growth and proliferation. Within the cell, Ca^{2+} is mainly stored in the endoplasmic reticulum (ER)[2] from where it is released upon activation of cell surface receptors and subsequent generation of the second messenger inositol 1,4,5-triphosphate, which binds and opens inositol 1,4,5-triphosphate receptors 1–3 at the ER membrane triggering Ca^{2+} release from the ER lumen. The following decrease in $[Ca^{2+}]_{ER}$ induces a strong Ca^{2+} influx from the extracellular space named store-operated Ca^{2+} entry (SOCE) (1, 2), which is followed by removal of cytosolic Ca^{2+} and replenishment of luminal Ca^{2+} through sarcoplasmic/endoplasmic reticulum Ca^{2+}-ATPases (SERCA). To ensure that the entering Ca^{2+} is promptly removed from the cytosol, subplasmalemmal mitochondria sequester parts of the entering Ca^{2+} ions and shuttle them to domains of the ER further apart from the membrane (3–5). As different enzymes of the Krebs cycle are activated by Ca^{2+} ions, mitochondrial Ca^{2+} uptake during activated SOCE increases matrix $[Ca^{2+}]$ and accelerates energy metabolism (6).

The Ca^{2+} sensor that conveys information about the Ca^{2+} load of the ER lumen to store-operated Ca^{2+} channels is stromal interaction molecule 1 (STIM1) (7, 8), a single transmembrane protein located in the ER membrane with a luminal EF hand and a cytosolic domain, which activates Ca^{2+} release-activated Ca^{2+} channels (7, 8). Upon store depletion, STIM1 clusters into punctae near the plasma membrane (9) and activates Ca^{2+} release-activated Ca^{2+} channels, mainly ORAI1 (10–12), resulting in a strong Ca^{2+} influx. Mutation of the luminal EF hand motif of STIM1 generates a constitutively active STIM1, which is located in punctae in close proximity to the plasma membrane and activates Ca^{2+} entry independently from ER Ca^{2+} stores (13, 14). In human embryonic kidney 293 cells, overexpression of ORAI1 alone inhibits SOCE, whereas expression of STIM1 alone just slightly increases Ca^{2+} entry during Ca^{2+} readdition after thapsigargin-induced store deple-

* This work was supported by Deutsche Forschungsgemeinschaft Grant ME1922/9-1 (to A. M.).
[1] To whom correspondence should be addressed: Johannes Gutenberg University Medical Center Mainz, Department of Neurology, Langenbeckstr. 1, D-55131 Mainz, Germany. Tel.: 49-6131-17-2695; Fax: 49-6131-17-5967; E-mail: axel.methner@gmail.com.
[2] The abbreviations used are: ER, endoplasmic reticulum; SOCE, store-operated Ca^{2+} entry; SERCA, sarcoplasmic/endoplasmic reticulum Ca^{2+}-ATPases; STIM1, stromal interaction molecule 1; MEF, mouse embryonic fibroblast; DA, dominant active; HBSS, Hanks' balanced salt solution; EYFP, enhanced yellow fluorescent protein; TMRE, tetramethylrhodamine ethyl ester; ANOVA, analysis of variance; BSO, L-buthionine-(*S*,*R*)-sulfoximine; ROS, reactive oxygen species; NRF, nuclear factor erythroid 2-related factor; KEAP, Kelch-like ECH-associated protein; PERK, protein kinase-like endoplasmic reticulum kinase; AIF, apoptosis-inducing factor.

tion. Only co-expression of ORAI1 and STIM1 increases SOCE pointing out the importance of the correct stoichiometry between STIM1 and ORAI1 (15). In addition to STIM1 and ORAI1, SERCA also co-assembles into punctae induced by store depletion and supposedly permits quick shuttling of entering Ca^{2+} into the ER (5, 16).

The link between Ca^{2+} and cell death is complex and has been extensively reviewed (17). Because STIM1 and ORAI1 are important players of SOCE, a link of these molecules to cell death appears possible and was investigated in different scenarios, yielding inconsistent results. STIM1 was first thought to be a tumor suppressor gene based on its genomic localization. In line with this hypothesis, transfection of STIM1 into cell lines derived from a rhabdoid tumor and a rhabdomyosarcoma-induced cell death (18). Similarly, inhibition of SOCE by siRNA-mediated knockdown of STIM1 increased survival of cervical epithelial cells on soft substrates (19). These reports suggested a negative effect of STIM1 and SOCE on cell survival. Malignant melanoma cells on the other hand were shown to depend on the intact SOCE machinery to sustain activation of the pro-survival factor protein kinase B/Akt (20) and silencing of STIM1-increased apoptosis of C6 glioma cells (21). Recently, Hawkins *et al.* (22) discovered that STIM1 can be glutathionylated in response to oxidative stress, which results in its constitutive activation and subsequent cell death.

In summary, the role of STIM1 in cell death still appears to be ambiguous. We therefore decided to compare cell death susceptibility to oxidative stress in STIM1 KO and WT mouse embryonic fibroblasts (MEFs) and in KO cells with reconstituted STIM1 and dominant-active STIM1 (DA-STIM1). Our data suggest that store-operated Ca^{2+} entry and STIM1 are involved in the regulation of mitochondrial shape and bioenergetics and play a role in oxidative stress.

EXPERIMENTAL PROCEDURES

Cell Culture—STIM1 KO and WT MEFs were a kind gift from Masatsugu Oh-Hora (Harvard University) and were cultured in DMEM high glucose with L-glutamine (PAA) containing 10% FCS (Thermo Fisher) and 100 units/ml penicillin and 100 μg/ml streptomycin (Invitrogen) and incubated in a humidified incubator with 5% CO_2 and 95% air. Stable cell lines were continuously selected using 1.5 mg/ml geneticin (Invitrogen).

Plasmids, siRNA, and Transfections—High purity plasmids pEYFP, STIM1-EYFP (8), STIM1-D76N/D78N-EYFP (14), and ORAI1-EYFP (a kind gift from Christoph Romanin, University of Linz, Linz, Austria) were prepared using Nucleobond AX 500 columns (Machery-Nagel). Flexitube siRNAs against ORAI1 were purchased from Qiagen (SI00972251 and SI00972258). Cells were grown to 70–80% confluency in 6-well plates and transfected with Attractene (Qiagen) in the case of plasmids or Lipofectamine RNAiMAX (Invitrogen) for siRNAs. Stable cell lines were generated by selection with geneticin and repeated fluorescence-activated cell sorting of EYFP positive cells on a MoFlo XDP (Beckman-Coulter).

Immunoblotting—The cells were lysed in ice-cold radioimmune precipitation assay buffer (Thermo Fisher Scientific) containing the mini complete protease inhibitor mixture (Roche Applied Science) and centrifuged for 30 min at 16,000 × *g*. The supernatants were separated on 8–16% polyacrylamide gels (Thermo Scientific), transferred onto nitrocellulose membranes using the iBlot System (Invitrogen), and blocked in 3% nonfat dry milk in phosphate-buffered saline or Tris-buffered saline for phosphorylation-sensitive antibodies containing 0.5% Tween 20 (PBS-T/TBS-T) for 1 h at room temperature. The membranes were incubated overnight with primary antibodies against STIM1 (Abnova, H00006786-M01, 1:1000), STIM2 (Cell Signaling, 4917, 1:1000), eIF2α (Cell Signaling, 9722, 1:1000), phospho-eIF2α (Cell Signaling, 9721, 1:1000), phospho-PERK (Cell Signaling, 3179, 1:1000), GAPDH (Cell Signaling, 2118, 1:5000), or actin (Millipore, MAB1501, 1:5000) followed by anti-mouse (rabbit) IgG (Fc) infrared fluorescence-conjugated (Licor, 1:30,000) secondary antibody. The membranes were scanned for infrared fluorescence at 680 or 800 nm using the Odyssey system (Licor). Intensity was quantitated with the image-processing software ImageJ.

Ca^{2+} Imaging—The cells were seeded in 24-well plates at a density of 100,000 cells per well and loaded 24 h later with Fura2-AM (Invitrogen) in HBSS (Invitrogen) at a concentration of 2 μM for 30 min at 37 °C. The cells were measured in HBSS or EGTA buffer (Ca^{2+}-free HBSS supplemented with 0.5 mM EGTA, 20 mM HEPES, 1 mM $MgCl_2$, and 1 g/liter glucose). Imaging was performed on an Olympus IX81 fluorescence microscope with cell^R imaging software. Images were taken at 340- and 380-nm excitation, and the ratio was calculated every 5 s for a period of 5 min for every single cell. The indicated substances were added 1 min after onset of the measurement.

For SOCE experiments, the cells were seeded on coverslips, loaded with Fura2, and placed into a flow chamber. Measurements were performed as described above. Base-line Ca^{2+} was recorded in HBSS for 2 min and then replaced by EGTA buffer with 2 μM thapsigargin to deplete ER Ca^{2+} stores. After 8 min, Ca^{2+} was readded by changing the buffer to HBSS again. In experiments with transfected cells, only EYFP-positive cells were analyzed.

Cell Survival Assays—The cells were seeded in 96-well plates at a density of 5000 cells/well in quintuplicate. Transiently transfected cells were seeded 24 h after transfection. Pharmacological agents were added the day after plating, and cell survival was quantified again 24 h later using the cell titer blue reagent (Promega). Either absorbance at 562 nm together with a reference value at 612 nm or fluorescence emission at 590 nm after exciting at 562 nm was measured using a GENios Pro microplate reader (Tecan). Alternatively, the cells were stained in DMEM without phenol red (PAA) with Hoechst 33342 (0.5 μg/ml; Sigma Aldrich) as a marker for all cells and Sytox Orange (0.5 μM; Molecular Probes) as a marker for dead cells and analyzed in a BD Pathway 855 high content imaging system (BD Bioscience). Regions of interest around the nuclei were defined by Hoechst signal, and double-positive cells were counted as dead cells.

GSH Assay—Total cellular GSH content was measured enzymatically recording NADPH consumption by GSH reductase. The cells, seeded in 6-well plates in duplicates on the day before the assay, were detached in 200 μl of PBS with EDTA, transferred into 100 μl of 10% sulfosalicylic acid, vortexed vigor-

ously, and incubated on ice for 10 min. After centrifugation for 10 min at 16,000 × *g*, the supernatants were transferred into 24 μl of 50% triethanolamine. The samples were diluted in an assay buffer containing 100 mM Na_2PO_4, 1 mM EDTA, pH 7.5, 0.6 mM 5,5′-dithiobis-(2-nitro-benzoic acid) and 0.8 mM NADPH. After addition of 1 unit/ml glutathione reductase, NADPH content was monitored at 390 nm using GENios Pro microplate reader (Tecan). Total cellular GSH was normalized to cellular protein amounts obtained from pellets after centrifugation solubilized in 100 μl of 0.2 N NaOH at 37 °C overnight analyzed with a BC assay protein quantification kit (Interchim).

Quantitative Real Time PCR—For expression analysis of antioxidant response genes, whole RNA was isolated using the ZR RNA MiniPrep Kit (Zymo) and subjected to cDNA synthesis with a high capacity cDNA reverse transcription kit (ABI). Real time analysis was performed on a 7500 Fast cycler (ABI) with FAST BLUE qPCR MasterMix (Eurogentec) running the 7500 standard program for TaqMan assays. Primers and probes for antioxidant response genes were designed by the universal probe library assay design center (Roche Applied Science). The hypoxanthine-phosphoribosyltransferase gene (*hprt*) served as endogenous control. Primers and *hprt* probe were purchased from MWG.

Mitochondrial Membrane Potential, Ca^{2+} Content, and Superoxide Production—Mitochondrial membrane potential, matrix Ca^{2+} content, and superoxide production were determined by flow cytometry using tetramethylrhodamine ethyl ester (TMRE) (Sigma), Rhod2-AM (ABD Bioquest), or dihydrorhodamine 6G (Invitrogen). The cells were seeded in 6-well plates in triplicate the day before the experiment. Staining was carried out at 37 °C in HBSS with 10 μM TMRE or 2 μM Rhod2-AM for 30 min or 1 μM dihydrorhodamine 6G for 15 min. After two wash steps, mean red fluorescence was analyzed on a FACSCalibur flow cytometer (BD Biosciences).

Immunofluorescence Staining and Nuclear Translocation Assay—The cells were seeded in 96-well imaging plates (BD Biosciences) coated with 0.1% gelatin and for AIF translocation assays subjected to glutamate treatment overnight 24 h later. For NRF2 staining, the cells were left untreated. After fixation in 4% paraformaldehyde for 10 min at 37 °C, the cells were permeabilized in 1× blocking solution (Roti-Block diluted in PBS; Carl Roth) supplemented with 0.1% Triton X-100 and subsequently incubated overnight in primary antibody solution (goat anti-AIF (D-20) sc-9416 from Santa Cruz or rabbit anti-NRF2 (H-300) sc-13032 from Santa Cruz both diluted 1:100 in blocking solution). After incubation with Cy3-labeled secondary antibody (Millipore) and nuclear staining with Hoechst 33342, nuclear translocation of AIF or NRF2 was measured on a BD Pathway 855 high content imaging system (BD Bioscience). Nuclear regions of interest were identified by Hoechst signal, and a concentric region around the nuclear region of interest was assessed as cytoplasm. The ratio of the nuclear and cytoplasmic Cy3 signal was calculated as the measure of translocation.

TEM Imaging—After trypsinization, the cells were pelleted, first fixed in 2.5% glutaraldehyde, 2% paraformaldehyde, and 0.05% tannic acid and afterward treated with 2% osmium tetroxide. After staining with 1.5% uranylacetate and 1.5% phosphotungstic acid, the pellets were embedded in epoxide resin (Spurr) and dissected in 70–80-nm-thick slices on an ultramicrotome (Reichert Ultracut, Vienna, Austria). Images (30 KO and 32 WT) were taken on a Hitachi H 600 transmission electron microscope in 15,000× magnification. Distances between mitochondria and ER membranes, as well as the length of the mitochondrial cut surface, were measured with the image analysis software Axiovision (Zeiss). In total, 523 mitochondria were analyzed for each cell type.

Analysis of Mitochondrial Shape—To visualize mitochondria of STIM1 WT and KO fibroblasts, the cells were transfected with mitochondrially targeted dsRed2 (kind gift of Axel Niemann, Zürich, Switzerland) and transferred to coverslips 24 h post-transfection. Again, 24 h later, 2.5 mM of glutamate or vehicle was added to the cell culture medium. After 16 h cells were fixed in 4% paraformaldehyde, stained with Hoechst 33342, and mounted in fluorescence mounting medium (Dako). Analysis of mitochondrial morphology was performed on an Olympus IX81 fluorescence microscope with a 60× oil immersion objective. For each condition, 100 cells were counted and categorized dependent on their mitochondrial morphology.

Statistical Analysis—The data were summarized as the means ± S.E., and the statistical significance was calculated using two-tailed *t* tests or analysis of variance (ANOVA) with Tukey's multiple comparison post hoc test as indicated using Graphpad Prism software. *p* values <0.05 were considered significant.

RESULTS

SOCE Deficiency Renders Cells More Susceptible to Oxidative Stress—To evaluate our model for SOCE deficiency, we first confirmed that mouse embryonic fibroblasts derived from STIM1 KO mice indeed did not express STIM1 (Fig. 1*A*). These cells showed no compensatory up-regulation of the STIM1 homologue STIM2 (Fig. 1*B*) and exhibited a remarkable reduction of Ca^{2+} re-entry after store depletion with the SERCA inhibitor thapsigargin compared with wild type control cells generated and passaged in parallel (Fig. 1*C*). We concluded that these cells constitute an adequate model of chronic SOCE deficiency and studied their susceptibility to oxidative stress using the model of oxidative glutamate toxicity, which is an excellent model of endogenous oxidative stress (23). In this paradigm, large amounts of extracellular glutamate block the glutamate-cystine antiporter system Xc^-. This leads to deprivation of cystine and its reduced form cysteine, the rate-limiting substrate for the synthesis of GSH, the most important intracellular antioxidant. The subsequent GSH depletion leads to accumulation of reactive oxygen species and cell death by oxidative stress (recently reviewed in Ref. 23). We also blocked GSH synthesis directly by using the glutamate-cysteine ligase inhibitor BSO (L-buthionine-(*S*,*R*)-sulfoximine). In all assays, cell viability was quantitated by survival assays utilizing reduction of resazurin to resorufin through metabolic activity of healthy cells. Using these paradigms, we observed an increased sensitivity of STIM1 KO MEFs to oxidative stress compared with WT MEFs (Fig. 1*D*). To rule out artifacts brought about by the resazurin method, we confirmed the results with an inde-

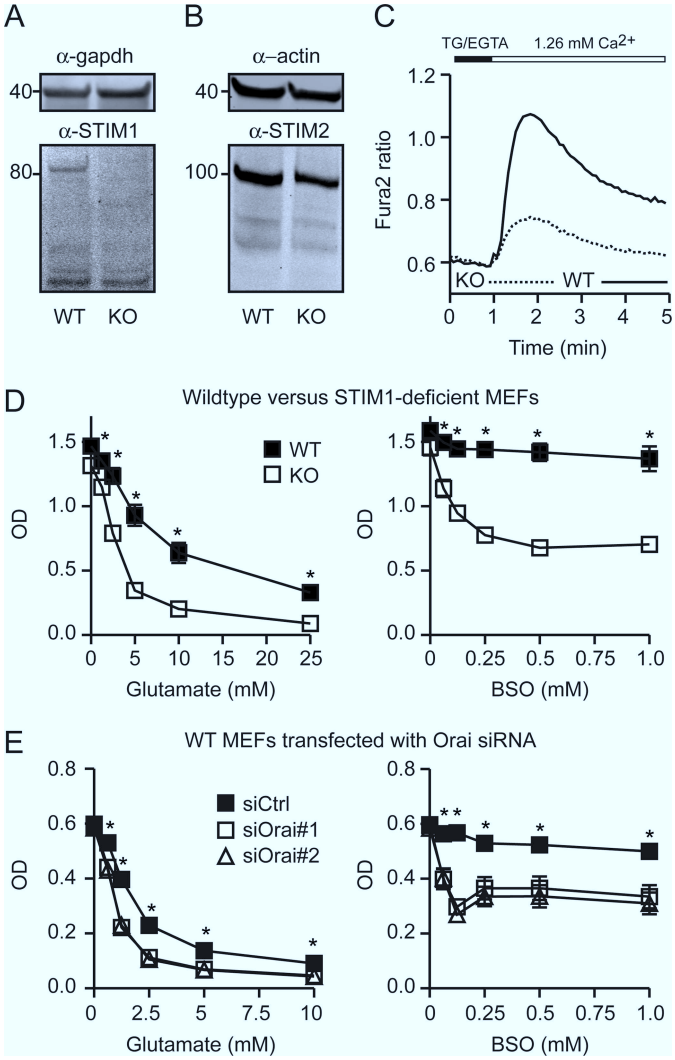

FIGURE 1. **SOCE deficiency renders cells more susceptible to oxidative stress.** *A* and *B*, immunoblots of STIM1 WT and KO cell lysates show lack of STIM1 (*A*) and no compensatory up-regulation of STIM2 (*B*). GAPDH and actin served as loading controls. Size is indicated. *C*, reduction of SOCE in STIM1 KO cells was quantitated by single cell microscopy using fura2-AM. Graphs show mean fura2 ratio of 164 (WT) and 170 (KO) cells. ER Ca^{2+} stores were emptied with 2 μM thapsigargin in Ca^{2+}-free conditions before readdition of HBSS containing 1.26 mM Ca^{2+}. Traces show only Ca^{2+} readdition. *D*, viability of STIM1 WT and KO cells treated for 16 h with the indicated concentrations of oxidative stress inductors glutamate or BSO. *E*, survival of WT cells transfected 48 h before oxidative stress induction with two independent siRNAs against ORAI1 or control siRNA. *D* and *E*, viability was quantitated by the cell titer blue assay. The graphs show mean ± S.E. absorbance values of 15 replicates for each condition obtained in three independent experiments. *, $p < 0.05$, Student's *t* test (*D*) or ANOVA with Tukey's post hoc test (*E*).

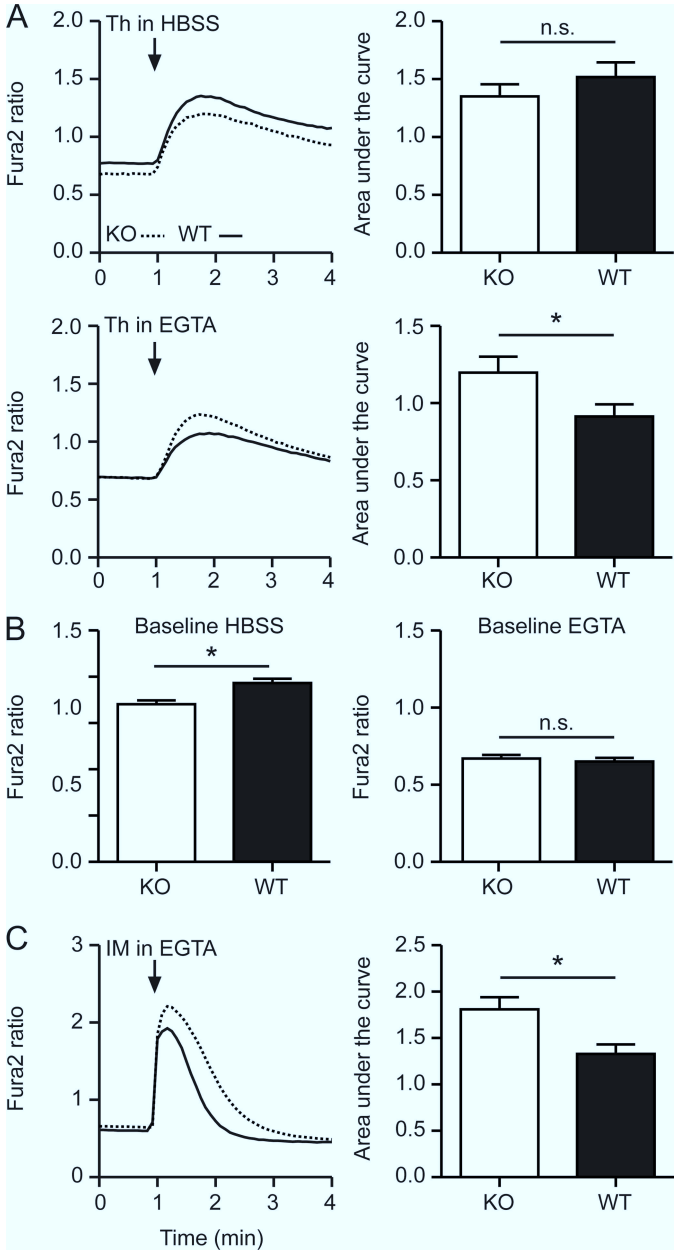

FIGURE 2. **Effects of STIM1 deficiency on the intracellular Ca^{2+} homeostasis.** fura2 single-cell imaging of WT and STIM1 KO cells. After 1 min of base-line recording, 2 μM thapsigargin (*A*) or 5 μM ionomycin (*C*) was added as indicated, and the fura2 signal was recorded for an additional 4 min. The graphs show mean fura2 ratio of >150 cells for each condition. For all experiments, the area under the curve (*A* and *C*) and the base-line fura2 ratio (*B*) of the first minute of measurement was calculated and plotted as the means ± S.E. *n.s.*, not significant; *, $p < 0.05$, Student's *t* test.

pendent method using high content imaging of live and dead cells stained with the dead cell marker Sytox Orange and Hoechst 33342 as a marker for all cells (not shown). We also reproduced these results by knocking down the other essential component of SOCE, ORAI1, the pore-forming subunit of store-operated Ca^{2+} channels. Consistent with the results obtained in the STIM1 knock-out condition, siRNA-mediated knockdown of ORAI1 in WT MEFs resulted in an increased susceptibility to oxidative stress induced by glutamate or BSO (Fig. 1*E*).

For a complete characterization of these cells, we also examined the thapsigargin-releasable Ca^{2+} pool in the presence and absence of extracellular Ca^{2+} as a measure of the ER $[Ca^{2+}]$ and the total cellular Ca^{2+} content by treatment with the Ca^{2+} ionophore ionomycin (Fig. 2). These experiments showed that STIM1 deficiency decreases slightly the cytosolic base-line Ca^{2+} and increases the total cellular Ca^{2+} content. We concluded that the intact SOCE machinery is important for cell survival under oxidative stress conditions and tried to rescue the phenotype by overexpressing wild type or dominant active STIM1 in STIM1 KO cells.

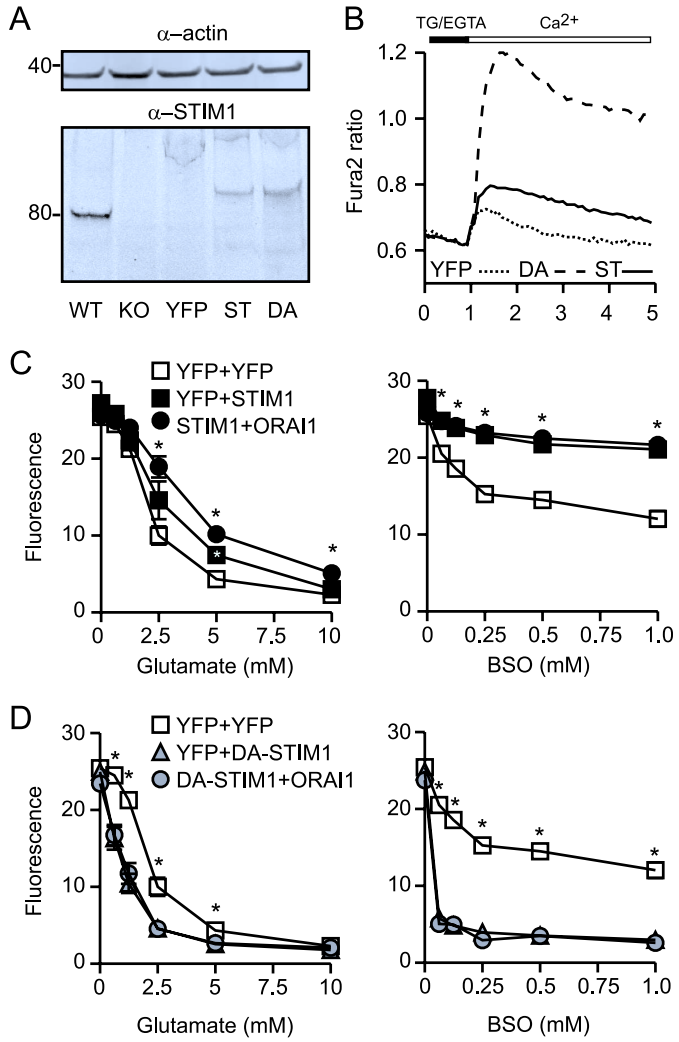

FIGURE 3. **STIM1 expression in STIM1 KO cells restores SOCE and protects from oxidative stress.** *A*, STIM1 KO MEFs were stably transfected with STIM1-EYFP (*ST*), dominant active DA-STIM1-EYFP (*DA*), or YFP, and the expression was verified by immunoblotting. Actin served as loading control. Size is indicated. *B*, reconstitution of SOCE quantitated by single cell microscopy using fura2-AM after ER Ca^{2+} stores were emptied with 2 μM thapsigargin in Ca^{2+}-free conditions. Graphs show mean fura2 ratio of 78 (*YFP*), 70 (STIM1-EYFP, *ST*), or 63 (DA-STIM1-EYFP, *DA*) cells. Traces show only Ca^{2+} readdition. *C* and *D*, survival of stably STIM1-EYFP (*C*) or DA-STIM1-EYFP (*D*) expressing STIM1 KO MEFs, additionally transfected with ORAI1-EYFP or YFP 48 h before induction of oxidative stress by glutamate or BSO. Viability in *C* and *D* was quantitated by the cell titer blue assay 16 h after addition of the indicated drugs. The graphs show the means ± S.E. of 15 replicates for each condition obtained in three independent experiments. *, $p < 0.05$, ANOVA with Tukey's post hoc test.

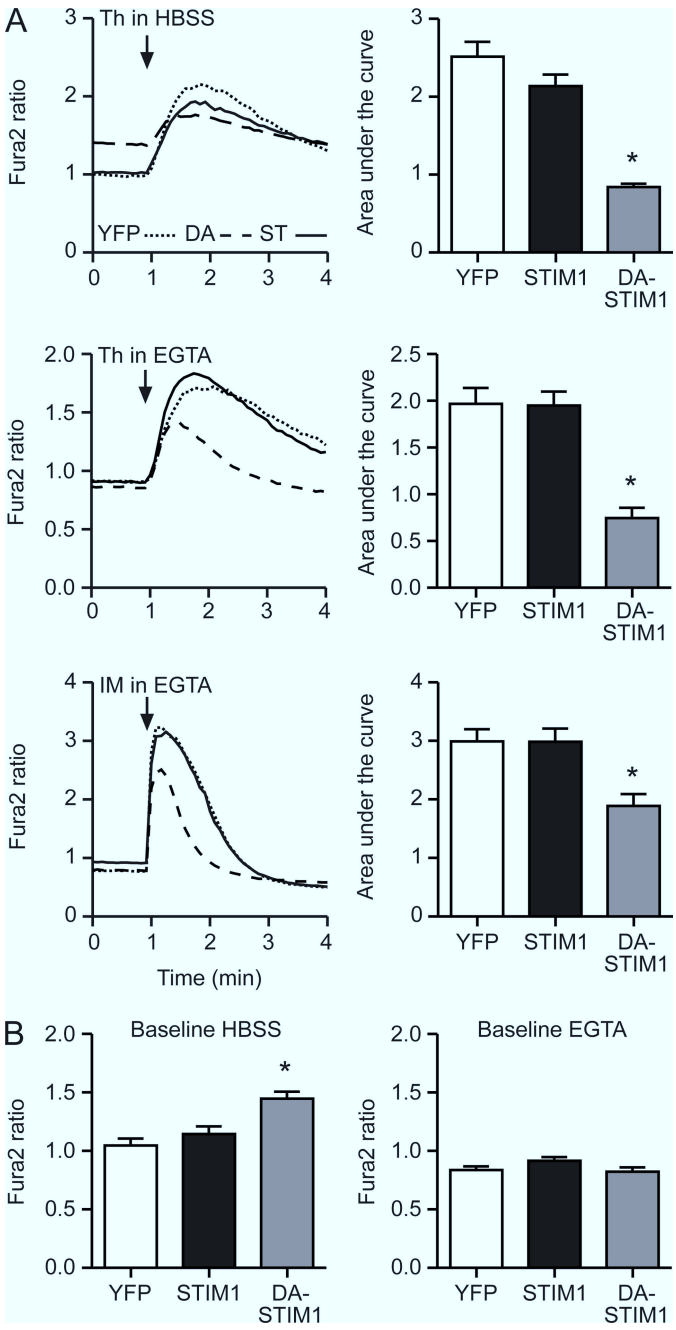

FIGURE 4. **Effects of STIM1 rescue on the intracellular Ca^{2+} homeostasis.** *A*, Fura2 single cell imaging of stably STIM1-EYFP or DA-STIM1-EYFP expressing STIM1 KO MEFs. After 1 min of base-line recording, 2 μM thapsigargin or 5 μM ionomycin was added as indicated, and the fura2 signal was recorded for additional 4 min. The graphs show mean fura2 ratio of >150 cells for each condition. For all experiments, the area under the curve (*A*) and the base-line fura2 ratio (*B*) of the first minute of measurement were calculated and plotted as the means ± S.E. *n.s.*, not significant; *, $p < 0.05$, ANOVA with Tukey's post hoc test.

STIM1 Expression in STIM1 KO Cells Restores SOCE and Protects from Oxidative Stress—We stably transfected STIM1-EYFP, DA STIM1-D76N/D78N-EYFP (14), or EYFP alone into STIM1 KO MEFs and verified the expression by immunoblotting (Fig. 3*A*). In line with the presumed dominant active phenotype of DA-STIM1, we observed an increased SOCE in DA-STIM1-EYFP > STIM1-EYFP > EYFP (Fig. 3*B*). This demonstrated a successful overexpression of both STIM1 isoforms. Survival assays with transfected cells showed that STIM1-EYFP-overexpressing cells were protected against oxidative glutamate toxicity and GSH depletion induced by BSO (Fig. 3*C*), which was even further increased by transient co-transfection of ORAI1-EYFP in the case of oxidative glutamate toxicity (Fig. 3*C*). DA-STIM1-EYFP-transfected cells, in contrast, were more susceptible to both stressors, which was independent of ORAI1 because transient ORAI1-EYFP co-expression had no further effect on the resistance of these cells (Fig. 3*D*).

We also examined the thapsigargin-releasable Ca^{2+} pool and the total cellular Ca^{2+} content in these cells and observed no differences between EYFP and STIM1-EYFP (Fig. 4*A*).

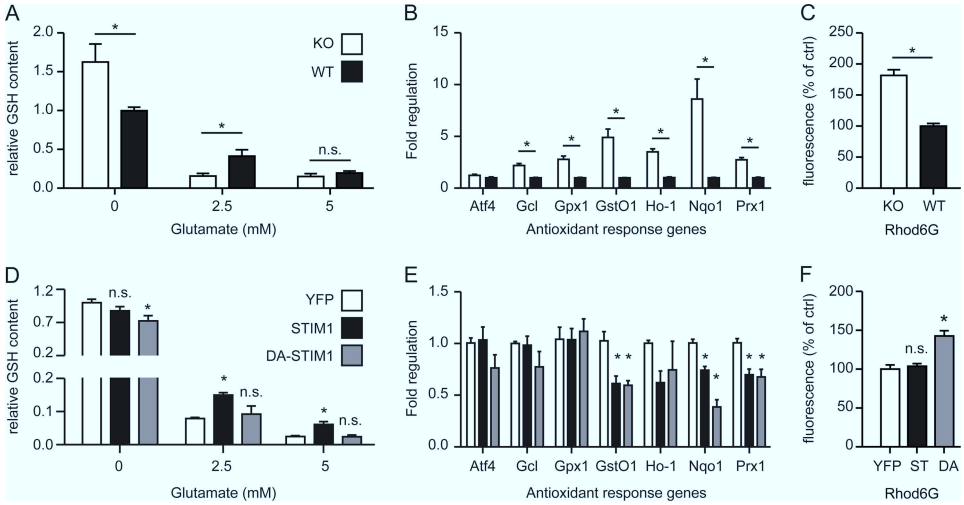

FIGURE 5. **Increased oxidative stress in STIM1 KO cells is overcompensated under basal conditions.** *A* and *D*, enzymatic determination of whole cellular GSH content in STIM1 WT and KO MEFs (*A*) or stably STIM1-EYFP and DA-STIM1-EYFP transfected KO cells (*D*) treated with the indicated concentrations of glutamate for 8 h in three independent experiments. GSH concentrations were normalized to cellular protein content and plotted as GSH content relative to untreated WT or YFP sample as the means ± S.E. *B* and *E*, real time RT-PCR analysis of mRNA levels of indicated antioxidant response genes in STIM1 WT and KO cells (*B*) or stably STIM1-EYFP expressing KO MEFs (*E*). The signals were normalized to *hprt* mRNA abundance and plotted in bar graphs as fold regulation over WT and EV samples. *C* and *F*, cellular ROS load of WT and STIM1 KO MEFs (*C*) or stably empty vector (*YFP*), STIM1-EYFP (*ST*), or DA-STIM1-EYFP (*DA*) expressing STIM1 KO MEFs (*F*) was quantitated by flow cytometry using rhodamine-6G fluorescence. The *bar graphs* represent mean relative fluorescence over WT and EYFP ± S.E. of three independent experiments each performed in triplicate. *n.s.*, not significant; *, $p < 0.05$, Student's *t* test (*A–C*) or ANOVA with Tukey's post hoc test (*D–F*).

DA-STIM1-EYFP, however, induced a reduction in ER and total cellular Ca^{2+} and a substantial increase of the base-line cytosolic [Ca^{2+}] in the presence of extracellular Ca^{2+} (Fig. 4*B*).

Our data suggest that STIM1 and SOCE play a role in oxidative stress, which is probably not mediated via the changes in the thapsigargin-releasable Ca^{2+} pool and the total cellular Ca^{2+} content. Also, STIM1 activation can apparently become detrimental, as shown by the deleterious effects of DA-STIM1-EYFP, which implies that SOCE must be delicately balanced and regulated to avoid unfavorable overactivation.

Increased Oxidative Stress in STIM1 KO Cells Is Overcompensated under Basal Conditions—In oxidative glutamate toxicity, cell death is mediated by GSH depletion. We therefore quantitated the GSH content of WT and STIM1 KO MEFs before and after glutamate challenge, which showed an elevated base-line GSH in STIM1 KO cells that nevertheless dropped to significantly lower levels after glutamate treatment (Fig. 5*A*). This increased GSH content at base line was also reflected by increased basal transcription of genes involved in the antioxidant response quantitated by real time PCR (Fig. 5*B*). We observed a significant up-regulation of glutamate-cysteine ligase (*Gcl*), glutathione peroxidase 1 (*Gpx1*), glutathione *S*-transferase ω-1 (*GstO1*), heme-oxygenase 1 (*Ho-1*), NAD(P)H quinone oxidoreductase 1 (*Nqo1*), and peroxiredoxin 1 (*Prx1*). These data suggested that STIM1 deficiency causes constitutive oxidative stress, which is counteracted by an up-regulation of the antioxidant response battery, which can still not cope with additional exogenous oxidative stress. We therefore quantitated reactive oxygen species (ROS) produced by the mitochondria of STIM1 KO and WT cells by using the fluorescent dye dihydrorhodamin 6G. In line with our hypothesis, we observed an increased ROS content of STIM1 KO mitochondria (Fig. 5*C*).

We were able to rescue these effects in our stably transfected cells. Here, DA-STIM1-EYFP overexpression had a negative effect on base-line GSH, whereas only STIM1-EYFP overexpression but not DA-STIM1-EYFP preserved GSH content after glutamate challenge (Fig. 5*D*). The induction of the antioxidant response gene expression was also significantly reversed for *GstO1*, *Nqo1*, and *Prx1* but not for *Gcl*, *Gpx1*, and *Ho-1* without a significant difference between the two STIM1 variants suggesting additional factors (Fig. 5*E*). The base-line mitochondrial ROS production, in contrast, was again similar to base-line GSH content, not different between EYFP and STIM1-EYFP-expressing cells but significantly increased in cells expressing the detrimental dominant active variant of STIM1 (Fig. 5*F*). We conclude that lack of STIM1, as well as constitutive STIM1 activity, results in an imbalance of ROS production and detoxification.

The Up-regulated Antioxidant Response in STIM1 KO Cells Is Mediated via NRF2 and Phosphorylated eIF2α—To identify the mechanisms responsible for the observed up-regulation of the antioxidant response battery in STIM1 KO cells, we considered enhanced expression and translocation of the transcription factor nuclear factor erythroid 2-related factor 2 (NRF2), which binds to antioxidant response elements in the promoters of the up-regulated protective genes. By high content fluorescence microscopy, we quantitated NRF2 immunofluorescence intensity in the nucleus, which was identified by Hoechst staining, and the surrounding cytoplasm resembled by a concentric ring around the nucleus (Fig. 6*A*). The ratio of nuclear fluorescence to cytoplasmic fluorescence serves as a quantitative and very sensitive measure for nuclear translocation. NRF2 was indeed found to be significantly increased in the nucleus of STIM1 KO cells (Fig. 6*A*). NRF2 is known to be regulated by Kelch-like ECH-associated protein 1 (KEAP1), which under normal con-

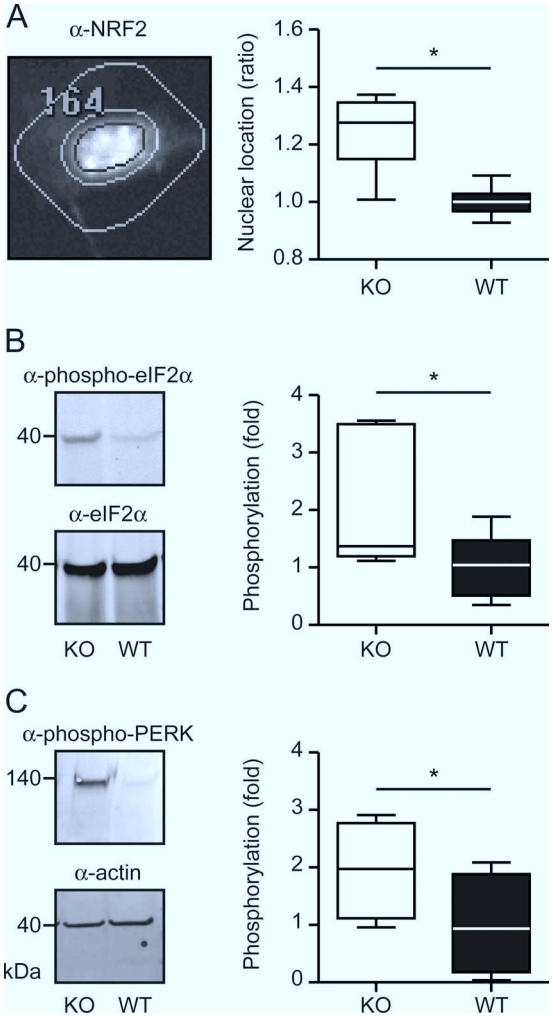

FIGURE 6. **The up-regulated antioxidant response in STIM1 KO cells is mediated via NRF2 and phosphorylated eIF2α.** *A*, translocation of NRF2 from the cytosol to the nucleus was analyzed by immunofluorescence in STIM1 WT and KO MEFs. NRF2 immunofluorescence intensity was quantified on a BD Pathway high content imaging system in the nucleus, which was identified by Hoechst staining, and the surrounding cytoplasm represented by a concentric ring around the nucleus. This method of segmentation is illustrated in the *left panel*. The ratio of nuclear to cytosolic NRF2 signal was calculated and normalized to WT signal. The graphs represent the means ± S.E. of 4468 WT and 3331 KO cells measured in three independent experiments each done in quintuplicates. *B* and *C*, immunoblot analysis of the phosphorylation state of eIF2α (*B*) or PERK (*C*). The blots were incubated with phosphorylation sensitive and insensitive antibodies against eIF2α (*B*) or phosphorylation-sensitive antibody against PERK and an antibody against actin as a loading control (*C*). Intensity values were calculated with the image analysis software ImageJ and normalized to WT control. The graphs represent the means ± S.E. of three independent experiments. *n.s.*, not significant; *, $p < 0.05$, Student's *t* test.

ditions binds NRF2 in the cytoplasm and marks it for degradation by the proteasome system (24). An increase in the cellular ROS level is sensed by KEAP1 through reactive cysteine groups, resulting in release of NRF2, which then translocates to the nucleus and activates antioxidant genes (25). Additionally, NRF2 can be activated by phosphorylated PERK (26). We therefore examined the phosphorylation state of PERK and an established PERK substrate, eIF2α, which plays a role in protection against oxidative stress (27), by immunoblotting. Both proteins were significantly hyperphosphorylated in STIM1 KO MEFs compared with WT MEFs (Fig. 6, *B* and *C*), proposing that phosphorylated PERK triggers NRF2 translocation, resulting in increased expression of antioxidant response genes in STIM1 KO cells. Moreover, the phosphorylated form of eIF2a can activate system Xc^- expression via nuclear factor ATF4, contributing to oxidative stress defense (27).

We conclude from these data that STIM1 KO cells exhibit a strong basal activation of antioxidative defense mechanisms triggered by NRF2 translocation and system Xc^- up-regulation through eIF2α phosphorylation. Despite these defense mechanisms, STIM1 KO cells are not able to cope with additional oxidative stress challenges.

Mitochondria of STIM1 KO Cells Are More Densely Packed and Have a Tubular Shape—Mitochondria are the main source of ROS in living cells, and their shape and function is critically dependent on intracellular Ca^{2+} signaling. Mitochondria also influence SOCE signals by shuttling Ca^{2+} released from the ER back to this intracellular store, which prevents luminal depletion (28), and they have a role in relaying Ca^{2+} signals from the plasma membrane to the ER (3). We therefore investigated mitochondrial shape and relationship with other organelles in WT and STIM1 KO MEFs by transmission electron microscopy and recognized distinct morphological differences. KO mitochondria appeared smaller, thinner, and more densely packed (Fig. 7*A*). This difference was statistically significant because the diameter of KO mitochondria, which were sectioned in a random fashion, amounted to KO 432 ($n = 523$, S.E. ±7.651) and WT 547.7 nm ($n = 523$, S.E. ±8.258) (Fig. 7*B*). Possible hot spots of ER mitochondria cross-talk like the distance between the ER and mitochondria (Fig. 7*D*) or areas of direct contact defined by a distance of less than 100 nm (Fig. 7*C*) were identical between KO and WT cells.

Mitochondria constantly fuse and divide, resulting in distinct shapes ranging from tubular to fragmented. These processes are highly dynamic and important for mitochondrial bioenergetics and cellular survival (reviewed in Ref. 29). Glutamate toxicity was previously shown to cause mitochondrial fragmentation and perinuclear accumulation (30). We therefore investigated the mitochondrial shape in STIM1 KO and WT cells and changes in response to glutamate in more detail. We transfected KO and WT cells with a mitochondrial targeted red fluorescent protein and treated the cells with 2.5 mM glutamate or vehicle overnight. After fixation, the mitochondrial shape was analyzed by fluorescence microscopy, and 100 cells for each condition were categorized by a blinded investigator. Categories were defined as healthy cells with fragmented mitochondria, healthy cells with tubular mitochondria, apoptotic cells with fragmented mitochondria, or apoptotic cells with tubular mitochondria (Fig. 7*E*). This analysis revealed a more tubular shape for mitochondria of STIM1 KO cells under basal conditions and also after overnight exposure to glutamate (Fig. 7*F*). Apparently, STIM1 KO cells possess more densely packed and elongated mitochondria, which raised the question about their metabolic activity.

Mitochondria from STIM1 KO Cells Are More Metabolically Active and More Susceptible to Nuclear Translocation of Apoptosis-inducing Factor—We therefore studied mitochondrial function by staining WT and KO cells with the mitochondrial Ca^{2+} reporter Rhod2-AM or the mitochondrial membrane

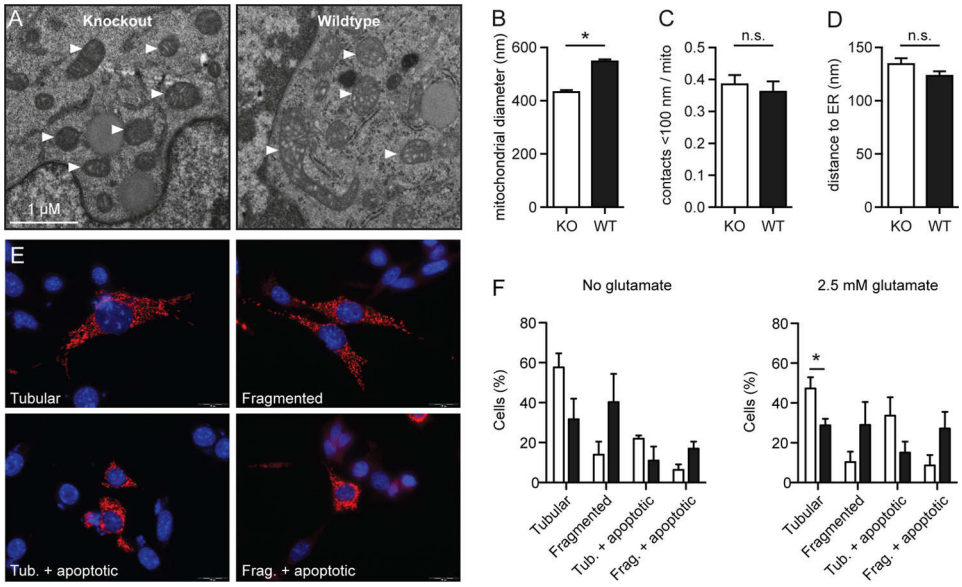

FIGURE 7. **Mitochondria of STIM1 KO cells are more densely packed and have a tubular shape.** *A*, electron microscopic images of STIM1 WT and KO MEFs were captured on a Hitachi H 600 microscope, and several morphological parameters from 523 KO mitochondria distributed over 30 visual fields and 523 WT mitochondria in 32 visual fields were quantitated and expressed as the means ± S.E. *B*, length of the mitochondrial cut surface. *C*, number of direct contacts of mitochondria to ER membranes defined by a distance of less than 100 nm divided by the number of mitochondria. *D*, distance between mitochondria and the nearest ER membrane. *E*, typical pictures of the four categories of mitochondrial shape. Healthy cells are flat and outstretched, whereas apoptotic cells appear smaller and rounded. Tubular mitochondria show a long filamentous shape, whereas fragmented mitochondria appear small and rounded. *F*, quantitative analysis of mitochondrial shape of WT and STIM1 KO cells with or without glutamate treatment (2.5 mM overnight). 100 cells of each condition were analyzed with a 60× objective and categorized by their mitochondrial shape by a blinded investigator. The *bar graphs* represent the means ± S.E. of three independently performed experiments. *n.s.*, not significant; *, $p < 0.05$, Student's *t* test. *Tub.*, tubular mitochondria; *Frag.*, fragmented mitochondria.

potential sensor TMRE. STIM1 KO MEFs exhibited significantly increased fluorescence of both Rhod2-AM (Fig. 8*A*) and TMRE (Fig. 8*B*), indicating high $[Ca^{2+}]_m$ and a higher mitochondrial membrane potential in line with the increased superoxide production shown in Fig. 5*C*. Mitochondria from STIM1 KO cells are thus elongated, densely packed, and more metabolically active, leading to an increased ROS concentration under basal conditions.

Oxidative glutamate toxicity proceeds in a well defined manner and includes release of apoptosis-inducing factor (AIF) from the mitochondria at the end of the cascade. AIF translocates to the nucleus in response to glutamate (Fig. 8*C*), where it triggers nuclear condensation and completion of the cell death program (31). Because this translocation is not only involved in endogenous oxidative stress but also dependent on the activity of the Ca^{2+}-dependent cysteine protease calpain 1 (32), we suspected that AIF might contribute to the observed susceptibility of STIM1-deficient cells to GSH depletion. In an imaging-based translocation assay, we indeed observed an increased amount of nuclear AIF relative to cytosolic AIF in STIM1 KO cells already under basal conditions, which increased in a concentration-dependent manner after glutamate treatment and always remained above WT levels in all conditions (Fig. 8*D*). Stable STIM1-EYFP expression did not serve to rescue the elevated ratio of nuclear/cytosolic AIF signal in untreated cells but impeded the translocation of AIF to the nucleus after glutamate exposure (Fig. 8*E*). Cells expressing DA-STIM1-EYFP instead showed an elevated base-line translocation of AIF together with a more pronounced translocation in response to glutamate, consistent with their increased susceptibility against oxidative stress.

DISCUSSION

Our results suggest that SOCE plays a role in cellular susceptibility to oxidative stress. We found that inhibition of SOCE by knock-out of STIM1 or knockdown of ORAI1 rendered fibroblasts more susceptible to oxidative stress, whereas re-expression of STIM1 in STIM1 KO MEFs restored SOCE activity and simultaneously protected from oxidative stress. STIM1-EYFP alone, thus without co-transfected ORAI1, did not restore SOCE to WT levels, probably because of a not-optimal ratio between STIM1 and endogenous ORAI1, which is important for SOCE (15). This is also reflected by the observation that co-transfection of ORAI1 together with STIM1-EYFP still increased the resistance of STIM1 KO cells to oxidative glutamate toxicity. We therefore conclude that the STIM1:ORAI1 ratio is difficult to adjust, which causes an incomplete repair of oxidative stress resistance. In contrast to this previous study, STIM1 was overexpressed in a STIM1-deficient background, which probably explains the effects on SOCE and cell death even in the absence of co-transfected ORAI1. It is also conceivable that the recently reported glutathionylation of STIM1 in response to oxidative stress, which results in its constitutive activation (22), renders the insufficient SOCE mediated by STIM1-EYFP rescue into just enough SOCE to be beneficial under the circumstances of glutathione depletion.

In contrast to our assumptions, we found that STIM1 KO cells contained more Ca^{2+} in the intracellular stores. In the presence of extracellular Ca^{2+}, the cytosolic Ca^{2+} concentration was reduced. This probably reflects the activity of compensating proteins like STIM2, which has been implicated in the control of cytosolic and ER Ca^{2+} levels (33), although we did

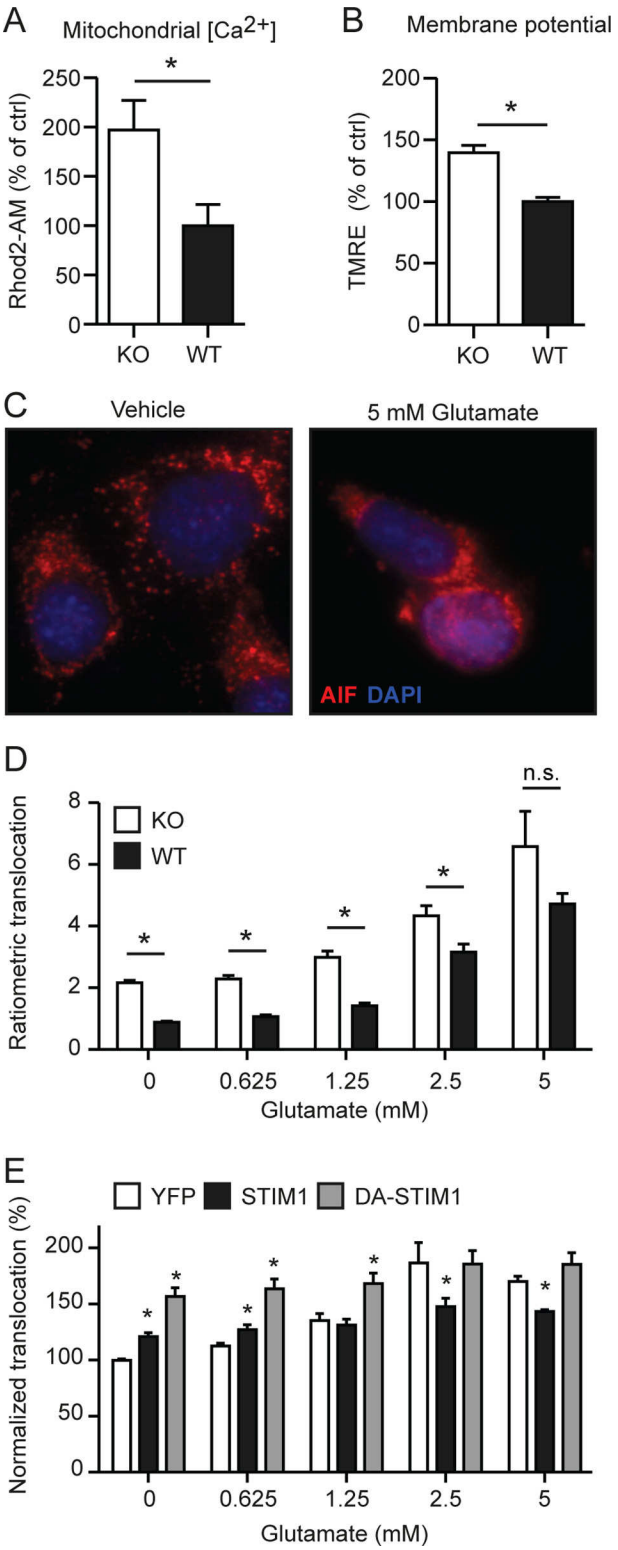

FIGURE 8. **Mitochondria from STIM1 KO cells are more metabolically active and more susceptible to nuclear translocation of apoptosis-inducing factor.** *A* and *B*, STIM1 KO MEFs show increased mitochondrial [Ca^{2+}] measured with Rhod2-AM (*A*) and increased membrane potential measured with TMRE (*B*). The mean fluorescence intensities were analyzed in triplicate on a flow cytometer in three independent experiments, normalized to WT samples, and plotted as the means ± S.E. *C*, immunocytochemistry of AIF shows nuclear translocation after 16 h of incubation with 5 mM glutamate. *D* and *E*, AIF localization was analyzed in STIM1 WT and KO MEFs (*D*) or stably empty vector (*YFP*), STIM1-EYFP (*STIM1*), or DA-STIM1-EYFP (*DA-STIM1*) transfected KO MEFs in response to glutamate (*E*). The cells were treated with indicated concentrations of glutamate for 16 h, 24 h after seeding in 96-well plates. After immunostaining, AIF fluorescence was analyzed on a BD Pathway high content imaging system, and the ratio of nuclear to cytosolic AIF signal was calculated. The *bar graphs* represent the means ± S.E. of three independent experiments each done in quintuplicate. In total, 80,099 WT and 42,750 KO cells were analyzed for *D*, and 45,238 YFP-expressing, 47,320 STIM1-EYFP expressing, and 22,092 DA-STIM1 expressing cells were analyzed for *E*. *n.s.*, not significant; *, $p < 0.05$, ANOVA with Tukey's post hoc test.

not observe any changes in the abundance of this protein (Fig. 1*B*). Alternatively, STIM1 deficiency might increase SERCA activity as a compensatory mechanism. Not all these differences were rescued by stable expression of STIM1-EYFP, probably because of the above mentioned difficulties in adjusting ORAI1 expression. DA-STIM1-EYFP, however, reversed the effects of STIM1 deficiency in regard to Ca^{2+} homeostasis; DA-STIM1-EYFP reduced the cellular Ca^{2+} content and increased the cytosolic Ca^{2+} concentration, which could be interpreted in a way that active STIM1 in the punctae inhibits SERCA activity. STIM1 and SERCA were already shown to co-localize in punctae (16) and to interact with each other upon store depletion (34). However, a physiologic inhibition of SERCA activity by STIM1 in the punctae conformation would be completely counterintuitive; active STIM1 should rather increase SERCA activity to rapidly remove cytosolic Ca^{2+} entering through SOCE. A possible explanation for such an inhibition might be that elevated amounts of reactive oxygen species, as found in DA-STIM1-EYFP-overexpressing cells, inhibit SERCA function (35) by the formation of a disulfide bond mediated via Erp57 (36), which was only recently discovered to interact with STIM1 and regulate SOCE activity (37). In any case, we think that it is very possible that such a constitutive inhibition of SERCA activity renders cells more susceptible to oxidative stress and thus mediates the detrimental effect of DA-STIM1-EYFP.

Because we observed an effect of STIM1-EYFP on oxidative stress but no significant effects on the intracellular Ca^{2+} homeostasis, we considered additional effects of STIM1 on the cellular redox regulation and analyzed the GSH content, ROS production, and expression of antioxidative defense genes in these cells. Under ideal conditions, we observed that the lack of STIM1 appeared to be even beneficial: there was an increase in cellular glutathione content, which was most likely mediated by an up-regulation of the antioxidant response through increased translocation of NRF2 to the nucleus where it binds antioxidant response elements in promoter regions and thereby triggers the expression of antioxidative defense genes. Under normal conditions NRF2 is prevented from entering the nucleus by binding to KEAP1 (24). Together with Cullin 3, KEAP1 builds an E3 ubiquitin ligase that actively targets NRF2 for degradation by the proteasome system, resulting in a very short half-life of NRF2 (38). Increased amounts of ROS as observed in STIM1 KO cells can modify reactive cysteine residues of KEAP1 releasing NRF2 and permitting its translocation to the nucleus (25). Additionally, PERK was found to be hyperphosphorylated in STIM1 KO cells, which also triggers NRF2 translocation (26) and promotes phosphorylation of eIF2α, a transcription factor enhancing expression of system Xc^- (27), an important component of the antioxidative defense machinery. In summary,

these results disclose that STIM1 KO MEFs suffer from an increased basal oxidative stress level, which promotes defense mechanisms to detoxify the high amount of ROS produced in these cells. However, under additional oxidative stress this system collapses, suggesting that this compensation is already at the edge under normal conditions or that it cannot be adapted to increased demand of antioxidant mechanisms.

Under unchallenged conditions, we also observed an increased mitochondrial Ca^{2+} concentration and a higher membrane potential. Both indicate increased mitochondrial respiratory activity probably necessary to generate ATP to run compensatory mechanisms. These changes in mitochondrial function were also accompanied by changes in mitochondrial shape and integrity. The changes in integrity mirrored the effects on protection against oxidative stress, which suggests a connection. We suspect that the increase in mitochondrial respiration, which elevates ROS production, renders the mitochondria more prone to release of AIF, which has been shown to play an imminent role in cell death mediated by glutathione depletion previously (31). We therefore conclude that the increased metabolic activity observed in STIM1 KO cells, which is probably necessary to compensate for SOCE deficiency, renders mitochondria more prone to permeabilization of the outer mitochondrial membrane and that this mediates the increased susceptibility to oxidative stress.

Our results indicate that the intact SOCE machinery enables the cell to carefully balance energy production and ROS detoxification. Loss of STIM1 or gain of function apparently precludes proper adaption to cellular energy needs and can be beneficial or detrimental depending on the cellular circumstances. This is well in line with the current literature where numerous different outcomes of cellular fate were reported in dependence of STIM1. In malignant melanoma cells or C6 glioma cells, STIM1-mediated signaling within an intact SOCE machinery was described to be essential for cell survival (20, 21). Ca^{2+}-independent activation of STIM1 through glutathionylation (22) or strong activation of SOCE on soft substrates in cervical endothelial cells (19) seems to be detrimental. These results suggest that STIM1 and SOCE play a role in the antioxidant response and are involved in the regulation of cellular energy production.

Acknowledgment—We thank Andrea Issberner for excellent technical support.

REFERENCES

1. Takemura, H., and Putney, J. W. (1989) Capacitative calcium entry in parotid acinar cells. *Biochem. J.* **258,** 409–412
2. Takemura, H., Hughes, A. R., Thastrup, O., and Putney, J. W. (1989) Activation of calcium entry by the tumor promoter thapsigargin in parotid acinar cells. Evidence that an intracellular calcium pool and not an inositol phosphate regulates calcium fluxes at the plasma membrane. *J. Biol. Chem.* **264,** 12266–12271
3. Malli, R., Frieden, M., Osibow, K., Zoratti, C., Mayer, M., Demaurex, N., and Graier, W. F. (2003) Sustained Ca^{2+} transfer across mitochondria is Essential for mitochondrial Ca^{2+} buffering, sore-operated Ca^{2+} entry, and Ca^{2+} store refilling. *J. Biol. Chem.* **278,** 44769–44779
4. Frieden, M., Arnaudeau, S., Castelbou, C., and Demaurex, N. (2005) Subplasmalemmal mitochondria modulate the activity of plasma membrane Ca^{2+}-ATPases. *J. Biol. Chem.* **280,** 43198–43208
5. Jousset, H., Frieden, M., and Demaurex, N. (2007) STIM1 knockdown reveals that store-operated Ca^{2+} channels located close to sarco/endoplasmic Ca^{2+} ATPases (SERCA) pumps silently refill the endoplasmic reticulum. *J. Biol. Chem.* **282,** 11456–11464
6. Jouaville, L. S., Pinton, P., Bastianutto, C., Rutter, G. A., and Rizzuto, R. (1999) Regulation of mitochondrial ATP synthesis by calcium. Evidence for a long-term metabolic priming. *Proc. Natl. Acad. Sci. U.S.A.* **96,** 13807–13812
7. Roos, J., DiGregorio, P. J., Yeromin, A. V., Ohlsen, K., Lioudyno, M., Zhang, S., Safrina, O., Kozak, J. A., Wagner, S. L., Cahalan, M. D., Veliçelebi, G., and Stauderman, K. A. (2005) STIM1, an essential and conserved component of store-operated Ca^{2+} channel function. *J. Cell Biol.* **169,** 435–445
8. Liou, J., Kim, M. L., Heo, W. D., Jones, J. T., Myers, J. W., Ferrell, J. E., Jr., and Meyer, T. (2005) STIM is a Ca^{2+} sensor essential for Ca^{2+}-store-depletion-triggered Ca^{2+} influx. *Curr. Biol.* **15,** 1235–1241
9. Wu, M. M., Buchanan, J., Luik, R. M., and Lewis, R. S. (2006) Ca^{2+} store depletion causes STIM1 to accumulate in ER regions closely associated with the plasma membrane. *J. Cell Biol.* **174,** 803–813
10. Zhang, S. L., Yeromin, A. V., Zhang, X. H., Yu, Y., Safrina, O., Penna, A., Roos, J., Stauderman, K. A., and Cahalan, M. D. (2006) Genome-wide RNAi screen of Ca^{2+} influx identifies genes that regulate Ca^{2+} release-activated Ca^{2+} channel activity. *Proc. Natl. Acad. Sci. U.S.A.* **103,** 9357–9362
11. Prakriya, M., Feske, S., Gwack, Y., Srikanth, S., Rao, A., and Hogan, P. G. (2006) Orai1 is an essential pore subunit of the CRAC channel. *Nature* **443,** 230–233
12. Mignen, O., Thompson, J. L., and Shuttleworth, T. J. (2008) Orai1 subunit stoichiometry of the mammalian CRAC channel pore. *J. Physiol.* **586,** 419–425
13. Zhang, S. L., Yu, Y., Roos, J., Kozak, J. A., Deerinck, T. J., Ellisman, M. H., Stauderman, K. A., and Cahalan, M. D. (2005) STIM1 is a Ca^{2+} sensor that activates CRAC channels and migrates from the Ca^{2+} store to the plasma membrane. *Nature* **437,** 902–905
14. Mercer, J. C., Dehaven, W. I., Smyth, J. T., Wedel, B., Boyles, R. R., Bird, G. S., and Putney, J. W. (2006) Large store-operated calcium selective currents due to co-expression of Orai1 or Orai2 with the intracellular calcium sensor, Stim1. *J. Biol. Chem.* **281,** 24979–24990
15. Soboloff, J., Spassova, M. A., Tang, X. D., Hewavitharana, T., Xu, W., and Gill, D. L. (2006) Orai1 and STIM reconstitute store-operated calcium channel function. *J. Biol. Chem.* **281,** 20661–20665
16. Manjarrés, I. M., Rodríguez-García, A., Alonso, M. T., and García-Sancho, J. (2010) The sarco/endoplasmic reticulum Ca^{2+} ATPase (SERCA) is the third element in capacitative calcium entry. *Cell Calcium* **47,** 412–418
17. Zhivotovsky, B., and Orrenius, S. (2011) Calcium and cell death mechanisms. A perspective from the cell death community. *Cell Calcium* **50,** 211–221
18. Sabbioni, S., Barbanti-Brodano, G., Croce, C. M., and Negrini, M. (1997) GOK. A gene at 11p15 involved in rhabdomyosarcoma and rhabdoid tumor development. *Cancer Res.* **57,** 4493–4497
19. Chiu, W.-T., Tang, M.-J., Jao, H.-C., and Shen, M.-R. (2008) Soft substrate up-regulates the interaction of STIM1 with store-operated Ca^{2+} channels that lead to normal epithelial cell apoptosis. *Mol. Biol. Cell* **19,** 2220–2230
20. Feldman, B., Fedida-Metula, S., Nita, J., Sekler, I., and Fishman, D. (2010) Coupling of mitochondria to store-operated Ca^{2+}-signaling sustains constitutive activation of protein kinase B/Akt and augments survival of malignant melanoma cells. *Cell Calcium* **47,** 525–537
21. Liu, H., Hughes, J. D., Rollins, S., Chen, B., and Perkins, E. (2011) Calcium entry via ORAI1 regulates glioblastoma cell proliferation and apoptosis. *Exp. Mol. Pathol.* **91,** 753–760
22. Hawkins, B. J., Irrinki, K. M., Mallilankaraman, K., Lien, Y.-C., Wang, Y., Bhanumathy, C. D., Subbiah, R., Ritchie, M. F., Soboloff, J., Baba, Y., Kurosaki, T., Joseph, S. K., Gill, D. L., and Madesh, M. (2010) *S*-Glutathionylation activates STIM1 and alters mitochondrial homeostasis. *J. Cell Biol.* **190,** 391–405
23. Albrecht, P., Lewerenz, J., Dittmer, S., Noack, R., Maher, P., and Methner, A. (2010) Mechanisms of oxidative glutamate toxicity. The glutamate/

cystine antiporter system Xc^- as a neuroprotective drug target. *CNS Neurol. Disord. Drug Targets* **9,** 373–382
24. Itoh, K., Wakabayashi, N., Katoh, Y., Ishii, T., Igarashi, K., Engel, J. D., and Yamamoto, M. (1999) Keap1 represses nuclear activation of antioxidant responsive elements by Nrf2 through binding to the amino-terminal Neh2 domain. *Genes Dev.* **13,** 76–86
25. Yamamoto, T., Suzuki, T., Kobayashi, A., Wakabayashi, J., Maher, J., Motohashi, H., and Yamamoto, M. (2008) Physiological significance of reactive cysteine residues of Keap1 in determining Nrf2 activity. *Mol. Cell. Biol.* **28,** 2758–2770
26. Cullinan, S. B., Zhang, D., Hannink, M., Arvisais, E., Kaufman, R. J., and Diehl, J. A. (2003) Nrf2 is a direct PERK substrate and effector of PERK-dependent cell survival. *Mol. Cell. Biol.* **23,** 7198–7209
27. Lewerenz, J., and Maher, P. (2009) Basal levels of eIF2α phosphorylation determine cellular antioxidant status by regulating ATF4 and xCT expression. *J. Biol. Chem.* **284,** 1106–1115
28. Arnaudeau, S., Kelley, W. L., Walsh, J. V., Jr., and Demaurex, N. (2001) Mitochondria recycle Ca^{2+} to the endoplasmic reticulum and prevent the depletion of neighboring endoplasmic reticulum regions. *J. Biol. Chem.* **276,** 29430–29439
29. Westermann, B. (2010) Mitochondrial fusion and fission in cell life and death. *Nat. Rev. Mol. Cell Biol.* **11,** 872–884
30. Grohm, J., Plesnila, N., and Culmsee, C. (2010) Bid mediates fission, membrane permeabilization and peri-nuclear accumulation of mitochondria as a prerequisite for oxidative neuronal cell death. *Brain Behav Immun.* **24,** 831–838
31. Landshamer, S., Hoehn, M., Barth, N., Duvezin-Caubet, S., Schwake, G., Tobaben, S., Kazhdan, I., Becattini, B., Zahler, S., Vollmar, A., Pellecchia, M., Reichert, A., Plesnila, N., Wagner, E., and Culmsee, C. (2008) Bid-induced release of AIF from mitochondria causes immediate neuronal cell death. *Cell Death Differ.* **15,** 1553–1563
32. Cao, G., Xing, J., Xiao, X., Liou, A. K., Gao, Y., Yin, X.-M., Clark, R. S., Graham, S. H., and Chen, J. (2007) Critical role of calpain I in mitochondrial release of apoptosis-inducing factor in ischemic neuronal injury. *J. Neurosci.* **27,** 9278–9293
33. Brandman, O., Liou, J., Park, W. S., and Meyer, T. (2007) STIM2 is a feedback regulator that stabilizes basal cytosolic and endoplasmic reticulum Ca^{2+} levels. *Cell* **131,** 1327–1339
34. Sampieri, A., Zepeda, A., Asanov, A., and Vaca, L. (2009) Visualizing the store-operated channel complex assembly in real time. Identification of SERCA2 as a new member. *Cell Calcium* **45,** 439–446
35. Kuster, G. M., Lancel, S., Zhang, J., Communal, C., Trucillo, M. P., Lim, C. C., Pfister, O., Weinberg, E. O., Cohen, R. A., Liao, R., Siwik, D. A., and Colucci, W. S. (2010) Redox-mediated reciprocal regulation of SERCA and Na^+-Ca^{2+} exchanger contributes to sarcoplasmic reticulum Ca^{2+} depletion in cardiac myocytes. *Free Radic. Biol. Med.* **48,** 1182–1187
36. Li, Y., and Camacho, P. (2004) Ca^{2+}-dependent redox modulation of SERCA 2b by ERp57. *J. Cell Biol.* **164,** 35–46
37. Prins, D., Groenendyk, J., Touret, N., and Michalak, M. (2011) Modulation of STIM1 and capacitative Ca^{2+} entry by the endoplasmic reticulum luminal oxidoreductase ERp57. *EMBO Rep.* **12,** 1182–1188
38. Zhang, D. D., Lo, S.-C., Cross, J. V., Templeton, D. J., and Hannink, M. (2004) Keap1 is a redox-regulated substrate adaptor protein for a Cul3-dependent ubiquitin ligase complex. *Mol. Cell. Biol.* **24,** 10941–10953

The plasma membrane channel ORAI1 mediates detrimental calcium influx caused by endogenous oxidative stress

Nadine Henke[1], Philipp Albrecht[1], Imane Bouchachia[1], Maria Ryazantseva[2], Katrin Knoll[1], Jan Lewerenz[3], Elena Kaznacheyeva[2], Pamela Maher[4], and Axel Methner[1,5#]

[1]Department of Neurology, Heinrich-Heine Universität Düsseldorf, Düsseldorf, Germany, [2]Institute of Cytology, St. Petersburg, Russia, [3]University of Ulm, Department of Neurology, Germany, [4]Cellular Neurobiology Laboratory, Salk Institute for Biological Studies, La Jolla, CA, USA, [5]Focus Program Translational Neuroscience (FTN), Rhine Main Neuroscience Network (rmn2), Johannes Gutenberg University Medical Center Mainz, Department of Neurology, Langenbeckstr. 1, D-55131 Mainz, Germany

The presented manuscript is submitted to the Journal “Cell Death and Disease” (73).

Contribution of Nadine Henke, first author:

Experimental design: 50%
Execution and analysis of experiments: 75%
Manuscript writing: first draft, overall 75%

Citation: Cell Death and Disease (2013) 4, e470; doi:10.1038/cddis.2012.216

www.nature.com/cddis

The plasma membrane channel ORAI1 mediates detrimental calcium influx caused by endogenous oxidative stress

N Henke[1], P Albrecht[1], I Bouchachia[1], M Ryazantseva[2], K Knoll[1], J Lewerenz[3], E Kaznacheyeva[2], P Maher[4] and A Methner*[,1,5]

The mouse hippocampal cell line HT22 is an excellent model for studying the consequences of endogenous oxidative stress. Addition of extracellular glutamate depletes the cells of glutathione (GSH) by blocking the glutamate – cystine antiporter system x_c^-. GSH is the main antioxidant in neurons and its depletion induces a well-defined program of cell death called oxytosis, which is probably synonymous with the iron-dependent form of non-apoptotic cell death termed ferroptosis. Oxytosis is characterized by an increase of reactive oxygen species and a strong calcium influx preceding cell death. We found a significant reduction in store-operated calcium entry (SOCE) in glutamate-resistant HT22 cells caused by downregulation of the Ca^{2+} channel ORAI1, but not the Ca^{2+} sensors STIM1 or STIM2. Pharmacological inhibition of SOCE mimicked this protection similarly to knockdown of ORAI1 by small interfering RNAs. Long-term calcium live-cell imaging after induction of the cell death program showed a specific reduction in Ca^{2+}-positive cells by ORAI1 knockdown. These results suggest that dysregulated Ca^{2+} entry through ORAI1 mediates the detrimental Ca^{2+} entry in programmed cell death induced by GSH depletion. As this detrimental Ca^{2+} influx occurs late in the course of the cell death program, it might be amenable to therapeutic intervention in diseases caused by oxidative stress.

Cell Death and Disease (2013) **4,** e470; doi:10.1038/cddis.2012.216; published online 24 January 2013
Subject Category: Neuroscience

Oxidative stress is a phenomenon involved in a broad range of pathological conditions of the nervous system such as Alzheimer's and Parkinson's disease, stroke and trauma. It is provoked by an imbalance between superoxide production in the mitochondria and insufficient clearance of reactive oxygen species (ROS) through antioxidative defense mechanisms of the cell. One major defense pathway of nerve cells against ROS depends on the production of glutathione (GSH), a tripeptide composed of glutamate, cysteine and glycine, via the enzymes glutamate – cysteine ligase and GSH synthetase. In its reduced state, GSH serves as electron donor to detoxify ROS and is thereby oxidized to form GSH disulfide. The recovery of GSH from GSH disulfide is mediated by GSH reductase under NADPH consumption.[1]

GSH depletion serves to study the effects of endogenous oxidative stress and can be excellently studied *in vitro* by treating cells with glutamate, which inhibits cystine uptake through the glutamate/cystine antiporter system x_c^-. Within the cell, cystine is rapidly converted to cysteine, the rate-limiting amino acid for GSH synthesis. Cystine deprivation then causes secondary GSH depletion and a programmed cell death by oxytosis or oxidative glutamate toxicity, which is clearly distinct from apoptosis, necrosis, and cell death associated with autophagy, but probably synonymous with the recently described iron-dependent form of non-apoptotic cell death termed ferroptosis, which seems to be involved in the selective elimination of some tumor cells and protection from neurodegeneration.[2]

A well-established model system for oxytosis/ferroptosis is glutamate-induced cell death in the hippocampal cell line HT22, which has been used extensively to clarify the cascade leading to cell death and to identify antioxidant pathways and

[1]Department of Neurology, Heinrich-Heine Universität Düsseldorf, Düsseldorf, Germany; [2]Institute of Cytology St. Petersburg, St. Petersburg, Russia; [3]University of Ulm, Department of Neurology, Ulm, Germany; [4]Cellular Neurobiology Laboratory, Salk Institute for Biological Studies, La Jolla, CA, USA and [5]Focus Program Translational Neuroscience (FTN), Rhine Main Neuroscience Network (rmn^2), Johannes Gutenberg University Medical Center Mainz, Department of Neurology, Mainz, Germany
*Corresponding author: Professor A Methner, Focus Program Translational Neuroscience (FTN), Rhine Main Neuroscience Network (rmn^2), Johannes Gutenberg University Medical Center Mainz, Department of Neurology, Langenbeckstr. 1, D-55131 Mainz, Germany, Tel: +49 6131 17 2695, Fax: +49 6131 17 5967; Email: axel.methner@gmail.com
Keywords: STIM1; SOCE; oxidative stress
Abbreviations: 2-APB, 2-aminoethoxydiphenyl borate; ANOVA, Analysis of variance; BSO, L-buthionine-(S,R) sulfoximine; cGMP, Cyclic guanosine monophosphate; CTB, Cell titer blue; EGTA, Ethylene glycol tetraacetic acid; ER, Endoplasmic reticulum; FCS, Fetal calf serum; GAPDH, Glyceraldehyde 3-phosphate dehydrogenase; GSH, Glutathione; HBSS, Hank's balanced salt solution; HPRT, Hypoxanthine-phosphoribosyltransferase; IP3, Inositol trisphosphate; IP3R, Inositol trisphosphate receptor; iPLA2β, Ca^{2+}-independent phospholipase A2; LOX, Lipoxygenase; MTT, 3-(4,5-Dimethylthiazol-2-yl)-2,5-diphenyltetrazolium bromide; NAC, *N*-acetyl-L-cysteine; NADPH, Nicotinamide adenine dinucleotide phosphate; PBS, Phosphate-buffered saline; pCPT-cGMP, 8-(4-chlorophenylthio)-guanosine 3′,5′-cyclic monophosphate; RFP, Red fluorescent protein; ROS, Reactive oxygen species; SEM, Standard error of the mean; SERCA, Sarcoplasmic/endoplasmic reticulum Ca2+-ATPase; SOCE, Store-operated calcium entry; STIM1, Stromal interaction molecule 1; STIM2, Stromal interaction molecule 2; TRPM7, Transient receptor potential melastatin 7
Received 4.10.12; revised 29.11.12; accepted 6.12.12; Edited by A Finazzi-Agro'

proteins (reviewed in[3]). In this system, GSH depletion leads to an exponential increase in ROS that mostly originates from mitochondrial complex I activity.[4] After ~6 h of glutamate exposure, the lipid-oxidizing enzyme 12/15-lipoxygenase (12/15- LOX; EC 1.13.11.33) is activated and generates 12- and 15- hydroxyeicosatetraenoic acids[5] that directly damage mitochondria, and cause mitochondrial depolarization and increased ROS production.[6] The eicosanoids produced by 12-LOX are, however, also activators of soluble guanylate cyclases and thereby increase the concentration of intracellular cyclic guanosine monophosphate (cGMP), resulting in a detrimental influx of calcium at the end of the cell death cascade through a yet uncharacterized cGMP-dependent calcium channel.[7] This Ca^{2+} influx is essential for the completion of the cell death program, as proven by the fact that glutamate-treated HT22 cells do not die when Ca^{2+} influx is blocked by $CoCl_2$ or in Ca^{2+}-free medium,[7–9] but the molecular identity of the contributing Ca^{2+} channels is still unknown.

To identify the mechanism of Ca^{2+} entry in the final phase of oxidative glutamate toxicity, we compared the cellular calcium state of glutamate-sensitive and resistant HT22 cells, which are resistant due to the increased expression of various proteins with antioxidant properties,[10–13] and found an isolated attenuation of store-operated calcium entry (SOCE) in the resistant cells. SOCE is activated when the endoplasmic reticulum (ER), the main cellular calcium store, is depleted, for example,. during inositol trisphosphate (IP3)-mediated signaling events. When a membrane receptor is activated by its ligand, IP3 is generated near the plasma membrane and quickly diffuses through the cytoplasm to reach its receptor (Inositol trisphosphate receptor, IP3R) at the ER membrane. Binding of IP3 to IP3R releases Ca^{2+} stored in the ER lumen and generates a cytosolic Ca^{2+} signal, resulting in ER Ca^{2+}-store depletion. To refill the ER, plasma membrane Ca^{2+} channels need to be activated to permit Ca^{2+} entry from the extracellular space, so-called SOCE. The molecule that transmits the information of $[Ca^{2+}]_{ER}$ to plasma membrane Ca^{2+} channels is stromal interaction molecule 1 (STIM1).[14,15] STIM1 clusters into punctae close to the plasma membrane upon store depletion and binds and activates ORAI1, a plasma membrane calcium channel.[16–18]

In this study, we provide evidence that dysregulated SOCE through ORAI1 is the main calcium entry mechanism during oxidative glutamate toxicity, suggesting that SOCE inhibition might be a valuable tool in the treatment of diseases associated with increased oxidative stress.

Results

Reduced store-operated Ca^{2+} entry in hippocampal cells resistant to oxidative stress. Glutamate-resistant HT22 cells are protected against oxidative glutamate toxicity (Figure 1a) mainly via an elevated GSH content due to an increased expression of the glutamate/cystine antiporter subunit xCT.[19] They also show an increased expression of other proteins with antioxidant properties.[10,11,13] We therefore reasoned that the function and expression of the sought-after detrimental Ca^{2+} channel might be altered in these cells and studied the content of the main cellular Ca^{2+} store, the ER, by staining the cells with the ratiometric Ca^{2+}-sensitive dye Fura2 followed by treatment with the irreversible sarcoplasmic/ER Ca^{2+}-ATPase (SERCA) inhibitor thapsigargin, which resulted in the expected biphasic cytosolic Ca^{2+} rise. Although HT22S and R cells behaved similarly during the first phase of Ca^{2+} rise, which corresponds to Ca^{2+} passively leaking out of the ER, the second phase of cytosolic Ca^{2+} rise was remarkably reduced in HT22R compared with HT22S cells (Figure 1b).

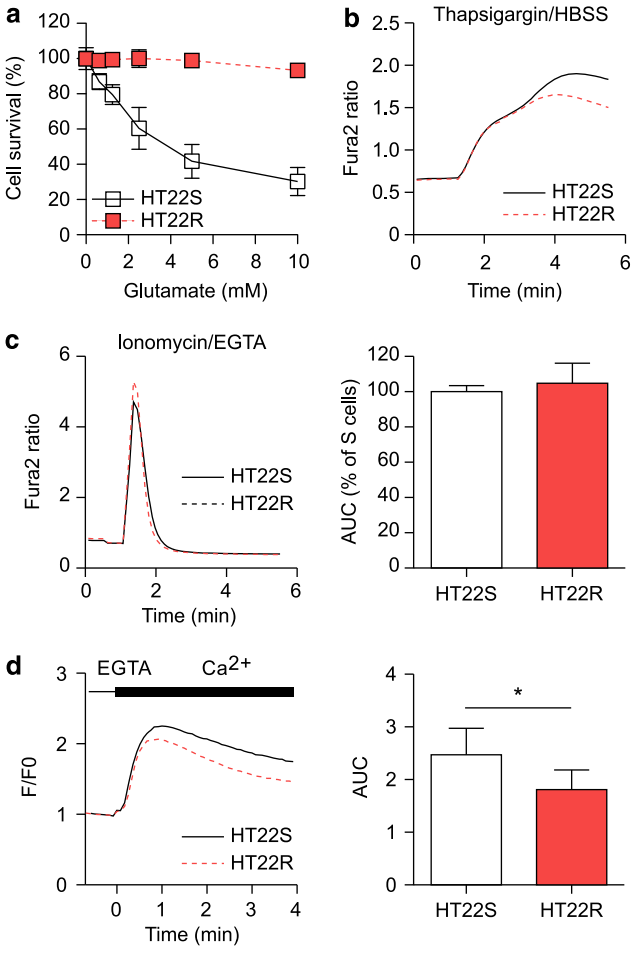

Figure 1 Reduced store-operated Ca^{2+} in hippocampal cells resistant to oxidative stress. (**a**) 5000 glutamate-sensitive and -resistant HT22S and R cells were seeded into 96-well plates and subjected to the indicated concentrations of glutamate 24 h later; viability was quantitated again 16 h later with the cell-titer blue reagent. Mean ± S.E.M. fluorescence values of three replicates obtained in three independent experiments were plotted against the glutamate concentration. (**b** – **d**) Fura2-live-cell imaging of glutamate-sensitive and -resistant HT22S and R cells. **(b)** After 1 min of baseline recording in HBSS, 2 μM of thapsigargin was added and the fura2 signal recorded for an additional 4 min. **(c)** After 30 s of baseline recording in HBSS with Ca^{2+}, EGTA was added. After a further 30 s, 5 μM of ionomycin was applied and the fura2 signal recorded for the following 4 min. (**d**) For measurement of SOCE, ER Ca^{2+} stores of HT22S and R cells were depleted by incubation in EGTA buffer supplemented with 2 μM thapsigargin. After 6 min of store depletion, the buffer was exchanged with HBSS supplemented with 1.26 mM Ca^{2+} and SOCE was recorded. Graph shows only Ca^{2+} readdition after store depletion. Graphs 1b and c show mean fura2 ratio of 20 – 30 individually-measured wells for each condition, containing altogether 2000 – 3000 cells. Graph 1d is pooled from nine wells for each condition containing >260 cells. For C and D, the area under the curve was calculated and plotted as mean ± S.E.M. in bar graphs. *$P<0.05$

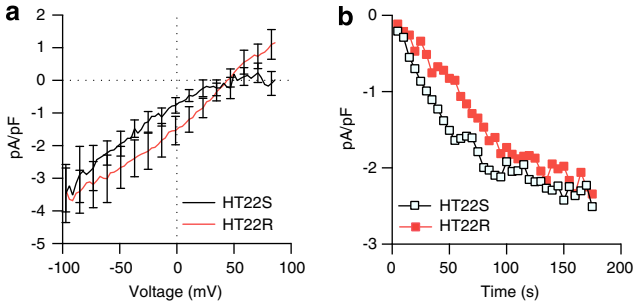

Figure 2 Different SOCE current characteristics in HT22S and glutamate-resistant HT22R cells. (**a**) Average I/V relationships for currents evoked by passive depletion of Ca^{2+} stores with 1 μM thapsigargin in HT22S (*black, n* = 6) and HT22R (*red, n* = 11) cells. The I/V relationships were measured when the currents reached the maximum. The data are shown as mean ± S.E.M., $P < 0.05$. (**b**) The average amplitude of SOCE currents recorded in whole-cell experiments is shown as a function of time after application of 1 μM thapsigargin to HT22S (black, *n* = 6) and HT22R (red, *n* = 11) cells. The current amplitudes were measured at each ramp at –80 mV test potentials. The data are shown as mean

We hypothesized that this second plateau corresponds to reduced SOCE and decided to delve further into this.

To distinguish between Ca^{2+} leaking from the ER and Ca^{2+} entering from outside the cell, we measured the whole-cellular Ca^{2+} store content and SOCE separately. Fura2-based Ca^{2+} live-cell imaging yielded no significant difference between HT22S and HT22R in the cytosolic Ca^{2+} rise induced by treatment with the Ca^{2+} ionophore ionomycin, which releases the whole-cellular Ca^{2+} content from the intracellular stores (Figure 1c). For measurement of SOCE activity, we depleted the ER Ca^{2+} store by addition of thapsigargin in EGTA buffer. After 6 min of store depletion, Ca^{2+} was readded and Ca^{2+} influx corresponding to SOCE was measured. In line with the data shown in Figure 1b, SOCE activity was significantly reduced in HT22R cells (Figure 1d).

To verify the reduced SOCE capacity of HT22R cells at the single cell level, we assessed SOCE activity by electrophysiological recordings using the whole-cell patch-clamp technique. Currents were evoked by application of 1 μM thapsigargin to achieve ER store depletion. Consistent with our results obtained in fura2 life – cell imaging experiments, HT22S and HT22R cells demonstrated different SOCE current – voltage (I/V) relation (Figure 2a). SOCE currents in HT22S cells revealed an inward rectification as expected for I_{CRAC} currents provided by ORAI1 channels, whereas SOCE currents in HT22R cells demonstrated a linear I/V relation with a reversal potential around + 40 mV. There was no difference in amplitude or speed of SOCE currents development in time in HT22S and HT22R cells (Figure 2b). These data are in line with an altered composition or abundance of I_{CRAC} channels in HT22R cells. We therefore set out to investigate the role of SOCE during oxidative glutamate toxicity.

Prolonged oxidative stress reduces the ER Ca^{2+} content and SOCE activity. Glutamate-resistant HT22R cells were continuously cultivated in medium containing 10 mM glutamate to preserve their resistant phenotype. To test whether glutamate directly or indirectly influences SOCE capacity, we aimed to measure SOCE activity in glutamate-treated HT22S cell. We also hypothesized that cytosolic cGMP might influence the SOCE capacity similarly to glutamate because the Ca^{2+} influx leading to cell death by oxytosis is preceded by a cytosolic increase of cGMP.[7] Application of 8-(4-chlorophenylthio)-guanosine 3′,5′-cyclic monophosphate (pCPT-cGMP), a cell-permeable cGMP analog, indeed induced death of HT22 cells in a concentration-dependent manner (Figure 3a) and opened plasma membrane Ca^{2+} channels resulting in a slow but pronounced cytosolic Ca^{2+} rise, which we measured with the genetically-encoded Ca^{2+} sensor GCaMP5, expressed from a bicistronic transcript together with the red fluorescent protein (RFP), to normalize the GCaMP5 signal to the level of transfection (Figure 3b).

We elicited SOCE by store depletion through thapsigargin-induced SERCA inhibition under Ca^{2+}-free conditions and subsequent restitution of Ca^{2+}. After 8 h of incubation with either glutamate or pCPT-cGMP, HT22S cells showed a reduced $[Ca^{2+}]_{ER}$ and reduced SOCE (Figure 3c). Addition of pCPT-cGMP or glutamate directly at the onset of measurement had no effect (Figure 3d). We therefore hypothesized that this reduction in $[Ca^{2+}]_{ER}$ and SOCE after induction of the cell death program might be a consequence of the endogenous oxidative stress that eventually kills the cells. And indeed, preventing oxidative stress with the antioxidant *N*-acetyl-L-cysteine (NAC) protected glutamate-treated cells from cell death (Figure 3e), and partially rescued the ER Ca^{2+} content as well as the SOCE capacity after 8 h of treatment (Figure 3f).

These results were of course not in line with our hypothesis that increased SOCE mediates the cytotoxic Ca^{2+} influx at the end of the cascade leading to cell death. We reasoned that the cell death program, which is already irreversible after 8 h of glutamate or 8-pCPT-cGMP treatments, alters many aspects of the intracellular Ca^{2+} homeostasis, which might obscure the effects on SOCE. We therefore decided to study the effect of SOCE on glutamate- and cGMP-induced cell death pharmacologically.

Pharmacological inhibition of SOCE protects against oxidative stress. We treated HT22 cells with a pharmacological inhibitor of SOCE, 2-aminoethoxydiphenyl borate (2-APB), and induced oxidative stress by addition of glutamate. 2-APB concentration-dependently protected against glutamate toxicity (Figure 4a) even when added up to 8 h after glutamate addition (Figure 4b). We also tested the ability of 2-APB to protect from pCPT-cGMP-induced cell death and observed a remarkable protective effect of 2-APB under these conditions, which was even stronger than that of the general Ca^{2+}-channel blocker $CoCl_2$ (Figure 4c). As 2-APB is a well-known inhibitor of SOCE and protects HT22 cells from oxidative glutamate toxicity and pCPT-cGMP even when applied several hours after induction of oxidative stress, these observations support the hypothesis that the detrimental, late-onset Ca^{2+} influx induced by endogenous oxidative stress is mediated via components of the SOCE machinery.

The SOCE Ca^{2+} influx channel ORAI1 is downregulated in glutamate-resistant HT22R cells. After clarifying that the observed reduction of SOCE in HT22R cells (Figures 1d

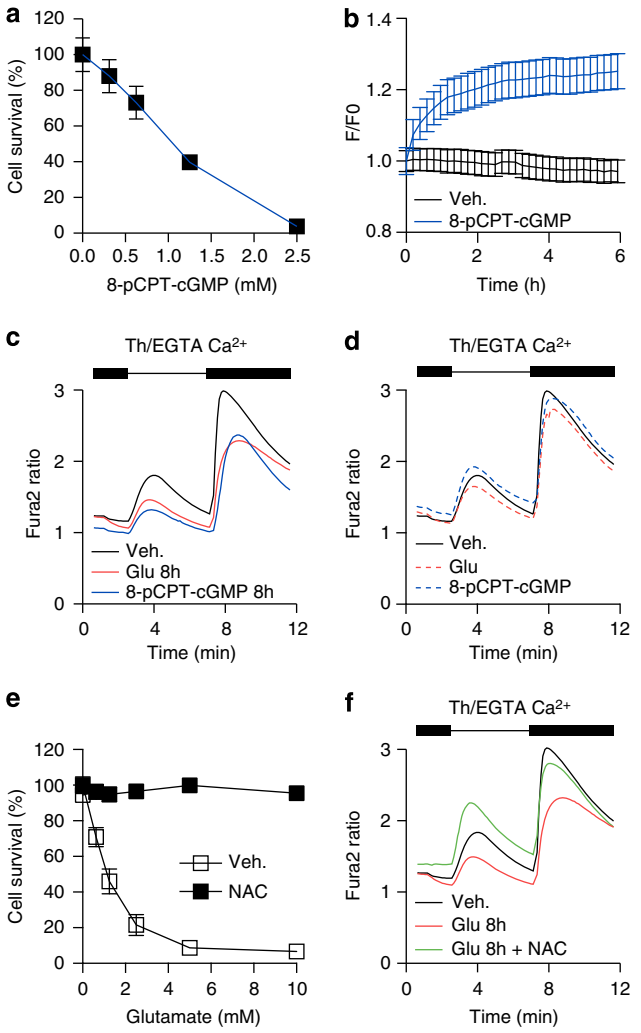

Figure 3 Prolonged oxidative stress reduces the ER Ca^{2+} content and SOCE activity. (**a**) Application of pCPT-cGMP-induces cell death in HT22 cells. Cells were subjected to the indicated concentrations of pCPT-cGMP and viability was measured 16 h later with the cell-titer blue reagent. The graph shows the mean fluorescence values ± S.E.M. of 11 replicate wells measured in two independent experiments plotted against glutamate concentration. (**b**) GCaMP5-based long-term Ca^{2+} live-cell imaging experiments reveals a pCPT-cGMP-induced cytosolic Ca^{2+} increase. Graphs show mean normalized GCaMP/RFP ratio of 10 wells each containing >30 cells obtained in two independent experiments. (**c**, **d** and **f**) Fura2-based SOCE measurements performed on a BD Pathway high content imaging system. Cells were either preincubated for 8 h with 2.5 mM glutamate, 2.5 mM glutamate together with 2 mM NAC or 2.5 mM pCPT-cGMP or supplemented with these substances directly at the onset of measurement as indicated. For measurement of SOCE after baseline recording in HBSS, ER Ca^{2+} stores were depleted by addition of 2 μM thapsigargin in 2 mM EGTA, which was necessary to bind the Ca^{2+} ions of the HBSS buffer. After 6 min of store depletion, 5 mM of Ca^{2+} was added to overload the EGTA and allow SOCE. Ca^{2+} influx was recorded for additional 4 min. Each trace represents the mean of five to six wells measured in three independent experiments. (**e**) Oxidative stress was induced in NAC or vehicle treated cells by application of indicated amounts of glutamate. Cell viability was quantitated 16 h after oxidative stress onset with the cell-titer blue reagent. The graph shows the mean ± S.E.M. of nine replicate wells measured in three independent experiments plotted against glutamate concentration

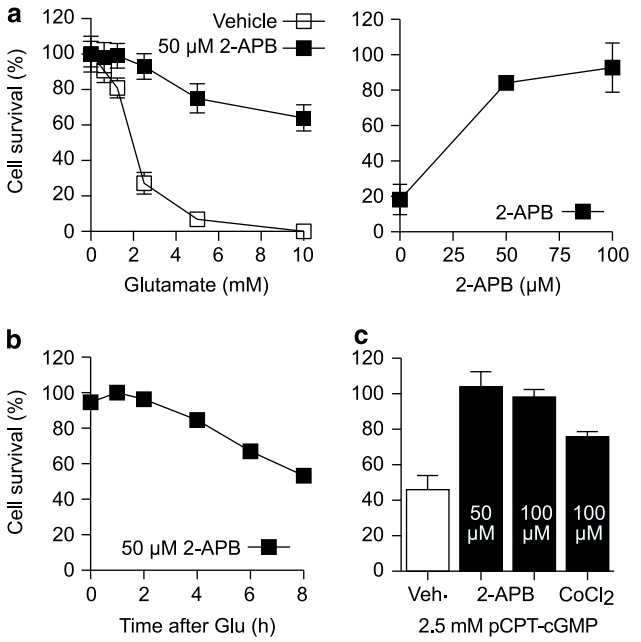

Figure 4 Pharmacological inhibition of SOCE protects against oxidative stress. (**a**) 2-APB or vehicle treated HT22S cells were subjected to oxidative stress by addition of the indicated amounts of glutamate. 16 h after stress onset, viability was quantitated with the CTB assay and normalized to controls without glutamate. Graphs show mean ± S.E.M. of nine replicates obtained in three independent experiments. (a right panel) The indicated concentrations of 2-APB were added to HT22 cells treated with 5 mM of glutamate. 20 h after stress, onset viability was quantified with the MTT-viability assay. **(b)** 2-APB was added to glutamate (5 mM)-treated HT22 cells at the indicated times after glutamate addition. After 20 h, cell viability was quantified by the MTT-assay. **(c)** Cells were treated with the indicated concentrations of 2-APB, $CoCl_2$ or vehicle and the MTT-assay was performed 20 h after addition of 2.5 mM pCPT-cGMP

and 2a) is relevant for the resistance against oxidative stress, we decided to identify the involved proteins. Resistance against oxidative stress in HT22R cells is mediated in part via transcriptional regulation of protective proteins.[10,11,13] We therefore hypothesized that the reduced SOCE observed in HT22R cells might be mediated via downregulation of components of the cellular SOCE machinery and analyzed the expression pattern of the SOCE-contributing proteins STIM1, STIM2 and ORAI1, as well the transient receptor potential melastatin 7 (TRPM7) channel, a Ca^{2+} permeable channel that is also blocked by 2-APB.[20] The protein levels of STIM1 and STIM2 were equal in HT22S and R (Figure 5a and b). TRPM7 expression was analyzed by quantitative real-time-PCR (qRT-PCR) and also found to be the similar in both cell types (Figure 5c). Immunoblotting against ORAI1 produced a ladder of bands between 50 and 100 kDa, which may be due to protein modifications for example, glycosylation, differential splicing,[21] dimerization or even tetramerization.[22] We quantified the 50 kDa band, which according to the datasheet of the antibody, should be ORAI1 and the more prominent 80 kDa band. Both bands were significantly downregulated in HT22R cells (Figure 5d), consistent with the reduced SOCE activity in these cells. Downregulation of these bands by small inhibitory RNA (siRNA) transfection, which correlated with mRNA quantification by RT-PCR (Figure 6h and i), also suggested specificity of the antibody used.

These results pointed to ORAI1 as being the protein that mediates the reduced SOCE observed in HT22R cells. To

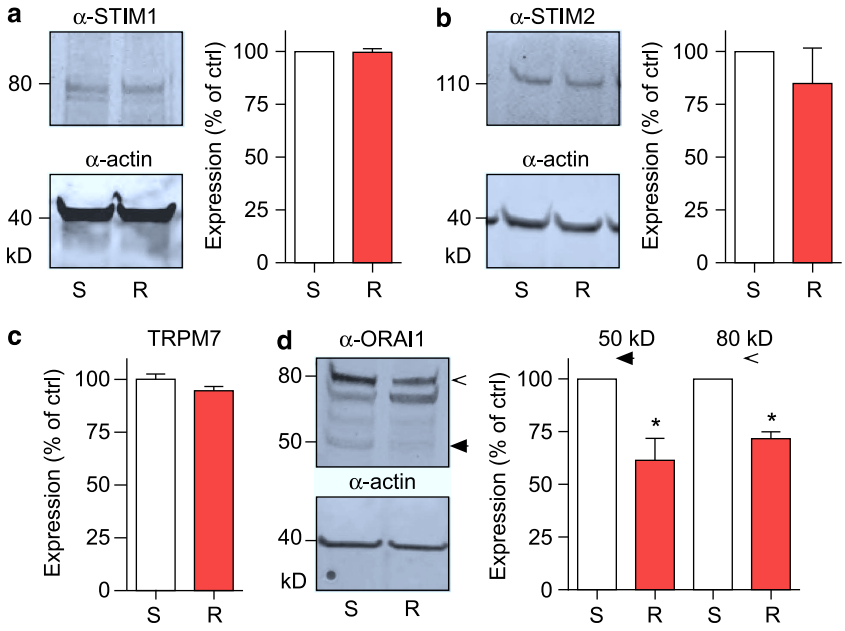

Figure 5 The SOCE Ca^{2+} influx channel ORAI1 is downregulated in glutamate-resistant HT22R cells. Expression analysis of key SOCE players and TRPM7 in HT22S and R cells. **(a, b** and **d)** Immunoblots were probed with antibodies against STIM1 **(a)** or 2 **(b)** and ORAI1 **(d)**; GAPDH served as loading control and was simultaneously recorded with the protein of interest on the same membrane with the Licor infrared imaging system. Quantification of immunoblots was done with ImageJ software. Intensity values were normalized to HT22S samples and plotted in bar graphs as expression in percentage. **(c)** RT-PCR analysis of *TRPM7* expression level in HT22S and R cells. The *TRPM7* signal was normalized to the endogenous control *hprt* and plotted as mean expression level ± S.E.M. in percentage. All graphs show the mean of at least three independently performed experiments. $^*P < 0.05$ using students *t*-test

complement this and to show that this downregulation is indeed involved in the resistance against oxidative stress observed in HT22R cells, we decided to knockdown the components of the SOCE machinery, STIM1, STIM2, ORAI1 and TRPM7 by siRNA and determine the susceptibility of the cells to oxidative glutamate toxicity.

Knockdown of ORAI1 protects from GSH depletion. We transfected HT22 cells with two different siRNAs against STIM1, STIM2 ORAI1 or TRPM7 and treated these cells with glutamate or L-buthionine-(S,R) sulfoximine (BSO), an inhibitor of the rate-limiting enzyme glutamate-cysteine ligase, 48 h after transfection. Successful knockdown was verified by RT-PCR analysis (Figure 6a, d, f and h) and immunoblotting (Figure 6b and i). In line with the protein expression pattern observed in glutamate-resistant cells (Figure 5), knockdown of STIM1 or STIM2 induced no significant protective effect against GSH depletion elicited either by glutamate or BSO (Figure 6c and e), whereas reduced ORAI1 levels strongly protected HT22 cells from oxidative stress (Figure 6j). Interestingly, siRNA-mediated knockdown of TRPM7 in HT22S cells significantly increased susceptibility to oxidative glutamate toxicity (Figure 6g).

We conclude from these data that the protective effect of 2-APB is unlikely to involve STIM1, STIM2 or TRPM7 inhibition, as reduction of these Ca^{2+} entry modulating proteins has either no or even the opposite effect of 2-APB. Rather, two lines of evidence suggest that ORAI1 is involved in oxidative stress-induced Ca^{2+} influx: ORAI1 is downregulated in glutamate-resistant cells and its knockdown protects glutamate-sensitive cells from cell death mediated by GSH depletion. We conclude that the protective effect of 2-APB is mediated by the inhibition of ORAI1-mediated Ca^{2+} influx and that reduced expression of ORAI1 is involved in the resistance of HT22R cells against oxidative stress.

Knockdown of ORAI1 inhibits cytosolic calcium elevation during oxytosis. To directly investigate the contribution of ORAI1 to the detrimental Ca^{2+} influx induced by glutamate, we continued with long-term Ca^{2+} live-cell imaging experiments to visualize the cytosolic Ca^{2+} rise during oxytosis. We transfected HT22 cells with the two different siRNAs against ORAI1 (Figure 6h, i) or non-targeting control-siRNA together with the Ca^{2+}-sensor GCaMP5. Knockdown efficiency was controlled by RT-PCR (data not shown). 48 h after transfection, the cells were exposed to glutamate overnight and the cytosolic calcium signal was monitored in a high-content microscope equipped with an environmental chamber to keep the temperature and CO_2 concentration constant. Two hours after glutamate addition, we started to acquire the GCaMP and the control RFP signal every 15 min for the next 14 h and calculated the GCaMP/RFP ratio. This showed that cells peak in a seemingly random manner between 5 – 16 h of glutamate exposure. After a sharp increase in GCaMP signal, the cells quickly lyse, which was visible through vigorous quenching of GCAMP and RFP fluorescence. A typical sequence of pictures is shown in Figure 7a. The appearance of these Ca^{2+} spikes was highly asynchronously spread over the whole-time frame (Figure 7a lower panel) and significantly less frequent in ORAI1 – siRNA-transfected cells compared

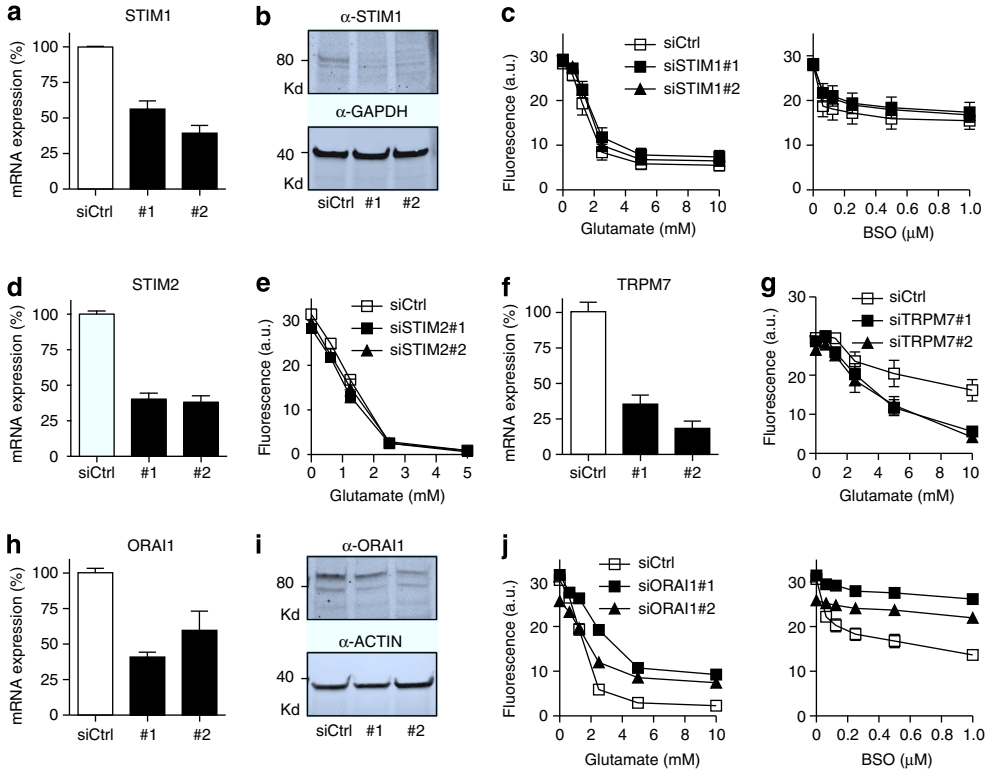

Figure 6 Knockdown of ORAI1 protects from GSH depletion. HT22S cells were transfected with two independent siRNAs against *STIM1, STIM2, ORAI1* and *TRPM7* or with non-targeting control siRNA and 48 h later subjected to cell survival experiments. **(a, d, f** and **h)** RT-PCR analyses of successful knockdown of *STIM1* **(a)**, *STIM2* **(d)**, *ORAI1* **(h)** and *TRPM7* **(f)**. Signals of genes of interest were normalized to *hprt* and plotted as expression in percentage relative to control-siRNA transfected samples. **(b** and **i)** Verification of successful knockdown by immunoblot. The membranes were simultaneously probed with antibody against either STIM1 **(b)** or ORAI1 **(i)** and GAPDH respectively actin as loading control and analyzed with the Licor infrared imaging system. **(c, e, g** and **j)** Survival experiments of siRNA-transfected cells. The indicated amounts of glutamate or BSO were added 48 h after transfection and viability was quantified with the CTB reagent 16 h after glutamate or BSO addition. The graphs show the mean fluorescence ± S.E.M. of 15 replicates obtained in three independent experiments plotted against glutamate or BSO concentration

with scrambled siRNA-transfected cells (Figure 7b). We also treated ORAI1 siRNA-transfected cells with pCPT-cGMP and immediately recorded the cytosolic Ca^{2+} level with GCaMP5 as described above. Interestingly, pCPT-cGMP did not evoke Ca^{2+} peaks similar to glutamate, but instead induced a slow but prominent cytosolic Ca^{2+} influx (Figure 3b). Because the cytosolic Ca^{2+} increase induced by cell-permeable cGMP occurs with a steady increase, we calculated the slope of Ca^{2+} influx over the first 2 h, which was significantly reduced by downregulation of ORAI1 (Figure 7c).

We conclude from these results that the SOCE-mediating channel protein ORAI1 significantly contributes to the detrimental Ca^{2+} influx elicited by cGMP or caused by oxidative stress in the course of GSH depletion.

Discussion

We conclude that ORAI1 channels has a major role in the detrimental Ca^{2+} influx caused by oxidative stress. We found that glutamate-resistant HT22R cells exhibit a reduction in SOCE and reduced amounts of ORAI1. Knockdown of ORAI1 protected against two different causes of GSH depletion; blocking cystine uptake with glutamate and inhibiting GSH synthesis with BSO. Pharmacological inhibition of SOCE using the well-established inhibitor 2-APB similarly protected against cell death induced by GSH depletion, but not against ER stress elicited with the N-glycosylation inhibitor tunicamycin (not shown), which suggests that dysregulation of ORAI1 function is not a general aspect of cell death, despite the fact that glutamate-resistant cells are also resistant against ER stress as well as direct activation of the caspase cascade caused by overexpression of the apoptotic protein BAX.[10] As 2-APB is a known inhibitor of Ca^{2+} influx, its cell survival-promoting action is most probably caused by its inhibitory action on the detrimental Ca^{2+} influx during oxidative stress. This hypothesis is strengthened by our time course experiments, which still showed a beneficial effect of 2-APB when applied up to 8 h after glutamate addition, further pointing to a mechanism of action that interferes with late events in the cell death program such as Ca^{2+} influx. In addition, pCPT-cGMP-induced cell death was prevented by 2-APB, and the observed effect was even stronger than that of the general Ca^{2+} channel blocker $CoCl_2$. Cytosolic elevation of cGMP through increased activity of soluble guanylate cyclases occurs very late in the cell death program induced by glutamate and is responsible for the opening of plasma membrane Ca^2 channels allowing detrimental Ca^{2+} influx.[7]

The fact that knockdown of the upstream initiator of SOCE STIM1 had no effect, speaks against a dysregulation of the whole SOCE machinery and points instead to ORAI1 as the major culprit in these cells. When we investigated the effects of STIM1 and ORAI1 knockdown using the same siRNAs in

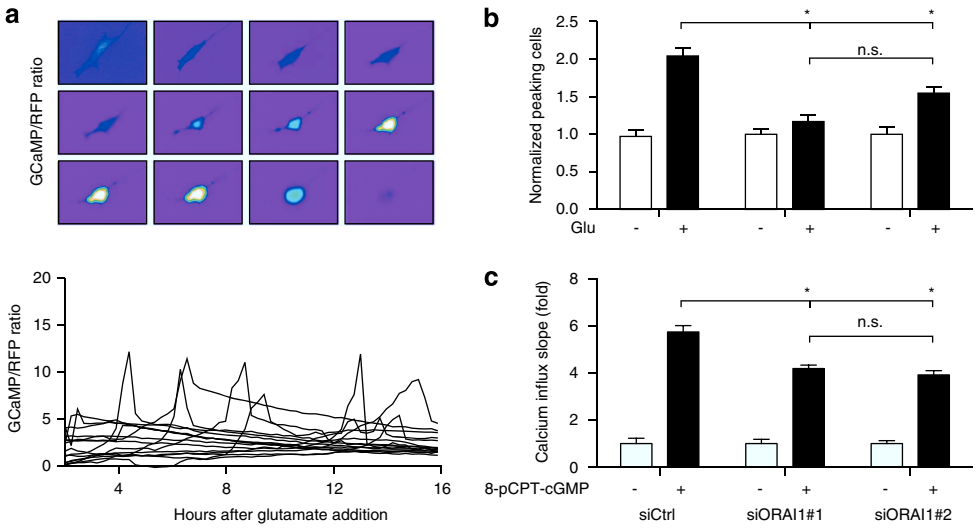

Figure 7 Knockdown of ORAI1 inhibits cytosolic calcium elevation during oxytosis. HT22S cells were transfected with two different siRNAs against ORAI1 or non-targeting siRNA as control together with a plasmid encoding the GCaMP5-IRES-RFP Ca^{2+} reporter gene and subjected to long-term live-cell imaging experiments to show the detrimental Ca^{2+} influx in the late phase of oxidative glutamate toxicity. **(a)** Typical GCaMP pictures of a control siRNA transfected cell under glutamate exposure. The cytosolic Ca^{2+} concentration stays low for several hours, but eventually rises quickly, leading to cell lysis assessed by quenching of the fluorescence signal. The lower panel shows sample traces from glutamate-treated cells transfected with control siRNA, which illustrate the asynchronous appearance of Ca^{2+}-spikes. For reasons of clarity, only Ca^{2+}-peak positive cells from one well are shown. **(b)** Analysis of long-term live-cell imaging of GCaMP-IRES-RFP and siRNA-transfected cells under glutamate exposure in comparison to vehicle treatment. For each picture, a GCaMP5/RFP ratio was calculated. To identify peaking cells, the maximal GCaMP/RFP ratio was divided by the average GCaMP/RFP ratio calculated over the whole measurement period. Each cell that reached a value above the average value of control siRNA transfected cells was counted as Ca^{2+}-peak positive. The amount of Ca^{2+}-peaking cells was normalized to vehicle control and plotted as a bar graph. The bars represent mean ± S.E.M. of 15 replicate wells measured in three independent experiments. **(c)** Analysis of the increase in the GCaMP/RFP ratio in pCPT-cGMP treated HT22 cells transfected with ORAI1 or control siRNA. The slope was normalized to vehicle and plotted as mean ± S.E.M. in bar graphs. Two independent experiments were performed containing >150 cells for each condition. N.S., not significant, $^*P<0.05$ by ANOVA with Tukey's *post hoc* test

mouse embryonic fibroblasts, we observed a detrimental effect for both transcripts, which suggests cell type-specific differences.[23] The protection conferred by ORAI1 knockdown in HT22 cells is in line with the recent observation that CD4-positive T cells from mice lacking ORAI1 robustly proliferate despite repetitive stimulations, and are strongly resistant against stimulation-induced cell death.[24] Our results suggest that ORAI1-mediated Ca^{2+} influx causes cytotoxic Ca^{2+} overload late in the course of oxidative stress-induced cell death. To prove this hypothesis, we performed long-term live-cell imaging of glutamate challenged cells transfected with a genetically-encoded cytosolic Ca^{2+} sensor. The direct observation of cytosolic calcium dynamics revealed a strong but short-lived calcium rise directly preceding cell death, which appeared completely asynchronously in the cell population within a time frame of $5-16$ h after the addition of glutamate. This perfectly resembles the time course of 2-APB protection. When applied 8 h after glutamate (Figure 4b), 50% of the cells were still rescued, which can be explained by the apparently random distribution of the final Ca^{2+} rise. Cells that have already opened their gates for external Ca^{2+} are irrecoverable, but those that have not induced Ca^{2+} influx at the time of 2-APB addition can still survive by the blockage of Ca^{2+} channels.

Our quantification of Ca^{2+} dynamics cells during glutamate or pCPT-cGMP treatment revealed a direct impact of ORAI1 expression levels on the Ca^{2+} influx after induction of the cell death program, which is perfectly in line with the protective effect of ORAI1 knockdown in the survival assays. Direct Ca^{2+} imaging over the whole-time course of oxidative glutamate toxicity also disclosed the time lag between cytosolic Ca^{2+} elevation and cell death. We demonstrated that the cytosolic Ca^{2+} rise directly precedes cell death, visible by disintegration of the plasma membrane and strong fluorescence quenching due to loss of GCaMP5. This short time period between the cytosolic Ca^{2+} signal and cell death suggests a direct detrimental role and renders further signaling events unlikely.

Although we showed that intracellular cGMP contributes to Ca^{2+} channel opening, it remains unclear whether it directly causes the opening of ORAI1 channels in endogenous oxidative stress or whether additional factors are needed. It is possible that the reduced amounts of STIM1 in siRNA-transfected cells (Figure 6a, b) are still sufficient to open ORAI1 channels during oxidative stress or that STIM2 can substitute for STIM1 under these conditions. Furthermore, ORAI1 might not only be activated by STIM1, but also through other factors such as the Ca^{2+}-independent phospholipase A_2 (iPLA2β).[25] Also a direct influence of the cellular redox state on ORAI1 activity seems possible. One study revealed that H_2O_2 enhanced I_{CRAC}-mediated Ca^{2+} influx (the electrophysiological equivalent of SOCE) through activation of IP3 receptors and subsequent store depletion without direct effect on ORAI1.[26] SERCA pumps in contrast were shown to be inhibited by H_2O_2.[27] One might speculate that during glutamate-induced oxidative stress, SERCA is inhibited and IP3 receptors activated, which eventually results in ER Ca^{2+} store depletion triggering ORAI1-mediated detrimental Ca^{2+} influx. This would be in line with our results, where 8 h of glutamate treatment resulted in a reduction of the

thapsigargin-releasable Ca^{2+} pool, implying reduced SERCA activity or increased ER Ca^{2+} efflux. Others, however, suggested a direct inhibitory effect of H_2O_2 on ORAI1-mediated Ca^{2+} influx induced by store depletion with thapsigargin, which was explained by the oxidation of cysteine residues located in an extracellular loop of ORAI1.[28] This could be interpreted as an attempt to withstand the cytotoxic Ca^{2+}-mediated by ORAI1.

We conclude from the presented data that dysregulated ORAI1-mediated Ca^{2+} influx contributes in a significant manner to programmed cell death induced by GSH depletion in neuronal cells. As this detrimental Ca^{2+} influx occurs late in the course of the cell death program, it might be amenable to therapeutic intervention in acute diseases where oxidative stress have a role.

Materials and Methods

Cell culture. The glutamate-resistant HT22R cell line was generated from the parental mouse hippocampal cell line HT22 as previously described.[19] Both cells lines, HT22S and HT22R, were cultured in DMEM high glucose (PAA Laboratories, Pasching, Austria) supplemented with 5% fetal calf serum (Thermo Fisher Scientific, Waltham, MA, USA) and 100 U per ml penicillin and 100 μg per ml streptomycin (Gibco, Darmstadt, Germany) in a humidified incubator with 5% CO_2 and 95% air.

Cell survival assays. HT22 cells were seeded in 96-well plates at a density of 5000 cells/well and 24 h later subjected to cell death experiments. siRNA-transfected cells were seeded 24 h post transfection. Pharmacological agents were added together with, or at specified time periods after, induction of cell death by the indicated drugs. Cell viability was quantified 16–24 h after stress onset with the cell titer blue (CTB) reagent (Promega, Madison, WI, USA). Alternatively, in some experiments, the 3-(4,5-Dimethylthiazol-2-yl)-2,5-diphenyltetrazolium bromide (MTT) assay was used.[19] For CTB fluorescence, emission was measured at 590 nm after excitation at 562 nm using a GENios Pro microplate reader (Tecan, Männedorf, Switzerland); for the MTT-assay, absorption was measured at 570 nm.

Calcium live-cell imaging. Fura2 Ca^{2+} imaging experiments were performed on a BD Pathway 855 High Content Imaging System (BD Biosciences, Heidelberg, Germany). The cells were seeded in 96-well imaging plate (BD Bioscience) the day before the experiment in a density of 5000 cells/well and loaded with 5 μM Fura2-AM (Molecular Probes, Darmstadt, Germany) in HBSS for 30 min before the experiment. Measurement was performed with excitation at 340 and 380 nm for ratiometric analysis and pictures were taken with a delay of 5 s. For comparison of SOCE in HT22S and HT22R, cells were seeded on 12 mm coverslips at a density of 100 000/well, loaded with Fura2-AM and placed into a flow chamber. The measurement was performed using an Olympus IX81 fluorescence microscope with the cell^R imaging software. Images were acquired at 340 and 380 nm excitation and the ratio was calculated every 5 s for every single cell. After 1 min of baseline recording, ER-calcium stores were depleted in EGTA buffer (Ca^{2+}-free HBSS supplemented with 0.5 mM EGTA, 20 mM HEPES, 1 mM $MgCl_2$ and 1 g per l Glucose) with 2 μM thapsigargin for 6 min and subsequently Ca^{2+} was readded by changing the buffer to HBSS.

Electrophysiology. We used whole-cell patch clamping to measure currents through ion channels of single cells. Whole-cell recordings were performed using an Axopatch 200B patch clamp amplifier (Axon Instruments, Sunnyvale, CA, USA) and digitized with Digidata 1332 (Axon Instruments). For SOC channels recordings the pipette solution contained (in mM) 120 CsCl, 5 Bapta-Na, 30 Cs-HEPES pH 7.3, 1.5 $MgCl_2$, 4 Na_2ATP, 0.4 Na_2GTP and 1.6 $CaCl_2$ (pCa 7.0). Extracellular solution contained (in mM) 140 NMDG-Asp, 10 $BaCl_2$, 10 Cs-HEPES, pH 7.3. During recording the currents were sampled at 5 kHz and filtered digitally at 500 Hz, the pClamp9 software (Axon Instruments) was used for data acquisition and analysis. In all whole-cell experiments the holding potential was −40 mV, periodically (once every 5 s) the membrane potential was stepped to −100 mV (for 30 ms) and a 200 ms voltage ramp to +100 mV was applied. Currents were evoked by application of 1 μM thapsigargin (Sigma, Munich, Germany) in external solution, which was added to the bath perfusion. The traces recorded before current activation were used as templates for leak subtraction. Whole-cell currents were normalized to the cell capacitance. The mean value of cell capacitance was 19 pF ± 5 (total number of experiments $n = 20$).

Quantitative RT-PCR. Whole-cellular RNA was isolated using ZR RNA MiniPrep Kit (Zymo, Irvine, CA, USA) and transcribed into cDNA with the High Capacity cDNA Reverse Transcription Kit (Applied Biosystems, Darmstadt, Germany). RT-PCR analysis was performed on a 7500 Fast cycler (Applied Biosystems) with FAST BLUE qPCR MasterMix (Eurogentec, Cologne, Germany) running the 7500 standard program. Primers and Probes for *STIM1* and *2, ORAI1* and *TRPM7* were designed by the universal probe library assay design center (Roche, Mannheim, Germany) and the hypoxanthine-phosphoribosyltransferase gene (*HPRT*) served as an endogenous control with individually designed primers and probe purchased from MWG (Ebersberg, Germany).

siRNA transfections. Flexitube siRNAs against ORAI1, STIM1, STIM2 and TRPM7 were purchased from Qiagen (Hilden, Germany) (no.SI00972251, no.SI00972272, no.SI1435623, no.SI1435637, no.SI01435665, no.SI01435672, no.SI02694727 and no.SI02742663) and transfected into cells with Lipofectamine RNAiMAX (Invitrogen, Darmstadt, Germany) when cells were grown to 70–80% confluence in six-well plates. Successful knockdown was verified by RT-PCR or immunoblot.

Immunoblotting. Cells were lysed in ice-cold RIPA buffer (Thermo Fisher Scientific) containing mini complete protease inhibitor cocktail (Roche) and centrifuged for 30 min at 16 000 g. The supernatants were separated on 8–16% polyacrylamide gels (Thermo Fisher Scientific), transferred onto nitrocellulose membranes with the iBlot System (Invitrogen, Darmstadt, Germany) and blocked in 3% nonfat dry milk in phosphate-buffered saline containing 0.5% Tween-20 (PBS-T) for 1 h at room temperature before overnight incubation with primary antibodies against STIM1 (BD Biosciences, no.610955 1 : 250), STIM2 (Cell Signaling, Danvers, MA, USA, no.4917 1 : 1000), ORAI1, Alomone Jerusalem, Israel, no.ACC-062 1 : 500), Actin (Millipore, Billerica, MA, USA, no.MAB1501 1 : 5000) or GAPDH (Cell Signaling, no.2118 1 : 5000) followed by α-mouse (respectively rabbit) IgG (Fc) infrared fluorescence − conjugated secondary antibody (Licor, Lincoln, NE, USA, 1 : 30 000). The membranes were scanned for infrared fluorescence at 680 or 800 nm using the Odyssey system (Licor) and the signal was analyzed quantitatively with the image-processing software ImageJ (http://rsbweb.nih.gov/ij/).

Long-term calcium live-cell imaging. GCaMP5 was a kind gift of Douglas S. Kim (Howard Hughes Medical Institute, Ashburn) and subcloned with EcoRI and NotI into the IRES-RFP-containing vector PB531A-1 (System Biosciences, Mountain View, CA, USA). Cells were transfected with GCaMP5-IRES-RFP together with two different siRNAs against ORAI1 or non-targeting control-siRNA with Lipofectamine 2000 (Invitrogen) in six-well plates and 24 h later transferred to 96-well imaging plates (BD Biosciences) at a density of 5000 cells/well. For calcium imaging, phenol red containing medium was replaced by colorless DMEM (PAA Laboratories, Pasching, Austria). Two hours before the onset of measurement, 25 mM glutamate was added to the cells, control wells were supplemented with vehicle and the plate was incubated in the BD Pathway 855 at 37 °C with 5% CO2 and 95% air. For pCPT-cGMP-induced Ca^{2+} influx, measurement was started immediately after addition of 2.5 mM pCPT-cGMP. Cytosolic calcium was monitored by GCaMP5 and normalized to RFP fluorescence; pictures were taken every 15 min. For analysis of glutamate-induced Ca^{2+} peaks, the maximal ratio was divided by the average ratio and a threshold was defined by the mean of control-siRNA transfected cells. Every cell above that threshold was counted as Ca^{2+} peak positive. For analysis of pCPT-cGMP-induced Ca^{2+} influx, the slope of Ca^{2+} increase was calculated over the first 2 h of the measurement.

Statistical analysis. Data were analyzed as mean ± S.E.M. and the statistical significance assessed using two-tailed *t*-tests or analysis of variance (ANOVA) with Tukey's Multiple Comparison Test as indicated.

Conflict of Interest

The authors declare no conflict of interest.

Acknowledgements. We thank Andrea Issberner and Caroline Sladek for excellent technical support and Christie Dietz for proofreading. This project was funded by Dr. Kurt and Irmgard Meister-Stiftung (AM), 'Molecular and Cellular Biology' RAS (EK), the OPTEC LLC (MR), and TargetSOCE (AM and EK).

1. Dringen R. Metabolism and functions of glutathione in brain. *Prog Neurobiol* 2000; **62**: 649–671.
2. Dixon SJ, Lemberg KM, Lamprecht MR, Skouta R, Zaitsev EM, Gleason CE *et al.* Ferroptosis: an iron-dependent form of nonapoptotic cell death. *Cell* 2012; **149**: 1060–1072.
3. Albrecht P, Lewerenz J, Dittmer S, Noack R, Maher P, Methner A *et al.* Mechanisms of oxidative glutamate toxicity: the glutamate/cystine antiporter system xc- as a neuroprotective drug target. *CNS Neurol Disord Drug Targets* 2010; **9**: 373–382.
4. Tan S, Sagara Y, Liu Y, Maher P, Schubert D. The regulation of reactive oxygen species production during programmed cell death. *J Cell Biol* 1998; **141**: 1423–1432.
5. Li Y, Maher P, Schubert D. A role for 12-lipoxygenase in nerve cell death caused by glutathione depletion. *Neuron* 1997; **19**: 453–463.
6. Pallast S, Arai K, Wang X, Lo EH, van Leyen K. 12/15-Lipoxygenase targets neuronal mitochondria under oxidative stress. *J Neurochem* 2009; **111**: 882–889.
7. Li Y, Maher P, Schubert D. Requirement for cGMP in nerve cell death caused by glutathione depletion. *J Cell Biol* 1997; **139**: 1317–1324.
8. Davis JB, Maher P. Protein kinase C activation inhibits glutamate-induced cytotoxicity in a neuronal cell line. *Brain Res* 1994; **652**: 169–173.
9. Murphy TH, Miyamoto M, Sastre A, Schnaar RL, Coyle JT. Glutamate toxicity in a neuronal cell line involves inhibition of cystine transport leading to oxidative stress. *Neuron* 1989; **2**: 1547–1558.
10. Dittmer S, Sahin M, Pantlen A, Saxena A, Toutzaris D, Pina AL *et al.* The constitutively active orphan G-protein-coupled receptor GPR39 protects from cell death by increasing secretion of pigment epithelium-derived growth factor. *J Biol Chem* 2008; **283**: 7074–7081.
11. Noack R, Frede S, Albrecht P, Henke N, Pfeiffer A, Knoll K *et al.* Charcot-Marie-Tooth disease CMT4A: GDAP1 increases cellular glutathione and the mitochondrial membrane potential. *Hum Mol Genet* 2012; **21**: 150–162.
12. Sahin M, Saxena A, Joost P, Lewerenz J, Methner A. Induction of Bcl-2 by functional regulation of G-protein coupled receptors protects from oxidative glutamate toxicity by increasing glutathione. *Free Radic Res* 2006; **40**: 1113–1123.
13. Toutzaris D, Lewerenz J, Albrecht P, Jensen LT, Letz J, Geerts A *et al.* A novel giant peroxisomal superoxide dismutase motif-containing protein. *Free Radic Biol Med* 2010; **48**: 811–820.
14. Roos J, DiGregorio PJ, Yeromin AV, Ohlsen K, Lioudyno M, Zhang S *et al.* STIM1, an essential and conserved component of store-operated Ca2 + channel function. *J Cell Biol* 2005; **169**: 435–445.
15. Liou J, Kim ML, Heo WD, Jones JT, Myers JW, Ferrell JE Jr *et al.* STIM is a Ca2 + sensor essential for Ca2 + -store-depletion-triggered Ca2 + influx. *Curr Biol* 2005; **15**: 1235–1241.
16. Zhang SL, Yeromin AV, Zhang XH, Yu Y, Safrina O, Penna A *et al.* Genome-wide RNAi screen of Ca(2 +) influx identifies genes that regulate Ca(2 +) release-activated Ca(2 +) channel activity. *Proc Natl Acad Sci USA* 2006; **103**: 9357–9362.
17. Prakriya M, Feske S, Gwack Y, Srikanth S, Rao A, Hogan PG *et al.* Orai1 is an essential pore subunit of the CRAC channel. *Nature* 2006; **443**: 230–233.
18. Mignen O, Thompson JL, Shuttleworth TJ. Orai1 subunit stoichiometry of the mammalian CRAC channel pore. *J Physiol (Lond)* 2008; **586**: 419–425.
19. Lewerenz J, Klein M, Methner A. Cooperative action of glutamate transporters and cystine/glutamate antiporter system Xc- protects from oxidative glutamate toxicity. *J Neurochem* 2006; **98**: 916–925.
20. Li M, Jiang J, Yue L. Functional characterization of homo- and heteromeric channel kinases TRPM6 and TRPM7. *J Gen Physiol* 2006; **127**: 525–537.
21. Fukushima M, Tomita T, Janoshazi A, Putney JW. Alternative translation initiation gives rise to two isoforms of orai1 with distinct plasma membrane mobilities. *J Cell Sci* 2012; **125**: 4354–4361.
22. Penna A, Demuro A, Yeromin AV, Zhang SL, Safrina O, Parker I *et al.* The CRAC channel consists of a tetramer formed by Stim-induced dimerization of Orai dimers. *Nature* 2008; **456**: 116–120.
23. Henke N, Albrecht P, Pfeiffer A, Toutzaris D, Zanger K, Methner A *et al.* Stromal interaction molecule 1 (STIM1) is involved in the regulation of mitochondrial shape and bioenergetics and plays a role in oxidative stress. *J Biol Chem* 2012; **287**: 42042–42052.
24. Kim KD, Srikanth S, Yee MK, Mock DC, Lawson GW, Gwack Y *et al.* ORAI1 deficiency impairs activated t cell death and enhances T cell survival. *J Immunol* 2011; **187**: 3620–3630.
25. Bolotina VM. Orai, STIM1 and iPLA2beta: a view from a different perspective. *J Physiol (Lond)* 2008; **586**: 3035–3042.
26. Grupe M, Myers G, Penner R, Fleig A. Activation of store-operated ICRAC by hydrogen peroxide. *Cell Calcium* 2010; **48**: 1–9.
27. Kuster GM, Lancel S, Zhang J, Communal C, Trucillo MP, Lim CC *et al.* Redox-mediated reciprocal regulation of SERCA and Na + -Ca2 + exchanger contributes to sarcoplasmic reticulum Ca2 + depletion in cardiac myocytes. *Free Radic Biol Med* 2010; **48**: 1182–1187.
28. Bogeski I, Kummerow C, Al-Ansary D, Schwarz EC, Koehler R, Kozai D *et al.* Differential redox regulation of orai ion channels: a mechanism to tune cellular calcium signaling. *Sci Signal* 2010; **3**: ra24.

Summary of the results

Store-operated calcium entry modulates neuronal network activity in a model of chronic epilepsy

In this study, we investigated the importance of SOCE in the brain and found convincing evidence for a contribution of the SOCE machinery to normal and pathological neuronal function. We confirmed the expression of STIM1 and STIM2 in primary neurons and astrocytes and measured the occurrence of SOCE in response to Ca^{2+}-store depletion in these cells. Application of pharmacological inhibitors of SOCE, ML9 and 2-APB, reduced neuronal network activity of neurons cultured on multielectrode arrays (MEAs) highlighting the importance of an intact SOCE response for neuronal function. As a model of disturbed excitability, we evoked chronic epileptic seizures in C57Bl6 mice and detected increased protein amounts of STIM1 and 2 in the brain of these animals. Also in human hippocampal specimens dissected from a patient suffering from medial temporal lobe epilepsy, we detected strong expression of STIM1 and STIM2. Pharmacological inhibition of SOCE in chronic epileptic slice cultures reduced occurrence of interrictal spikes and rhythmized epileptic bursts.

Stromal interaction molecule 1 (STIM1) is involved in the regulation of mitochondrial shape and bioenergetics and plays a role in oxidative stress

To investigate the role of STIM1 and SOCE during oxidative stress, we used genetically modified mouse embryonic fibroblasts (MEF) from STIM1 KO mice, in which we stably re-expressed STIM1 or a dominant active variant of STIM1 (DA-STIM1). We also knocked down ORAI1, the main Ca^{2+} channel of the SOCE machinery by small interfering RNA. Using these models, we observed a strongly reduced resistance against endogenous oxidative stress in STIM1 KO or ORAI1 knock down cells. This increased susceptibility was caused by higher basal oxidative stress levels of STIM1 KO MEFs compared to their WT counterparts, indicated by stronger antioxidative signaling through the NRF2 pathway. We showed evidence for reduced fragmentation of STIM1 KO mitochondria, together with increased metabolic activity and ROS production, which resulted in an elevated basal oxidative stress level in these cells. Obviously without STIM1 the cells failed to adjust their energy production to their needs and balance generation and detoxification of cellular ROS, what rendered SOCE-deficient cells more prone to oxidative stress-induced injury.

The plasma membrane channel ORAI1 mediates detrimental calcium influx caused by endogenous oxidative stress

In this contribution, we investigated the effect of a reduced SOCE capacity in neuronal HT22 cells and found a protective effect of pharmacological inhibition of SOCE. In contrast to the effects observed in MEF cells, knock down of STIM1 had no effect on survival of HT22 cells, whereas knock down of ORAI1 strongly protected from oxidative-glutamate toxicity. We directly recorded the strong cytosolic Ca^{2+} rise in the final phase of the oxidative-glutamate toxicity cell death program and observed an inhibitory effect of ORAI1-knock down. We concluded from these data that ORAI1 is the main Ca^{2+}-influx channel during oxidative-stress induced injury and that channel opening is unlikely to be mediated by STIM1.

Discussion

Several studies on STIM1 and STIM2 expression in neurons have been published since the discovery of STIM1 as SOCE-regulating protein (74) (75) (76). These studies report fairly different results ranging from prominent expression of STIM1 in pyramidal neurons and Purkinje cells (77) to nearly undetectable levels of STIM1 expression in primary hippocampal neurons (51).

With the first publication presented in this thesis, we confirmed the expression of STIM1 in the murine and human brain. The analysis of different cell types isolated from rat brains revealed expression of STIM1 and 2 in astrocytes as well as in neurons. The STIM1 signal was stronger in astrocytes compared to neurons whereas the opposite was the case for STIM2, which was in line with previously published results presenting a twofold higher expression of STIM2 compared to STIM1 in hippocampal neurons (76).

Based on the established expression of STIM1 and 2 in neurons and astrocytes, we next attempted to clarify the role of SOCE in neuronal function. The importance of STIM1 is best characterized in non-excitable cells of the immune system. Here, SOCE is an indispensable signaling mechanism in response to receptor activation leading to nuclear translocation of nuclear factor of activated T-cells (NFAT) and transcriptional up-regulation of immune-modulatory genes, e.g. different cytokines (78). The relevance of this signaling cascade is reflected by different immune deficiencies caused by mutations of STIM1 or ORAI1 (79). In contrast to the detailed knowledge about the relevance of SOCE in immune cells, less is known about the role of STIM1 in neurons. We therefore analyzed the effect of pharmacological SOCE inhibition on physiologic neuronal network activity on MEA chips and the role of SOCE in pathological hyperexcitability as observed in epilepsy. We found a clear reduction in network activity on MEA chips and observed a decrease in the neuronal cytosolic Ca^{2+} concentration in fura2 based live-cell imaging experiments in response to inhibition of SOCE. Because changes in the cytosolic Ca^{2+} concentration directly change the membrane potential of the neuron, the excitability of the cell is influenced. A cytosolic increase in Ca^{2+} is furthermore necessary for synaptic transmitter release and a reduction in cytoplasmic Ca^{2+} therefore impedes synaptic activity, what most likely provoked the reduced neuronal network activity observed in the MEA experiments. An intact SOCE machinery is therefore indispensable for physiologic neuronal activity.

Interestingly, in situations of pathologic hyperexcitability, STIM1 and STIM2 expression levels were significantly increased, potentially contributing to the generation of the hyperexcitability. Alternatively, one might speculate, that the up-regulation of STIM1 in epileptic neurons might resemble an attempt of the cell to reduce the pathologically increased excitability, because STIM1 was described to inhibit depolarization-induced opening of $Ca_V1.2$ thereby reducing excitability (27) (28).

In further experiments, we pharmacologically inhibited SOCE on chronic epileptic rat-brain slices and observed a clear modulatory action of SOCE in this epileptic model. Application of ML9 or 2-APB induced an increase in burst activity but suppressed interictal spikes after drug washout which resembled rythmization of neuronal activity probably correlating to the increased synchrony observed in MEA

experiments. However the increased burst activity during treatment resembled enhanced epileptic activity, which appeared in contrast to the reduced network activity in MEA experiments. This difference between MEA and slice-recording experiments might be developed from reduced accessibility of the slices to the pharmacon in contrast to the dissociated cultures on MEA chips, which rendered the effects in slice cultures less pronounced than in the MEA experiments.

One might also speculate that ML9 or 2-APB not only block SOCE but also impact on the described interaction between STIM1 and $Ca_V1.2$. If the observed up-regulation of STIM1 indeed resembled a compensatory mechanism to suppress $Ca_V1.2$ activity and reduced excitability, an interruption of this connection would also increase burst activity. Thus, further experiments, extending the possibilities of this thesis, have to be performed to clarify the role of the inhibitory action of STIM1 on $Ca_V1.2$ in epileptic condition and to find out how ML9 and 2-APB are linked to this phenomenon.

However we can conclude that STIM1 and STIM2 are not only expressed in neurons and astrocytes, but also contribute to normal neuronal activity. In pathologic hyperexcitability, as observed in epilepsy, the deregulation of STIM protein expression and inhibition of SOCE impact on neuronal firing.

Based on the finding that STIM1 and SOCE are indeed of relevance in the brain and even contribute to pathological hyperexcitability, we decided to further investigate the influence of the SOCE machinery on neuronal physiology. Interestingly epileptic patients suffer from neuronal loss through high oxidative stress levels in the brain (80) (81). Also, epileptic seizures are energy consuming processes and lead to increased cellular glucose uptake and elevated metabolic rates in the cells to keep sufficient ATP levels (82). We therefore started to investigate the role of STIM1 during oxidative stress.

Caused by its high metabolic rate and strong O_2 consumption, the brain is extremely prone to oxidative stress induced injury which plays an important role not only during the progression of epilepsy (83) but also in neurodegenerative diseases like Alzheimer's and Parkinson's disease (56) or ischemia and reperfusion injuries as observed after stroke or traumatic brain injury (56). ROS are continuously produced in the brain either by electron leakage from the mitochondrial electron transport chain, by free radical reactions catalyzed by iron ions, which are found in high concentrations in the brain, and as a by-product of different receptor-signaling events (84) (85). Several antioxidative defense mechanisms are active in the brain, e.g. the GSH or thioredoxin systems, SODs and direct ROS scavengers like α-tocopherol or coenzyme Q. When these detoxifying strategies are not sufficient to balance the produced amount of ROS, oxidative stress develops. Due to ROS overload, DNA, lipids and proteins of the cell are damaged and if the oxidative stress persists, the cell is eventually prone to death.

In order to elucidate the role of SOCE during oxidative stress-induced cell death, we first studied oxidative stress resistance in WT and STIM1 KO MEF cells as a model for reduced SOCE capacity and, in addition, evoked hyper-activated SOCE by expression of a dominant active form of STIM1. Interestingly, suppression of SOCE as well as permanent activation of SOCE led to a significantly reduced resistance against oxidative stress. We found that a disturbance of the physiological SOCE activity, which could either be over-activation or reduction, impeded accurate balancing of energy

production and ROS detoxification. STIM1 KO MEF cells contained elongated mitochondria and exhibited a stronger mitochondrial membrane potential in comparison to WT counterparts. We analyzed the expression of several antioxidative-defense genes regulated by ARE-driven promoters, the level of GSH and ROS and found a significantly enhanced activity of the antioxidative-signaling cascade in STIM1 KO MEFs together with high ROS load, which led to increased consumption of GSH under additional oxidative stress induced by glutamate addition. The enhanced expression of ARE-driven genes was caused by enhanced translocation of NRF2 to the nucleus, which might have been induced directly through ROS-mediated regulation of KEAP1 activity (86) or through phosphorylation of protein kinase-like endoplasmic reticulum kinase (PERK) (87) which we found to be increased in STIM1 KO MEF cells. PERK is usually known as an ER-stress marker with signaling functions during the unfolded protein response (UPR) (88). Thus one could hypothesize that STIM1 MEFs suffer from ER stress, which could also, as a side effect, trigger the enhanced oxidative stress observed in these cells (89). We therefore analyzed the ER-stress level of STIM1 KO cells but did not find further evidence for increased ER stress. The KO cells, compared to WT counterparts, were even less susceptible to ER stress induced through thapsigargin or tunicamycin and showed equal or reduced levels of spliced X-box binding protein 1 (Xbp1) mRNA (data not shown), a transcription factor which is differentially spliced in response to ER-stress (88). As the enhanced phosphorylation level of PERK in STIM1 KO MEFs cannot be explained by an increased ER-stress level in these cells, the mechanism of PERK phosphorylation in STIM1 KO conditions needs further investigation.

In conclusion, our data suggest that STIM1 impacts on the mitochondrial fusion/fission machinery and thereby allows adaption of cellular energy production to the cellular energy needs, a mechanism which is impaired through knock out of STIM1, rendering STIM1 KO MEFS highly susceptible to oxidative stress. Interestingly, not only reduction but also over-activation of SOCE increased the susceptibility towards oxidative stress induced injury. Therefore, one might speculate that the increase in STIM1 and 2 expression in epileptic neurons, which we demonstrated in the first study presented here, might contribute to the increased oxidative stress level in neurons from epileptic patients (80) (81).

Others already highlighted a connection between movement of STIM1 in response to store depletion and the mitochondrial membrane potential (90) and identified mitofusin 2 (MFN2), which is one of the main factors facilitating mitochondrial fusion (91), as a regulatory link. In MFN2-deficient cells, Ca^{2+}-store regulated STIM1 punctae formation was uncoupled from mitochondrial membrane potential. It is well possible that this MFN2-mediated interconnection between STIM1 and mitochondria also helps to shape mitochondrial morphology. In the case of STIM1 deficiency, MFN2 might lose a necessary connection to adjacent cellular structures. As STIM1 is located in ER- and plasma membranes, it possibly provides an anchoring site for mitochondrial fusion- and fission-mediating proteins, which might be missing in STIM1 KO cells. This association between the SOCE machinery and the mitochondrial network could make sense as mitochondria are themselves important Ca^{2+} stores and mitochondrial Ca^{2+} uptake promotes SOCE (92) whereas the Ca^{2+} content of mitochondria critically shapes energy metabolism (93)

on the other hand. Reduction of mitochondrial Ca^{2+} uptake through a combination of mitochondrial membrane potential depletion and inhibition of the mitochondrial Na^{+}/Ca^{2+} antiporter NCX_{mito} also reduced Ca^{2+} influx in response to store depletion whereas inhibition of mitochondrial motility had no effect (94). However mitochondrial motility and an active fusion and fission machinery might be required to adapt energy metabolism to SOCE activity. This appears reasonable, as SOCE-mediated Ca^{2+} influx in response to receptor activation alters cellular effector functions like secretion, migration or proliferation, which are energy-consuming processes. Even the shuttling of entering Ca^{2+} ions through SERCA pumps into the ER consumes ATP. The other side of the coin is that Ca^{2+}, which is sequestered by mitochondria, actively regulates energy production by releasing ROS as by-products, which in turn can trigger oxidative stress. Therefore regulation of the mitochondrial network shape is necessary to adapt energy production and ROS load to Ca^{2+} uptake.

As we were interested in the role of SOCE in the brain and its impact on oxidative stress in nerve cells we switched to a more neuronal model in the third study. We chose HT22 cells, which are derived from embryonic mouse hippocampal neurons and lack ionotropic glutamate receptors. Addition of glutamate to these cells does therefore not evoke excitotoxicity, as it would do in mature neurons, but causes endogenous oxidative stress by inhibition of the glutamate-cystine antiporter system X_c^- and subsequent GSH depletion through inhibition of cystine uptake.

It is of interest that the effect of SOCE reduction on susceptibility to oxidative stress was quite different in neuronal HT22 cells compared to embryonic fibroblasts. In HT22 cells, knock down of STIM1 did not affect cell death susceptibility, which, together with the low expression level of STIM1 in neurons, suggests a minor relevance of STIM1 in neurons compared to other cell types. In MEF cells, STIM1-mediated signaling was indispensable for proper adjustment of metabolic activity whereas HT22 cells appeared to be independent from STIM1 mediated SOCE at least concerning energy metabolism.

The major difference between MEFs and neurons is excitability. As shown in the literature and by our data in non-excitable cells like immune cells or fibroblasts STIM1 expression is strong and important for several signaling events, whereas in excitable cells like neurons STIM1 expression is rather low. Although HT22 cells are also non-excitable, they are derived from neurons which might be the reason for the low expression level of STIM1 in these cells. As we showed in the first contribution presented in this thesis, a deregulation of STIM1 expression likely contributes to hyperexcitability as observed in epilepsy. Therefore it appears reasonable that STIM1 expression needs to be tightly regulated in neurons to keep excitability at a physiological level and that STIM1-dependent signaling, regulating metabolic activity as observed in fibroblasts, is not possible in neurons as it would risk deregulation of neuronal firing like observed in epilepsy. Although HT22 cells lost neuronal excitability, a fact which precludes neuronal firing, one might speculate that they still possess neuron-like regulatory mechanisms for STIM1 and therefore do not rely on STIM1 mediated regulation of energy production.

Instead ORAI1 expression remarkably contributed to oxidative stress sensitivity in HT22 cells. As we showed by expression analysis in glutamate-resistant and -sensitive HT22 cells and by siRNA-mediated

knock down, a reduced expression level of ORAI1 protected HT22 cells from oxidative glutamate toxicity. In Ca^{2+}-live cell imaging experiments, we were able to show a direct impact of ORAI1 on the detrimental Ca^{2+} influx in the late phase of oxidative glutamate toxicity.

In ER-Ca^{2+} store dependent activity of ORAI1, STIM1 is the main switch which opens ORAI1 channels. Here we show that STIM1 is not important for oxidative stress induced cell death in HT22 cells but still ORAI1 opening is the detrimental Ca^{2+} influx pathway. Therefore it is of high interest which mechanisms activate ORAI1 in the course of oxidative stress. One might hypothesize a contribution of STIM2, which is also expressed in neurons (76) or iPLA2β, which was shown to be involved in store-dependent Ca^{2+} influx already before STIM1 was discovered (95) (96). Also cGMP needs to be considered as ORAI1-gatekeeper, because it was shown, that during the well-defined cell death program of oxidative-glutamate toxicity soluble guanylyl cyclase was activated, leading to increased intracellular cGMP levels, what was shown to be indispensable for Ca^{2+} influx (70).

As the detrimental Ca^{2+} influx during oxidative stress induced cell death occurs very late in the cell death cascade it resembles an interesting target for a potential therapeutic intervention in neurological diseases which are known to involve oxidative stress-induced cell death. Therefore further investigation concerning the ORAI1 gating mechanism is of high interest.

In conclusion the SOCE machinery plays an ambivalent role in cellular oxidative stress resistance. On one hand it allows the cell to adjust ATP production to energy needs and on the other hand it contributes to detrimental Ca^{2+} influx. These two sides of the coin also differ in their mode of activation. For beneficial SOCE signaling, STIM1 is indispensable, whereas channel opening for detrimental Ca^{2+} influx can occur independently from STIM1. Different modes of ORAI1 channel opening can be imagined and will be further investigated in the future. Also in the current literature this divergent role of STIM1 and SOCE is reflected. Several studies performed with fairly different cellular stress model found protective (48) (49) as well as detrimental effects of SOCE activity (45) (46) (47). However even in one cellular stress model applied to different cell lines, fibroblasts versus neuronal HT22 cells, STIM1 and ORAI1 respectively SOCE activity can impact very differently on cell survival and furthermore need to be tightly regulated especially in neurons as SOCE activity significantly impacts on excitability. Therefore a general conclusion about the effect of STIM1 or ORAI1 expression during cellular stress conditions cannot be drawn. It is rather dependent on the individual constitution of the investigated cell type if SOCE activity promotes beneficial and pro-survival or detrimental signaling cascades.

References

1. *Calcium signaling.* **Clapham, DE.** 2007, Cell, Vol. 131(6), pp. 1047-58.
2. *Calcium signalling: dynamics, homeostasis and remodelling.* **Berridge MJ, Bootman MD, Roderick HL.** 2003 Jul, Nat Rev Mol Cell Biol., Vol. 4(7), pp. 517-29.
3. **Bruce Alberts, Alexander Johnson, Peter Walter, Julian Lewis, Martin Raff, Keith Roberts,.** *Molecular Biology of the cell.* 5. s.l. : Garland Science Taylor and Francis Group, 2007. pp. 687-692.
4. *Three types of neuronal calcium channel with different calcium agonist sensitivity.* **Nowycky MC, Fox AP, Tsien RW.** 1985 Aug, Nature, Vol. 316(6027), pp. 440-3.
5. *Exocytotic Ca2+ channels in mammalian central neurons.* **Dunlap K, Luebke JI, Turner TJ.** 1995 Feb;, Trends Neurosci., Vol. 18(2), pp. 89-98.
6. *N-methyl-D-aspartate receptors are critical for mediating the effects of glutamate on intracellular calcium concentration and immediate early gene expression in cultured hippocampal neurons.* **Bading H, Segal MM, Sucher NJ, Dudek H, Lipton SA, Greenberg ME.** 1995 Feb, Neuroscience. , Vol. 64(3), pp. 653-64.
7. *Molecular mechanisms controlling calcium entry through AMPA-type glutamate receptor channels.* **Jonas P, Burnashev N.** 1995 Nov, Neuron., Vol. 15(5), pp. 987-90.
8. *Inositol 1,4,5-trisphosphate (IP3)-mediated Ca2+ release evoked by metabotropic agonists and backpropagating action potentials in hippocampal CA1 pyramidal neurons.* **Nakamura T, Nakamura K, Lasser-Ross N, Barbara JG, Sandler VM, Ross WN.** 2000 Nov 15, J Neurosci., Vol. 20(22), pp. 8365-76.
9. *Modulation of calcium wave propagation in the dendrites and to the soma of rat hippocampal pyramidal neurons.* **Watanabe S, Hong M, Lasser-Ross N, Ross WN.** 2006 Sep 1, J Physiol. , Vol. 575(Pt 2), pp. 455-68.
10. *Complex interactions between mGluRs, intracellular Ca2+ stores and ion channels in neurons.* **Fagni L, Chavis P, Ango F, Bockaert J.** 2000 Feb, Trends Neurosci., Vol. 23(2), pp. 80-8.
11. *Calcium ions in neuronal degeneration.* **Wojda U, Salinska E, Kuznicki J.** 2008 Sep, IUBMB Life., Vol. 60(9), pp. 575-90.
12. *Activation of calcium entry by the tumor promoter thapsigargin in parotid acinar cells. Evidence that an intracellular calcium pool and not an inositol phosphate regulates calcium fluxes at the plasma membrane.* **Takemura H, Hughes AR, Thastrup O, Putney JW Jr.** 1989 Jul 25, J Biol Chem. , Vol. 264(21), pp. 12266-71.
13. *Capacitative calcium entry in parotid acinar cells.* **Takemura H, Putney JW Jr.** 1989 Mar 1, Biochem J., Vol. 258(2), pp. 409-12.
14. *CIF and other mysteries of the store-operated Ca2+-entry pathway.* **Bolotina VM, Csutora P.** 2005 Jul, Trends Biochem Sci., Vol. 30(7), pp. 378-87.
15. *Calcium oscillations.* **MJ., Berridge.** 1990 Jun 15, J Biol Chem., Vol. 265(17), pp. 9583-6.
16. *Emptying of intracellular Ca2+ stores releases a novel small messenger that stimulates Ca2+ influx.* **Randriamampita C, Tsien RY.** 1993 Aug 26, Nature., Vol. 364(6440), pp. 809-14.
17. *A novel mechanism for the store-operated calcium influx pathway.* **Smani T, Zakharov SI, Csutora P, Leno E, Trepakova ES, Bolotina VM.** 2004 Feb, Nat Cell Biol., Vol. ;6(2), pp. 113-20.
18. *STIM1, an essential and conserved component of store-operated Ca2+ channel function.* **Roos J, DiGregorio PJ, Yeromin AV, Ohlsen K, Lioudyno M, Zhang S, Safrina O, Kozak JA, Wagner SL, Cahalan MD, Veliçelebi G, Stauderman KA.** 2005 May 9, J Cell Biol., Vol. 169(3), pp. 435-45.
19. *STIM is a Ca2+ sensor essential for Ca2+-store-depletion-triggered Ca2+ influx.* **Liou J, Kim ML, Heo WD, Jones JT, Myers JW, Ferrell JE Jr, Meyer T.** 2005 Jul 12, Curr Biol., Vol. 15(13), pp. 1235-41.
20. *Ca2+ store depletion causes STIM1 to accumulate in ER regions closely associated with the plasma membrane.* **Wu MM, Buchanan J, Luik RM, Lewis RS.** 2006 Sep 11, J Cell Biol., Vol. 174(6), pp. 803-13.
21. *STIM1 clusters and activates CRAC channels via direct binding of a cytosolic domain to Orai1.* **Park CY, Hoover PJ, Mullins FM, Bachhawat P, Covington ED, Raunser S, Walz T, Garcia KC, Dolmetsch RE, Lewis RS.** 2009 Mar 6, Cell. , Vol. 136(5), pp. 876-90.
22. *STIM1 is a Ca2+ sensor that activates CRAC channels and migrates from the Ca2+ store to the plasma membrane.* **Zhang SL, Yu Y, Roos J, Kozak JA, Deerinck TJ, Ellisman MH, Stauderman KA, Cahalan MD.** 2005 Oct 6, Nature., Vol. 437(7060), pp. 902-5.
23. *Large store-operated calcium selective currents due to co-expression of Orai1 or Orai2 with the intracellular calcium sensor, Stim1.* **Mercer JC, Dehaven WI, Smyth JT, Wedel B, Boyles RR, Bird GS, Putney JW Jr.** 2006 Aug 25, J Biol Chem., Vol. 281(34), pp. 24979-90.
24. *Orai1 and STIM reconstitute store-operated calcium channel function.* **Soboloff J, Spassova MA, Tang XD, Hewavitharana T, Xu W, Gill DL.** 2006 Jul 28, J Biol Chem. , Vol. 281(30), pp. 20661-5.

25. *The sarco/endoplasmic reticulum Ca(2+) ATPase (SERCA) is the third element in capacitative calcium entry.* **Manjarrés IM, Rodríguez-García A, Alonso MT, García-Sancho J.** 2010 May, Cell Calcium., Vol. 47(5), pp. 412-8.
26. *STIM1 knockdown reveals that store-operated Ca2+ channels located close to sarco/endoplasmic Ca2+ ATPases (SERCA) pumps silently refill the endoplasmic reticulum.* **Jousset H, Frieden M, Demaurex N.** 2007 Apr 13, J Biol Chem. , Vol. 282(15), pp. 11456-64.
27. *The CRAC channel activator STIM1 binds and inhibits L-type voltage-gated calcium channels.* **channels., The CRAC channel activator STIM1 binds and inhibits L-type voltage-gated calcium.** 2010 Oct 1, Science., Vol. 330(6000), pp. 101-5.
28. *The calcium store sensor, STIM1, reciprocally controls Orai and CaV1.2 channels.* **Wang Y, Deng X, Mancarella S, Hendron E, Eguchi S, Soboloff J, Tang XD, Gill DL.** 2010 Oct 1, Science., Vol. 330(6000), pp. 105-9.
29. *Cell biology. How to STIMulate calcium channels.* **MD., Cahalan.** 2010 Oct 1, Science. , Vol. 330(6000), pp. 43-4.
30. *Apoptosis in development.* **Meier P, Finch A, Evan G.** 2000 Oct 12, Nature., Vol. 407(6805), pp. 796-801.
31. *Intracellular adenosine triphosphate (ATP) concentration: a switch in the decision between apoptosis and necrosis.* **Leist M, Single B, Castoldi AF, Kühnle S, Nicotera P.** 1997 Apr 21, J Exp Med., Vol. 185(8), pp. 1481-6.
32. *Apoptosis: a basic biological phenomenon with wide-ranging implications in tissue kinetics.* **Kerr JF, Wyllie AH, Currie AR.** 1972 Aug, Br J Cancer., Vol. 26(4), pp. 239-57.
33. *Glucocorticoid-induced thymocyte apoptosis is associated with endogenous endonuclease activation.* **AH., Wyllie.** 1980 Apr 10, Nature. , Vol. 284(5756), pp. 555-6.
34. *Regulation of cell death: the calcium-apoptosis link.* **Orrenius S, Zhivotovsky B, Nicotera P.** 2003 Jul, Nat Rev Mol Cell Biol., Vol. 4(7), pp. 552-65.
35. *Requirement of biphasic calcium release from the endoplasmic reticulum for Fas-mediated apoptosis.* **Wozniak AL, Wang X, Stieren ES, Scarbrough SG, Elferink CJ, Boehning D.** 2006 Dec 4, J Cell Biol., Vol. 175(5), pp. 709-14.
36. *Calcium and cell death mechanisms: a perspective from the cell death community.* **Zhivotovsky B, Orrenius S.** 2011 Sep, Cell Calcium., Vol. 50(3), pp. 211-21.
37. *Participation of the conventional calpains in apoptosis.* **Lu T, Xu Y, Mericle MT, Mellgren RL.** 2002 Jun 12, Biochim Biophys Acta., Vols. 1590(1-3), pp. 16-26.
38. *Ubiquitous calpains promote both apoptosis and survival signals in response to different cell death stimuli.* **Tan Y, Wu C, De Veyra T, Greer PA.** 2006 Jun 30, J Biol Chem., Vol. 281(26), pp. 17689-98.
39. *Plasma membrane Ca2+ATPase isoform 4b is cleaved and activated by caspase-3 during the early phase of apoptosis.* **Pászty K, Verma AK, Padányi R, Filoteo AG, Penniston JT, Enyedi A.** 2002 Mar 1, J Biol Chem., Vol. 277(9), pp. 6822-9.
40. *Cleavage of plasma membrane calcium pumps by caspases: a link between apoptosis and necrosis.* **Schwab BL, Guerini D, Didszun C, Bano D, Ferrando-May E, Fava E, Tam J, Xu D, Xanthoudakis S, Nicholson DW, Carafoli E, Nicotera P.** 2002 Aug, Cell Death Differ., Vol. 9(8), pp. 818-31.
41. *Bcl-2-mediated alterations in endoplasmic reticulum Ca2+ analyzed with an improved genetically encoded fluorescent sensor.* **Palmer AE, Jin C, Reed JC, Tsien RY.** 2004 Dec 14, Proc Natl Acad Sci U S A., Vol. 101(50), pp. 17404-9.
42. *Bcl-2 and calcium: controversy beneath the surface.* **Distelhorst CW, Shore GC.** 2004 Apr 12, Oncogene., Vol. 23(16), pp. 2875-80.
43. *BAX and BAK regulation of endoplasmic reticulum Ca2+: a control point for apoptosis.* **Scorrano L, Oakes SA, Opferman JT, Cheng EH, Sorcinelli MD, Pozzan T, Korsmeyer SJ.** 2003 Apr 4, Science., Vol. 300(5616), pp. 135-9.
44. *Selective regulation of IP3-receptor-mediated Ca2+ signaling and apoptosis by the BH4 domain of Bcl-2 versus Bcl-Xl.* **Monaco G, Decrock E, Akl H, Ponsaerts R, Vervliet T, Luyten T, De Maeyer M, Missiaen L, Distelhorst CW, De Smedt H, Parys JB, Leybaert L, Bultynck G.** 2012 Feb, Cell Death Differ., Vol. 19(2), pp. 295-309.
45. *Soft substrate up-regulates the interaction of STIM1 with store-operated Ca2+ channels that lead to normal epithelial cell apoptosis.* **Chiu WT, Tang MJ, Jao HC, Shen MR.** 2008 May, Mol Biol Cell., Vol. 19(5), pp. 2220-30.
46. *Orai1 contributes to the establishment of an apoptosis-resistant phenotype in prostate cancer cells.* **Flourakis M, Lehen'kyi V, Beck B, Raphaël M, Vandenberghe M, Abeele FV, Roudbaraki M, Lepage G, Mauroy B, Romanin C, Shuba Y, Skryma R, Prevarskaya N.** 2010 Sep 16, Cell Death Dis., Vol. 1:e75.
47. *Requirement for store-operated calcium entry in sodium butyrate-induced apoptosis in human colon cancer cells.* **Sun S, Li W, Zhang H, Zha L, Xue Y, Wu X, Zou F.** 2012 Feb, Biosci Rep., Vol. 32(1), pp. 83-90.

48. *Coupling of mitochondria to store-operated Ca(2+)-signaling sustains constitutive activation of protein kinase B/Akt and augments survival of malignant melanoma cells.* **Feldman B, Fedida-Metula S, Nita J, Sekler I, Fishman D.** 2010 Jun, Cell Calcium. , Vol. 47(6), pp. 525-37.
49. *Calcium entry via ORAI1 regulates glioblastoma cell proliferation and apoptosis.* **Liu H, Hughes JD, Rollins S, Chen B, Perkins E.** 2011 Dec, Exp Mol Pathol., Vol. 91(3), pp. 753-60.
50. *S-glutathionylation activates STIM1 and alters mitochondrial homeostasis.* **Hawkins BJ, Irrinki KM, Mallilankaraman K, Lien YC, Wang Y, Bhanumathy CD, Subbiah R, Ritchie MF, Soboloff J, Baba Y, Kurosaki T, Joseph SK, Gill DL, Madesh M.** 2010 Aug 9, J Cell Biol., Vol. 190(3), pp. 391-405.
51. *STIM2 regulates capacitive Ca2+ entry in neurons and plays a key role in hypoxic neuronal cell death.* **Berna-Erro A, Braun A, Kraft R, Kleinschnitz C, Schuhmann MK, Stegner D, Wultsch T, Eilers J, Meuth SG, Stoll G, Nieswandt B.** 2009 Oct 20, Sci Signal., Vol. 2(93):ra67.
52. *Localization of the site of oxygen radical generation inside the complex I of heart and nonsynaptic brain mammalian mitochondria.* **Herrero A, Barja G.** 2000 Dec, J Bioenerg Biomembr., Vol. 32(6), pp. 609-15.
53. *Complex I-mediated reactive oxygen species generation: modulation by cytochrome c and NAD(P)+ oxidation-reduction state.* **Kushnareva Y, Murphy AN, Andreyev A.** 2002 Dec 1, Biochem J., Vol. 368(Pt 2), pp. 545-53.
54. *A model of O2.-generation in the complex III of the electron transport chain.* **Demin OV, Kholodenko BN, Skulachev VP.** 1998 Jul, Mol Cell Biochem., Vols. 184(1-2), pp. 21-33.
55. *Production of reactive oxygen species by mitochondria: central role of complex III.* **Chen Q, Vazquez EJ, Moghaddas S, Hoppel CL, Lesnefsky EJ.** 2003 Sep 19, J Biol Chem., Vol. 278(38), pp. 36027-31.
56. *Free radicals and antioxidants in normal physiological functions and human disease.* **Valko M, Leibfritz D, Moncol J, Cronin MT, Mazur M, Telser J.** 2007, Int J Biochem Cell Biol., Vol. 39(1), pp. 44-84.
57. *Oxidative stress in ALS: key role in motor neuron injury and therapeutic target.* **Barber SC, Shaw PJ.** 2010 Mar 1, Free Radic Biol Med., Vol. 48(5), pp. 629-41.
58. *Oxidative stress in schizophrenia - focusing on the main markers.* **Ciobica A, Padurariu M, Dobrin I, Stefanescu C, Dobrin R.** 2011 Sep, Psychiatr Danub., Vol. 23(3), pp. 237-45.
59. *Superoxide radicals as precursors of mitochondrial hydrogen peroxide.* **Loschen G, Azzi A, Richter C, Flohé L.** 1974 May 15, FEBS Lett. , Vol. 42(1), pp. 68-72.
60. *Mitochondrial metabolism of reactive oxygen species.* **Andreyev AY, Kushnareva YE, Starkov AA.** 2005 Feb, Biochemistry (Mosc)., Vol. 70(2), pp. 200-14.
61. *The Nrf2-antioxidant response element signaling pathway and its activation by oxidative stress.* **Nguyen T, Nioi P, Pickett CB.** 2009 May 15, J Biol Chem. , Vol. 284(20), pp. 13291-5.
62. *Oxidative stress sensor Keap1 functions as an adaptor for Cul3-based E3 ligase to regulate proteasomal degradation of Nrf2.* **Kobayashi A, Kang MI, Okawa H, Ohtsuji M, Zenke Y, Chiba T, Igarashi K, Yamamoto M.** 2004 Aug, Mol Cell Biol., Vol. 24(16), pp. 7130-9.
63. *Keap1 represses nuclear activation of antioxidant responsive elements by Nrf2 through binding to the amino-terminal Neh2 domain.* **Itoh K, Wakabayashi N, Katoh Y, Ishii T, Igarashi K, Engel JD, Yamamoto M.** 1999 Jan 1, Genes Dev., Vol. 13(1), pp. 76-86.
64. *The effects of stress and aging on glutathione metabolism.* **P., Maher.** 2005 May, Ageing Res Rev., Vol. 4(2), pp. 288-314.
65. *Glutathione: overview of its protective roles, measurement, and biosynthesis.* **Forman HJ, Zhang H, Rinna A.** 2009 Feb-Apr, Mol Aspects Med., Vols. 30(1-2), pp. 1-12.
66. *Redox environment of the cell as viewed through the redox state of the glutathione disulfide/glutathione couple.* **Schafer FQ, Buettner GR.** 2001 Jun 1, Free Radic Biol Med., Vol. 30(11), pp. 1191-212.
67. *Identification of S-glutathionylated cellular proteins during oxidative stress and constitutive metabolism by affinity purification and proteomic analysis.* **Lind C, Gerdes R, Hamnell Y, Schuppe-Koistinen I, von Löwenhielm HB, Holmgren A, Cotgreave IA.** 2002 Oct 15, Arch Biochem Biophys., Vol. 406(2), pp. 229-40.
68. *Mechanisms of oxidative glutamate toxicity: the glutamate/cystine antiporter system xc- as a neuroprotective drug target.* **Albrecht P, Lewerenz J, Dittmer S, Noack R, Maher P, Methner A.** 2010 Jul, CNS Neurol Disord Drug Targets., Vol. 9(3), pp. 373-82.
69. *A role for 12-lipoxygenase in nerve cell death caused by glutathione depletion.* **Li Y, Maher P, Schubert D.** 1997 Aug, Neuron., Vol. 19(2), pp. 453-63.
70. *Requirement for cGMP in nerve cell death caused by glutathione depletion.* **Li Y, Maher P, Schubert D.** 1997 Dec 1, J Cell Biol., Vol. 139(5), pp. 1317-24.
71. *Store-operated calcium entry modulates neuronal network activity in a model of chronic epilepsy.* **Steinbeck JA, Henke N, Opatz J, Gruszczynska-Biegala J, Schneider L, Theiss S, Hamacher N, Steinfarz B, Golz S, Brüstle O, Kuznicki J, Methner A.** 2011 Dec, Exp Neurol., Vol. 232(2), pp. 185-94.

72. *Stromal interaction molecule 1 (STIM1) is involved in the regulation of mitochondrial shape and bioenergetics and plays a role in oxidative stress.* **Henke N, Albrecht P, Pfeiffer A, Toutzaris D, Zanger K, Methner A.** 2012 Dec 7, J Biol Chem., Vol. 287(50), pp. 42042-52.
73. *The plasma membrane channel ORAI1 mediates detrimental calcium influx caused by endogenous oxidative stress.* **Henke N, Albrecht P, Bouchachia I, Ryazantseva M, Knoll K, Lewerenz J, Kaznacheyeva E, Maher P, Methner A.** 2013 Jan 24, Cell Death Dis.
74. *Store-operated Ca2+ entry in sensory neurons: functional role and the effect of painful nerve injury.* **Gemes G, Bangaru ML, Wu HE, Tang Q, Weihrauch D, Koopmeiners AS, Cruikshank JM, Kwok WM, Hogan QH.** 2011 Mar 9, J Neurosci., Vol. 31(10), pp. 3536-49.
75. *Regulation of STIM1 and SOCE by the ubiquitin-proteasome system (UPS).* **Keil JM, Shen Z, Briggs SP, Patrick GN.** 2010 Oct 18, PLoS One., Vol. 5(10):e13465.
76. *Differential roles for STIM1 and STIM2 in store-operated calcium entry in rat neurons.* **Gruszczynska-Biegala J, Pomorski P, Wisniewska MB, Kuznicki J.** 2011 Apr 26, PLoS One., Vol. 6(4):e19285.
77. *Expression of STIM1 in brain and puncta-like co-localization of STIM1 and ORAI1 upon depletion of Ca(2+) store in neurons.* **Klejman ME, Gruszczynska-Biegala J, Skibinska-Kijek A, Wisniewska MB, Misztal K, Blazejczyk M, Bojarski L, Kuznicki J.** 2009 Jan, Neurochem Int., Vol. 54(1), pp. 49-55.
78. *Signalling to transcription: store-operated Ca2+ entry and NFAT activation in lymphocytes.* **Gwack Y, Feske S, Srikanth S, Hogan PG, Rao A.** 2007 Aug, Cell Calcium., Vol. 42(2), pp. 145-56.
79. *Immunodeficiency due to mutations in ORAI1 and STIM1.* **Feske S, Picard C, Fischer A.** 2010 May, Clin Immunol., Vol. 135(2), pp. 169-82.
80. *The potential role of mitochondrial dysfunction in seizure-associated cell death in the hippocampus and epileptogenesis.* **Chen SD, Chang AY, Chuang YC.** 2010 Dec, J Bioenerg Biomembr., Vol. 42(6), pp. 461-5.
81. *Mitochondria, oxidative stress, and temporal lobe epilepsy.* **Waldbaum S, Patel M.** 2010 Jan, Epilepsy Res., Vol. 88(1), pp. 23-45.
82. *Mitochondrial dysfunction and oxidative stress: a contributing link to acquired epilepsy?* **Waldbaum S, Patel M.** 2010 Dec, J Bioenerg Biomembr., Vol. 42(6), pp. 449-55.
83. *Role of oxidative stress in epileptic seizures.* **Shin EJ, Jeong JH, Chung YH, Kim WK, Ko KH, Bach JH, Hong JS, Yoneda Y, Kim HC.** 2011 Aug, Neurochem Int., Vol. 59(2), pp. 122-37.
84. *Oxidative stress and neurodegeneration: where are we now?* **B., Halliwell.** 2006 Jun, J Neurochem. , Vol. 97(6), pp. 1634-58.
85. *Reactive oxygen species in cell signaling.* **Thannickal VJ, Fanburg BL.** 2000 Dec, Am J Physiol Lung Cell Mol Physiol. , Vol. 279(6), pp. L1005-28.
86. *Physiological significance of reactive cysteine residues of Keap1 in determining Nrf2 activity.* **Yamamoto T, Suzuki T, Kobayashi A, Wakabayashi J, Maher J, Motohashi H, Yamamoto M.** 2008 Apr, Mol Cell Biol., Vol. 28(8), pp. 2758-70.
87. *Nrf2 is a direct PERK substrate and effector of PERK-dependent cell survival.* **Cullinan SB, Zhang D, Hannink M, Arvisais E, Kaufman RJ, Diehl JA.** 2003 Oct, Mol Cell Biol., Vol. 23(20), pp. 7198-209.
88. *The unfolded protein response: controlling cell fate decisions under ER stress and beyond.* **Hetz C.** 2012 Jan 18, Nat Rev Mol Cell Biol., Vol. 13(2), pp. 89-102.
89. *Integrating the mechanisms of apoptosis induced by endoplasmic reticulum stress.* **Tabas I, Ron D.** 2011 Mar, Nat Cell Biol., Vol. 13(3), pp. 184-90.
90. *Mitofusin 2 regulates STIM1 migration from the Ca2+ store to the plasma membrane in cells with depolarized mitochondria.* **Singaravelu K, Nelson C, Bakowski D, de Brito OM, Ng SW, Di Capite J, Powell T, Scorrano L, Parekh AB.** 2011 Apr 8, J Biol Chem., Vol. 286(14), pp. 12189-201.
91. *Mitofusins and OPA1 mediate sequential steps in mitochondrial membrane fusion.* **Song Z, Ghochani M, McCaffery JM, Frey TG, Chan DC.** 2009 Aug, Mol Biol Cell., Vol. 20(15), pp. 3525-32.
92. *Sustained Ca2+ transfer across mitochondria is Essential for mitochondrial Ca2+ buffering, sore-operated Ca2+ entry, and Ca2+ store refilling.* **Malli R, Frieden M, Osibow K, Zoratti C, Mayer M, Demaurex N, Graier WF.** 2003 Nov 7, J Biol Chem. , Vol. 278(45), pp. 44769-79.
93. *Regulation of mitochondrial ATP synthesis by calcium: evidence for a long-term metabolic priming.* **Jouaville LS, Pinton P, Bastianutto C, Rutter GA, Rizzuto R.** 1999 Nov 23, Proc Natl Acad Sci U S A. , Vol. 96(24), pp. 13807-12.
94. *Mitochondrial Ca2+ uptake and not mitochondrial motility is required for STIM1-Orai1-dependent store-operated Ca2+ entry.* **Naghdi S, Waldeck-Weiermair M, Fertschai I, Poteser M, Graier WF, Malli R.** 2010 Aug 1, J Cell Sci., Vol. 123(Pt 15), pp. 2553-64.
95. *Ca2+-independent phospholipase A2 is a novel determinant of store-operated Ca2+ entry.* **Smani T, Zakharov SI, Leno E, Csutora P, Trepakova ES, Bolotina VM.** 2003 Apr 4, J Biol Chem., Vol. 278(14), pp. 11909-15.
96. *Orai, STIM1 and iPLA2beta: a view from a different perspective.* **Bolotina VM.** 2008 Jul 1, J Physiol., Vol. 586(13), pp. 3035-42.

Appendix

Abbreviations

12-LOX	12-lipoxygenase
2-APB	2-aminoethoxydiphenyl borate
AMPA	2-amino-3-(3-hydroxy-5-methyl-isoxazol-4-yl)propanoic acid
ARE	antioxidant response element
ATP	adenosine triphosphate
BAK	Bcl-2 homologous antagonist killer
BAX	Bcl-2–associated X protein
BCL-2	B-cell lymphoma 2
BCL-XL	BCL2-like 1
cGMP	cyclic guanosinemonophosphate
CIF	Ca^{2+}-influx factor
CRAC	Ca^{2+}-release activated Ca^{2+} channel
DAG	diacylglycerol
DA-STIM1	dominant-active STIM1
ER	endoplasmic reticulum
GCL	γ-glutamylcysteine ligase
GSH	glutathione
GSSG	GSH disulfide
IP3	inositol 1,4,5-triphosphate
IP3R1-3	IP3-receptors 1-3
$iPLA_2$	Ca^{2+}-independent phospholipase A_2
KEAP1	kelch-like ECH-associated protein 1
KO	knock out
LGCC	ligand-gated Ca^{2+} channel
MEA	multi-electrode array
MEF	mouse embryonic fibroblast
MFN2	mitofusin-2
mGluR	metabotropic glutamate receptor
NADPH	nicotinamide adenine dinucleotide phosphate
NCX	Na^{+}/Ca^{2+} transporter type 1
NFAT	nuclear factor of activated T-cells
NMDA	N-Methyl-D-aspartate
NRF2	nuclear factor (erythroid-derived 2)-like 2

PERK	protein kinase-like endoplasmic reticulum kinase
PIP2	phosphatidylinositol 4,5-bisphosphate
PLC	phospholipase C
PMCA	plasma membrane Ca^{2+} ATPase
RNAi	RNA interference
ROS	reactive oxygen species
SERCA	sarcoplasmic/endoplasmic reticulum Ca^{2+} ATPase
sGC	soluble guanylyl cyclase
SOCE	store operated Ca^{2+} entry
SOD	superoxide dismutase
STIM1	stromal interaction molecule 1
UPR	unfolded protein response
VDCC	voltage-dependent Ca^{2+} channel
WT	wild type
Xbp1	X-box binding protein 1

List of publications

Publications prepared in the context of this PhD study:

The plasma membrane channel ORAI1 mediates detrimental calcium influx caused by endogenous oxidative stress, **Henke N**, Albrecht P, Bouchachia I, Knoll K, Lewerenz J, Maher P, Methner A, submitted to Cell Death & Disease

Extracellular cyclic GMP and its derivatives GMP and guanosine protect from oxidative glutamate toxicity, Albrecht P, **Henke N**, Tran Tien ML, Issberner A, Bouchachia I, Maher P, Lewerenz J, Methner A, submitted to Neurochemistry International

Stromal interaction molecule 1 (STIM1) is involved in the regulation of mitochondrial shape and bioenergetics and plays a role in oxidative stress., **Henke N**, Albrecht P, Pfeiffer A, Toutzaris D, Zanger K,, Methner A, J Biol Chem. 2012 Oct 17. [Epub ahead of print]

Effects of dimethyl fumarate on neuroprotection and immunomodulation. Albrecht P, Bouchachia I, Zimmermann C, Hofstetter HH, Kovacs Z, **Henke N**, Lisak D, Issberner A, Lewerenz J, Maher P, Goebels N, Quasthoff K, Mausberg AK, Hartung HP, Methner A. J Neuroinflammation. 2012 Jul 7;9(1):163.

A case of relapsing-remitting neuroborreliosis? Challenges in the differential diagnosis of recurrent myelitis. Albrecht P, **Henke N**, Lehmann HC, Macht S, Hefter H, Goebels N, Mackenzie C, Rupprecht TA, Fingerle V, Hartung HP, Methner A.; Case Rep Neurol. 2012 Jan;4(1):47-53.

The C terminus of Bax inhibitor-1 forms a Ca^{2+}-permeable channel pore. Bultynck G, Kiviluoto S, **Henke N**, Ivanova H, Schneider L, Rybalchenko V, Luyten T, Nuyts K, De Borggraeve W, Bezprozvanny I, Parys JB, De Smedt H, Missiaen L, Methner A.; J Biol Chem. 2012 Jan 20;287(4):2544-57.

Mutation of ATF4 mediates resistance of neuronal cell lines against oxidative stress by inducing xCT expression. Lewerenz J, Sato H, Albrecht P, **Henke N**, Noack R, Methner A, Maher P.; Cell Death Differ. 2012 May;19(5):847-58. doi: 10.1038/cdd.2011.165.

Charcot-Marie-Tooth disease CMT4A: GDAP1 increases cellular glutathione and the mitochondrial membrane potential. Noack R, Frede S, Albrecht P, **Henke N**, Pfeiffer A, Knoll K, Dehmel T, Meyer Zu Hörste G, Stettner M, Kieseier BC, Summer H, Golz S, Kochanski A, Wiedau-Pazos M, Arnold S, Lewerenz J, Methner A.; Hum Mol Genet. 2012 Jan 1;21(1):150-62.

Store-operated calcium entry modulates neuronal network activity in a model of chronic epilepsy. Steinbeck JA*, **Henke N***, Opatz J, Gruszczynska-Biegala J, Schneider L, Theiss S, Hamacher N, Steinfarz B, Golz S, Brüstle O, Kuznicki J, Methner A.; Exp Neurol. 2011 Dec;232(2):185-94. *equally contributed

The ancient cell death suppressor BAX inhibitor-1. **Henke N***, Lisak DA*, Schneider L, Habicht J, Pergande M, Methner A. Cell Calcium. 2011 Sep;50(3):251-60. Review. *equally contributed

Induction of Nrf2 and xCT are involved in the action of the neuroprotective antibiotic ceftriaxone in vitro. Lewerenz J, Albrecht P, Tien ML, **Henke N**, Karumbayaram S, Kornblum HI, Wiedau-Pazos M, Schubert D, Maher P, Methner A.; J Neurochem. 2009 Oct;111(2):332-43.

Publications obtained from the work as diploma student:

The B cell mutator AID promotes B lymphoid blast crisis and drug resistance in chronic myeloid leukemia. Klemm L, Duy C, Iacobucci I, Kuchen S, von Levetzow G, Feldhahn N, **Henke N**, Li Z, Hoffmann TK, Kim YM, Hofmann WK, Jumaa H, Groffen J, Heisterkamp N, Martinelli G, Lieber MR, Casellas R, Müschen M.; Cancer Cell. 2009 Sep 8;16(3):232-45.

Activation-induced cytidine deaminase acts as a mutator in BCR-ABL1-transformed acute lymphoblastic leukemia cells. Feldhahn N, **Henke N**, Melchior K, Duy C, Soh BN, Klein F, von Levetzow G, Giebel B, Li A, Hofmann WK, Jumaa H, Müschen M.; J Exp Med. 2007 May 14;204(5):1157-66.

Acknowledgment/Danksagung

An dieser Stelle möchte ich zunächst Prof. Methner danken, unter dessen Anleitung ich diese Arbeit anfertigen durfte. Vielen Dank für die zahlreichen guten Idee, viele spannende Projekte, Beharrlichkeit und Optimismus auch bei Ergebnissen die auf den ersten Blick nicht zusammen passten, konstruktive Kritik und das seltene aber dafür umso wertvollere Lob! Ich freue mich, dass ich die Möglichkeit hatte viel Neues zu lernen und Gelerntes weitergeben zu können, und dass ich durch zahlreiche Kooperationen und die Teilnahme an spannenden Kongressen viele interessante Menschen kennen gelernt habe.

Des Weiteren möchte ich mich bei Prof. Willbold bedanken für seine Bereitschaft als Koreferent zur Verfügung zu stehen. Vielen Dank für das Lesen und die Begutachtung dieser Arbeit!

Und auch bei Prof. Hartung bedanke ich mich für die Anschaffung des BD Pathway 855, womit wir das Live-Cell Imaging automatisieren konnten, was mir effektiv Lebenszeit geschenkt hat!

Mein Dank gilt ebenso allen Koautoren für die produktive Zusammenarbeit, besonders aber Julius Steinbeck für seine Expertise zur Epilepsieforschung, Pamela Maher für ihre Erfahrung im Bereich der oxidativen Glutamattoxizität und Jan Lewerenz für konstruktive Kritik rund um die Uhr, auch am Samstagabend.

Bedanken möchte ich mich auch bei allen aktuellen und fast allen ehemaligen Mitgliedern der Arbeitsgruppe und allen Kollegen aus dem Labor im Life Science Center. Es ist schön mit euch zusammen zu arbeiten, mit einigen besonders schön. Ich danke Andrea für Glutamatzugaben um sieben Uhr morgens, ohne die manche Versuche gar nicht möglich gewesen wären. Vielen Dank auch an Annika für das manuelle kategorisieren zahlreicher Mitochondrien und an Astrid für ihren Beitrag zum AIG1 Projekt. Dima möchte ich danken für Statistikunterricht und Feuerzangenbowle und Lars für das unermüdliche Training meiner Soft Skills. Ein großer Dank gilt auch Teresa und Caro, dafür, dass Teresa mich versteht, wenn ich einfach nur mal schimpfen und meckern muss damit es mir besser geht und Caro für ihren unerschütterlichen Glauben daran, dass alles gut wird und ihr tägliches „Ich wünsch dir noch nen schönen Abend!“. Manchmal ist es tatsächlich überraschend noch ein schöner Abend geworden. Danke auch an Zsuzsa, für ihre unerwarteten, trockenen Kommentare zu diversen Situationen, die passender nicht hätten sein können und vielen Dank an Sven, dass er mich nie vergessen hat, wenn er zum REWE gegangen ist. Ein großes Dankeschön geht auch an Janine, die immer ein offenes Ohr für mich hatte wenn‘s stressig war und auch für ein entspanntes Kaffeeschwätzchen immer zu haben war/ist.

Ich bedanke mich auch bei „meinen Mädels“ Jenni, Steffi (lila) und Steffi (blond) dafür, dass sie sich auch nach längerer Funkstille über ein Lebenszeichen freuen ohne sich über ausgebliebene Anrufe oder email-Antworten zu beschweren. Und dafür, dass wir uns auch nach einer halben Ewigkeit wieder treffen können und alles ist wie immer. Besonders bedanke ich mich aber bei Sonja, die vom anfänglichen „Lab Buddy“ sehr schnell zu einer sehr guten, wenn nicht sogar meiner besten Freundin geworden ist, einfach für alles, da ich gar nicht weiß wo ich anfangen soll.

Ich bin sehr froh in den letzten Jahren ein Teil der Hipkendahler „Ponyfarm“ gewesen zu sein und bedanke mich bei allen Reiterfreunden, von denen sich glücklicherweise niemand für Paper oder Doktorarbeiten interessiert, für die entspannten Stunden mit oder zu Pferd.

Bedanken möchte ich mich natürlich auch bei meinen Eltern, die mich auf meinem Weg stets bestmöglich unterstützt haben.

Der größte Dank aber geht zum Abschluss an meinen Partner Jari, der in den letzten zehn Jahren immer an meiner Seite war und der mich einfach glücklich macht! Jari, mit dir würde ich auch bis ans Ende dieser Welt gehen!

Declaration/Erklärung

Hiermit erkläre ich, die vorliegende Arbeit selbstständig und ohne unerlaubte Hilfe verfasst und die verwendeten Quellen kenntlich gemacht zu haben. Diese Dissertation wurde bei keiner anderen Institution in dieser oder ähnlicher Form bisher eingereicht und es wurden keine erfolglosen Promotionsversuche unternommen.

Nadine Henke